RE-190

IMPROVED PARTICLE CHARGING TECHNIQUE

October 1964

Grumman

RESEARCH DEPARTMENT

GRUMMAN AIRCRAFT ENGINEERING CORPORATION
BETHPAGE NEW YORK

Grumman Research Department Report RE-190

IMPROVED PARTICLE-CHARGING TECHNIQUE

by

Frank Swanson

Paul Grinoch

Anthony Favale

Nuclear Research Section

October 1964

NATIONAL AERONAUTICS AND SPACE ADMINISTRATION NAS 1-2309

FINAL REPORT

Approved by: Charles E. Mack, Jr.
Charles E. Mack, Jr.
Director of Research

ABSTRACT

This final report describes the work which is a continuation of previous studies for imposing unusually high electrical charges on micro-particles so that they may be accelerated in a controllable electrostatic accelerator to hypervelocities. The approach pursued utilizes a high-current ion beam (low milliampere range) as a charging medium in conjunction with automatic electrostatic confinement of the microparticles during the charging process. Two important criteria employed as guidelines in this study are the development of a technique inherently compatible with the production of hypervelocity particles in per second or per minute availability and the development of a system which is completely containable in the high voltage end of the accelerators presently being employed to accelerate charged microparticles.

ACKNOWLEDGMENT

We wish to express our appreciation for the contributions of Messrs. E.T. Kruszewski and R.A. Golub of the Protective Structures Section, Structures Research Division, Langley Research Center. Their many comments and suggestions were valuable both in the course of the study and in the preparation of this Final Report. We also wish to acknowledge the contributions of Grumman personnel M. Rossi, A. St. Laurent, and F. Lotito to various phases of the study.

TABLE OF CONTENTS

LIST OF ILLUSTRATIONS

I. INTRODUCTION AND SUMMARY

A. Particle Charging Concept

The work described in this final report was performed under Contract NAS 1-2309 in continuation of studies initiated under Contract NASw-149, which was published as Grumman Research Department Report RE-152 (Ref. 1). The over-all aim of this work has been the development of a means for imposing unusually high electrical charge on microparticles so that they may be accelerated readily, in a controllable electrostatic accelerator (of the low Mv Van de Graaff type, for example), to velocities far in excess of those presently obtainable by other means in the laboratory. This would provide a tool valuable for both the simulation of micrometeorite impact and the study of microparticle hypervelocity impact in general.

The approach pursued in this investigation has been to utilize a high-current ion beam as a charging medium in conjunction with automatic electrostatic confinement of the microparticles during the charging process. Although one alternative charging concept, known as "contact" or "induction" charging, has been very successfully pursued by others (Refs. 2 and 3), we believe that the general concept of ion beam charging is potentially superior in that it offers a means of surpassing the more limited capability inherent in contact charging (Ref. 2, p. 32). At the same time, in pursuing the use of high-current beams and automatic confinement, we have sought to avoid certain severe limitations on routine use that are inherent in the otherwise highly successful low-current ion beam approach pursued by others (Ref. 4).

Our aim has been the development of a technique inherently compatible with the production of hypervelocity particles in per second or per minute availability rather than in per day availability or per week availability. An equally important, and somewhat related, criterion in our concept has been that the charging system be

completely containable in the high voltage end of the accelerator, with the impact target specimens located at the ground end. The advantage of this polarity becomes obvious when one considers the expenditure of time and effort required for "unbuttoning" an Mv electrostatic accelerator after each run to retrieve target specimens. In principle, the polarity problem could be overcome by employing a specially designed linear accelerator. However, at a given setting, this type of machine could only handle particles with charge-to-mass ratios in a very tight range about a central value corresponding to the machine setting. In practice, this would require the use of a system that charges only one particle at a time, and a high percentage of rejection of these individually charged particles. Thus, the over-all flavor of such a system may not be compatible with engineering laboratory requirements.

For these reasons, our efforts have centered on the use of milliamperes of beam current for charging rather than fractions of a microampere; the charging of many particles simultaneously at a high rate (albeit only a small fraction of the total number of particles initially injected) rather than the charging of one particle at a time; and automatic confinement of the particles rather than manipulation of a single particle. It should also be pointed out that, in a given vacuum environment, high-current ion beam charging (short charging time) is inherently capable of achieving higher charge accumulation than is low-current (long charging time) charging, because of charge neutralization processes that can become overwhelming in the latter mode (see Appendix IV). Low-current charging requires the use of bulky cryogenic pumping equipment in close proximity to the charging region to reduce the rate of impingement of ambient gas molecules attracted to the electrified microsphere. Such equipment cannot be fitted into the high-voltage terminal of an electrostatic accelerator.

B. Previous Work

During the period of time between Contract NASw-149 and the present contract, it had been found experimentally that the electrostatic particle injector previously designed was not suitable for injecting particles with sufficient velocity to traverse the ion beam. A modification of this injector (shown in Fig. 1 of this report), which makes use of an auxiliary high velocity air stream (together with baffling and differential pumping to protect the vacuum of the ion beam tube) was developed during this interim period and found to operate satisfactorily. Experimental velocity studies with the injector in vacuum, based on observation of the vertical fall of particles while traversing a fixed horizontal distance, showed that the particles had injection velocities in excess of 30 meters/sec, and thus would pass through milliampere ion beams.

C. Charge Retention Determination.

Subsequent experimentation (during proton beam operation) with "bucking" potentials on an electrode placed at the first-pass end position showed that the injection velocities were not too high for confinement of particles carrying the small first-pass charge accumulation, and therefore would also be satisfactory for confinement of particles more highly charged after additional passes through the beam.

By being able to set a reliable lower limit on injection velocities obtained with particles of known size distribution, and from the experimental determination of bucking potentials required to stop the particles after single pass through proton beams of known intensities, we were able to calculate a lower limit for the amount of charge actually retained after first pass. These calculations from experiment (see Appendix VII.) agreed with our previous theoretical charge accumulation calculations performed on the basis of zero net charge leakage (Ref. 1, p. 59). Since protons may be expected to leak almost instantaneously from micron size particles at the temperatures attained during our first-pass operation (Ref. 1, pp. 17-21 and 57),

these measurements provided striking confirmation of our previous contention (see Appendix V and Ref. 1, p. 21) that leaking protons would carry electrons off with them in virtually a one-to-one correspondence, even in the presence of considerable field strengths and high temperature.

To the best of our knowledge, this was the first time that this basic process of solid state surface physics had ever been observed. Although others had previously inferred charge retention by observing the behavior of particles constrained to circulate in ion beams (for example, Ref. 2), and subsequent to our measurements others had published results (Ref. 4) from which the retention of net charge on particles after extraction from the ion beam can be inferred, the work reported in both Ref. 2 and Ref. 4 was performed with very low beam intensities (and hence with the particles at room temperature), and seems to have been principally with low diffusivity heavy ions such as argon. During the period of our studies, we have investigated several confinement systems: radial, plane, and line.

D. Radial Confinement System

Earliest efforts in the studies pursued during the present contract consisted of attempts to extract and detect highly charged particles at the exit port of the cylindrical grid confinement system developed under Contract NASw-149. In previous preliminary work, small quantities of particles had been captured on greased filter paper targets placed well within the detector port, presumably well shielded from the influence of stray scattering of particles by material surfaces in the charging tube. Then, alternately with filter paper targets and with our capacitive detector mounted in place, we attempted to optimize various parameters of the charging system to pass particles through the detector in sufficient quantity to allow dependable measurement of charge-to-mass ratio and velocity. These measurements required that the particles pass through the detector in sufficient abundance that the detection pulses could be reliably distinguished from stray noise pulses. In these

attempts we varied such parameters as ion beam current, beam focus, confinement grid voltage, and extractor focusing. On a number of occasions, we were by this means able to catch, on filter paper targets placed at the detector position, some 10 particles over a three hour run. This poor yield was much too low for us to detect reliably by electrical means,-and completely out of the range of our goal - particles per second or per minute. This result led us to re-examination of the first-pass conditions as the initial step in an attempt to trace the trajectories of the particles through the charging system.

We next decided to try to obtain measurement of charges retained and particle velocities, initially at the first-pass through the beam and subsequently at later points in the progress of the particles. Because the charge on the particles is very low in the early history of the process, the development and use of extremely high amplification, low noise, circuitry was required. Beam noise, consisting of a very pronounced 120 cycle component and a much lower (significant but tolerable) incoherent component, proved to be troublesome to this detection system for low-charge particles. This placed us in the position of not being able to detect first-pass (low-charge) particles electrically, while at the same time requiring the velocity-charge-mass information to be able to obtain usable quantities of multiple-pass (high charge) particles through the detector at the exit port of the charging system.

The need to eliminate the 120 cycle signal led to the development of a "dummy" detector and low-noise difference amplifier system. The dummy detector was made to view the beam simultaneously with the particle detector and the inputs of both were fed to the difference amplifier, whose output was then fed to the main amplifier and display system. By adjusting the gain in each leg of the difference amplifiers separately, we were able to reduce the 120 cycle noise to insignificant levels for short periods of time; but we soon found that this balance was unstable

and could not be adequately maintained, which meant that the spatial distribution of the noise was time-dependent in a random fashion.

We subsequently abandoned first-pass studies and examined the distribution of particles at points in the charging chamber, utilizing filter paper targets. Our results showed that the particle yields toward the lower end of the system were much lower than had been anticipated, in spite of the high injection rate. It had always been anticipated that the nonlinear electrical field around the grid wires would increase their effective geometric size, thus cutting down on the yield. We had hoped to overcome this by using high particle injection rates and grid wire thickness and spacing that were considerably narrower and wider, respectively, than the initial width of the microparticle beam. Our results, however, indicated that the field distortion in the complex geometry was too large for a helical grid wire system to be workable. Consequently, more suitable electrode geometries were sought.

E. Plane Confinement System

Proceeding to a slightly more complex concept, a brief attempt was made to acquire tighter control of the particle trajectories by electrostatically focusing them to the vicinity of a single plane during their descent through the charging system. The confinement system, which was very simple, obtained its focusing action from the voltages impressed on verticle insulated conducting plates. In this design, which is discussed herein in Section III, a certain amount of benefit was still sought from the combination of high injection rate and diversity of particles as to size and initial vector velocity. It was found that adequate focusing could only be achieved over a short descent distance. Because the charge-to-kinetic energy ratio of the particles rose as the particles fell, focusing voltages proper for the first-pass (a necessary condition) were increasingly less suitable at later times in the history of the particles. This eventually led to intolerable over-focusing and loss

of the particles. Although this result was not unexpected, the study had seemed advisable in view of the small amount of time required for its completion.

F. Line Confinement System

Preceding work having shown the need for tight confinement of the particles during charging, our attention was directed to confining the particles to the vicinity of a line perpendicular to the ion beam and passing through its axis. Electrostatic focusing was selected for this purpose because magnetic focusing would require impractically high magnetic field strengths for the charge-to-momentum ratios of the particles in our system. Confinement to a line (with temporal modulation of electrode voltages) was chosen over confinement to a plane (with spatial modulation of electrode voltages) because this would lead to an inherently smaller system with no greater penalty in design complexity. For tight confinement, voltage modulation is required because the charge accumulated on the particles increases as a function of time, while focusing characteristics depend on charge-to-momentum ratio. In line confinement, the particles must see electrode voltages gradually decreasing in time in order to avoid over-focusing. In plane confinement, the spatial modulation must be correlated to the rate of fall of the particles.

Tight focusing also acts more readily to reject particles having inappropriate charge-to-kinetic energy ratios, by over-focusing the more highly charged particles and under-focusing the less highly charged particles. This decreases the number of particles available for charging. By contrast, for example, our previous grid confinement system had the virtue of confining all the particles (preventing the particles from hitting the exterior housing of the system) when adjusted to confine those having the lowest charge-to-kinetic energy ratios. For this reason, and because the line confinement can only synchronize with a very briefly pulsed injection of particles, we were anxious to obtain an increased particle injection rate capability and particle collimation properties superior to the 1° spread typical of

our old injector. These attributes would be especially highly desirable in initial efforts to obtain a semiempirical tuning in on the electrode voltages and modulation required. Our efforts in this direction lead to the design and testing of the modified injector shown in Fig. 18. This device provides superior collimation through the use of an auxiliary peripheral gas stream. This attribute at the same time provides greater particle yield because fewer particles are rejected by the collimation slit. Although the design objectives, as to greatly improved collimation ($1/6^{\circ}$ compared to 1°), and yield were attained with the new injector hardware, the higher injection velocities characteristic of the collimation scheme presented an unexpected problem.

Our scheme for electrical confinement of the particles requires that the potentials employed be at all times capable of repelling the particles back into the ion beam. The electrode voltage requirement is highest during the first few passes of the particles through the beam, since the charge on a given particle is very low during this period. Previously, with the old injector, we had found that a bucking potential of some 2 kv was adequate for turning particles back after a single pass through a 1-ma proton beam. With the higher velocities characteristic of the new injector, higher voltages and higher beam currents (more charge on first pass) were required for repelling the particles. In particular, it was found that the new injector required bucking potentials of at least 6 kv with a 3-ma proton beam. Since, the bucking potential required for first pass, should vary as the cube of the injection velocity and inversely as the first power of the beam current, it can be inferred that the velocities obtained with the new injector were twice as high as those obtained with the old injector.

Within the vacuum capabilities of the existing pumping system we were unable to maintain the 6-kv bucking operation reliably, because of concomitant intermittent electrical discharge of the electrodes through the ambient partially ionized gaseous

environment. At the same time, it was found that attempts to obtain lower particle velocities by drastically reducing the upstream gas pressures in the injector resulted in impairment of the improved injection rate sought in this new device. Since improvement of the system vacuum to allow use of the required 6-kv bucking voltage would have required revisions in major portions of the equipment, the new injector was set aside for future use and the old injector was installed on the line confinement charging system. This decision amounted to making a modest, but high risk, investment in an effort to avoid a possible unnecessary delay in reaching the basic objective - the extraction of highly charged particles in quantities that could be reliably detected and analyzed as to mass-velocity-charge correlations.

Subsequent efforts have consisted of attempts to extract highly charged particles from the system by hand-and-eye tuning of the electrical and timing parameters while observing pulses from the detector on an oscilloscope. Meaningful pulses have not been obtained, which we interpret as a deficiency in either our particle injection rate or our lens configuration.

An interesting sidelight of this investigation has been the reduction of detector noise to a minimum, and the consequent enhancement of detection sensitivity. This has been important to us because first-pass studies are very basic to our work on confinement. The electrical detection of first-pass particles requires the use of very high amplification and low noise instrumentation, because these particles only carry about 1 percent of the design final charge. The major portion of our detector noise was previously established to be associated with beam noise during the early "first-pass" detection experimentation, in which a dummy detector and a difference amplifier were used to reduce detector noise. It is state of the art knowledge that positive ion beam systems in vacuum invariably give rise to secondary electrons due to the collision of ions with residual gas and due to the impact of stray ions on the structure of the apparatus. The latter effect usually predominates, especially

in the presence of metals. In the earlier work we had not considered secondary electrons as a source of noise in the detector because the surrounding geometric and field configurations seemed to preclude this possibility automatically. Instead, we had attributed the pickup to stray fields resulting from 120 cycle ripple in the beam. By using battery biasing during work with the line confinement system we discovered that this 120 cycle ripple noise is caused by electron currents flowing through the detector's 1,000 meg input impedance; this current is very small (50 μ μamp) and is probably due to beam-noise-dependent secondary emission from proton impacts on various metallic surfaces. A small permanent magnet, mounted so as to sweep the electrons away before they reach the detection cylinder, was effective in reducing the detector noise to much more acceptable levels.

At the time of this writing we are engaged in minimizing low level microphonic random noise that may be masking low yield detection. At the same time, we are initiating a full-scale mathematical analysis of our lens systems to refine analysis previously performed by extrapolating results obtained with a two dimensional electrical analog plotting board. We are also starting on the redesign of vacuum pumping capabilities of our system to allow the use of higher electrode voltages, and thus to allow use of the new injector.

II. EXPERIMENTAL WORK ON RADIAL CONFINEMENT SYSTEM (INITIAL SYSTEM)

A. Particle Injector

The design of an electrostatic injector was presented in Ref. 1 (p. 67). The injection system employed a parallel plate capacitor ("dust chamber") and an external electrical field to accelerate slightly negatively charged particles into the charging chamber. The dust chamber consists of two parallel conducting disks capping a 1-1/4-inch hollow cylindrical insulator, this assembly being mounted with the axis of the cylinder in line with the earth's gravitational field. Microparticles loaded into the evacuated chamber initially lie at rest on the lower conducting plate under the influence of gravity. In operation, a dc excitation voltage is applied across the conducting plates, establishing an electric field with vector direction running from the positive upper plate to the negative lower plate. As the voltage is raised, particles resting on the lower plate acquire increasingly greater amounts of excess negative charge. At a sufficiently high voltage (several kv), gravity and cohesive forces are overcome, and the particles jump to the upper plate, where they become positively charged, and then accelerated back to the lower plate where they become negatively charged again. The net effect is to fill the entire volume of the dust chamber with finely separated agitated dust particles. A small channel in the upper plate provides a "particle leak" through which some of the slightly negatively charged particles travel up into the accelerating chamber. The constructional details of the accelerating chamber are not pertinent to the present discussion. The function of this chamber is to accelerate the particles into the ion beam with sufficient velocity to allow the particles to penetrate that beam fully. As the particles travel into the beam, their slight negative charge is quickly neutralized and they begin to acquire positive charge, as a result of ion bombardment. As soon as they become positively charged, the particles are subjected

to an electrostatic force directed away from the center of the beam. The initial injection velocity must be sufficiently high to take the particles through the center of the beam, if the full charging capability of the beam is to be employed.

For a given mechanical and electrical configuration in this scheme, the injection velocity of the particles depends upon the amount of negative charge acquired by particles of a given mass before they exit the dust chamber. This quantity, in turn, depends upon the gravitational and cohesive forces to which the particles are subjected in the dust chamber. For illustration, in principle, even an excess of one electronic charge would lift a particle off the negative (lower) plate in the absence of these forces . The cohesive forces seem to be strongly dependent on humidity, and possibly on unevaluated other factors. For this reason, it is difficult to calculate precisely the injection velocity provided by an injection system of this type.

Initial experimental attempts with a device of this design proved unsatisfactory from the standpoint of injection velocity with the injection voltages employable in our over-all system. A quick solution based on the incorporation of a high velocity air stream, and differential pumping to protect the vacuum in the ion beam charging chamber, worked satisfactorily for a while. However, under repeated use, difficulties were encountered with clogging of the injection orifice by accumulated particles. Subsequent work, under the present contract, led to the design shown in Fig. 1, which has been employed in the bulk of the present work. It was found that for proper functioning of this injector, dry bottled nitrogen should be employed as the gas vehicle, rather than air, to minimize orifice clogging by the particles; in this connection "O-ring" seals are employed in the assembly of the device to exclude ambient air from the system, which is typically run with an upstream gas pressure of between 1.0 atmosphere and 0.1 atmosphere. In addition, the dust chamber capacitor

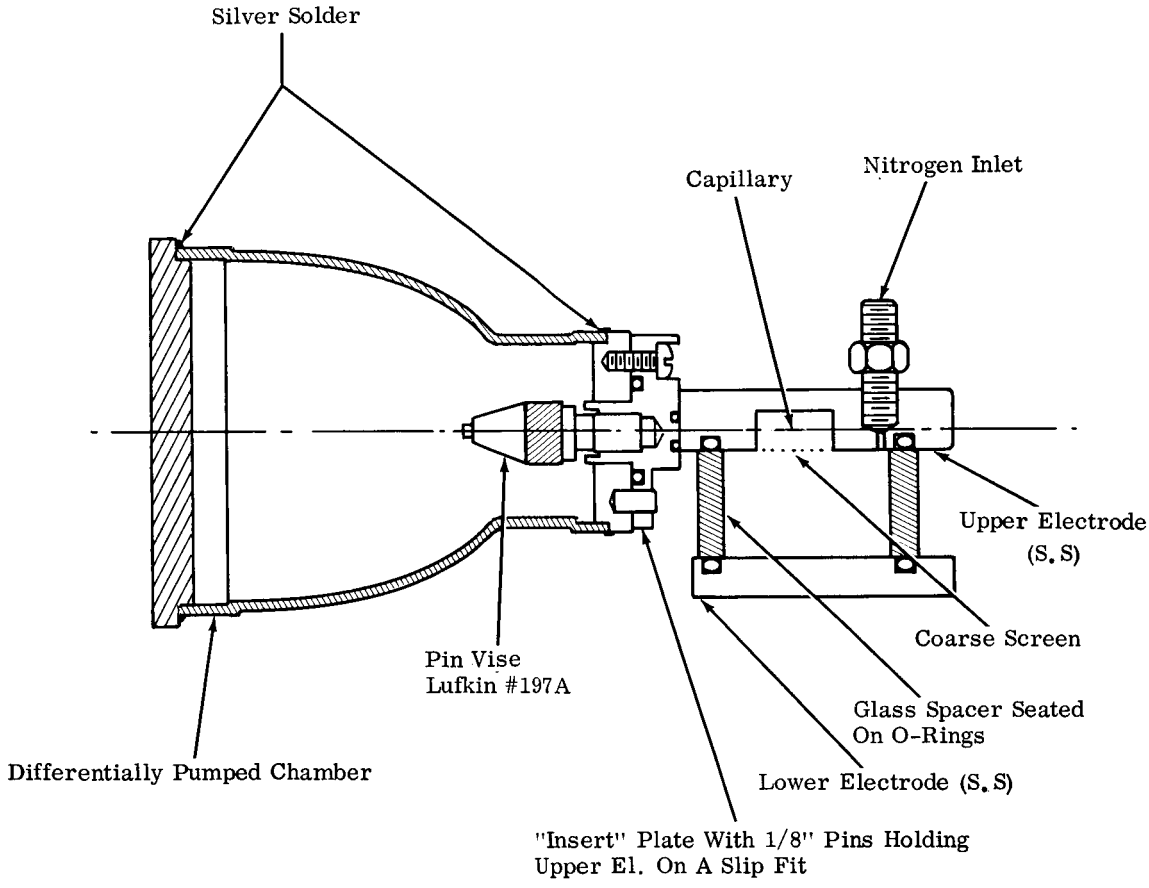

Fig. 1 Particle Injector

plates are made of stainless steel rather than brass, since brass plates were found to be overly subject to erosion that results in the production of extraneous brass dust. With these precautions, the present injector device operates over 8-hour runs reliably, and provides measured particle feed rates of about 500 particles/minute. We estimate that considerably higher feed rates will be readily obtainable, when needed, through relatively minor changes in the design, such as the use of higher upstream pressures and higher excitation voltages in the dust chamber.

In use, the injector is mounted via a glass stand-off attached to the outer structure of the ion beam charging chamber. Gas and particles are drawn through the capillary (which is a 4-mil inside diameter, 2-inch long stainless steel tube) under the influence of the airstream resulting from the difference in static pressure at the tube ends (upstream side at about 1 atmosphere, downstream side at about 60 microns). They then pass into the differentially pumped chamber, where most of the gas is removed with a roughing pump, to maintain a pressure of 60 microns. The particles pass through this chamber unimpeded, entering the ion beam charging chamber through the 1/32-inch chamber collimating hole. In traveling through the capillary tube the particles are rapidly accelerated under the influence of the high velocity gas stream. Theoretical calculations of injection velocities obtained, based on a greatly simplified calculational model, are given in Appendix VI. It is seen in Fig. A15, that particle velocities are only imperceptably affected by gross changes in upstream gas pressure (due to sonic choking of the gas flow), but are highly dependent on particle size. A lower limit on particle velocity has been determined experimentally by allowing the particles to traverse a 15-inch-long vacuum tube in which the particles were allowed to fall under gravity and where the amount of measured vertical displacement is proportional to the particle velocity. In this manner the lower limit was set at $v_0 > 30$ m/sec.

The operation of the injector is occasionally subject to clogging of the capillary tube with particles; the exact reasons for this phenomenon have neither been determined nor sought in the present investigation. The gas that we employ is bottled "dry" nitrogen, and the microparticles are passed through a No. 500 mesh and thoroughly dried under heat and vacuum before being loaded into the injector. For this reason, moisture does not appear to be responsible for the clogging. On the other hand, although the capillary tube diameter is only on the order of ten times that of a single particle, purely mechanical jamming seems improbable. Although clogging does slow our studies at times, and is thus an occasional source of frustration, the percentage of down time is very low in the present application. In later work, however, it would be advisable to minimize this factor if the injector is to be employed in a "buttoned-up" Mv accelerator.

B. First Pass Studies

Previous work, presented in (Ref. 1) had led to the design of the helical grid confinement ion beam charging system. This design had been predicated on the use of a high input rate of particles diverse in mass and velocity, in an admittedly high-loss confinement system, to produce large numbers of charged particles. In preliminary studies with operation of the full system, we had collected small quantities of particles in the extraction port of the device, at a point presumably well-shielded from the influence of stray scattering of particles by material surfaces in the charging chamber. In the current work we attempted to optimize various parameters, such as ion beam current, beam focus, confinement grid voltage, and extractor focusing, in an attempt to extract highly charged particles in an abundance sufficient that reliable measurements of charge, velocity, and mass correlation could be readily accomplished against the background of stray electrical noise pulses. By this means we were able to obtain, on a number of occasions, some 10 particles over a three-hour run. This poor yield was much too low for us to

detect reliably, and completely out of the range of our goal, - particles per second or per minute. This result led us to an experimental re-examination of the first-pass conditions as the first step in an attempt to trace the trajectories of the particles, and the influence working on them, during their descent through the charging system.

Optimization of system parameters necessary for automatic confinement of charged particles is highly dependent on a knowledge of particle mass-velocity-charge. Toward this end and to establish the physical validity of the beam charging method [mindful of our previous concern with proton leakage from microspheres at high material temperatures (Ref. 1, and Appendix V) , we concentrated our earliest efforts on measuring the charge retained by the particles during a single traversal of the beam. For this purpose, a target chamber was designed, built, and mounted directly across from the injection port, on the opposite side of the ion beam. Lightly greased paper targets were employed for collecting the particles, the targets being examined under a microscope before and after each run. It was found that particles passed through the proton beam at all beam currents employed (up to 4 ma), and that the bucking voltages required for a given proton beam current in that range corresponded to net charge accumulations previously calculated on the basis of zero charge leakage (Appendix VII and Ref. 1). Because this implied that leaking protons were carrying off electrons in essentially a one-to-one correspondence, it constituted a basic validation of the applicability of high-current proton beams for particle charging.

More definitive data on charge retained was now sought, since the particle velocities were only known on the basis of an experimentally measured lower limit, and since the particles lie in a size distribution, rather than all being exactly of the same size. Earlier measurements had indicated that the velocities acquired by the particles during the injection process were far in excess of those that

could be obtained from subsequent electrical forces in the course of a single pass through the beam. From this, it had been concluded that the velocities of the particles could at this time be treated as constant, independent of size, and that indeed the velocity involved during a single pass was essentially due to the injection gas stream, with all particles attaining a single basic asymptotic velocity. (This was found later to be erroneous). On this basis, a simple electrostatic deflection system was devised to obtain charge data. In this type of system the deflection is actually proportional to the ratio of charge-to-energy; however, for identical velocities, this amounts to a separation according to charge-to-mass. Since the amount of charge acquired during a first pass should be, to a first order approximation, proportional to the surface area of the particle, we essentially had expected to find particles of a single size at a given deflection point. Our failure to observe this indicated that the injection velocity is not the same for all particles. Strong dependence of particle velocity on particle size is indicated in a theoretical calculation presented in Appendix VI. The calculation is not necessarily definitive on an absolute basis, however, because the calculational model employed is greatly simplified and idealized.

Our attention then turned to employment of a version of the capacitive detector instrumentation outlined on page 43 of Ref. 1. This type of system provides a measurement of charge from the amplitude of a voltage pulse induced on a known cylindrical capacitor, and a measurement of velocity from the duration of the pulse. The detection system consists of a dural cylindrical capacitor (15 $\mu\mu$f total capacitance when connected to the amplifier tube). When a charged particle passes through this cylinder, image charges appear on the cylinder and are detected electronically. The electronic system is composed of a low noise pre-amp, with a gain of 100, mounted adjacent to the detection cylinder, and an oscilloscope on which the particle pulses are displayed. Calibration of the detector is obtained

by measuring the gain of the pre-amp and the capacitance of the detection cylinder; particle charge is then obtained by dividing pulse amplitude by the gain and multiplying by capacitance.

Since the anticipated detection pulse was of the order of 50 microvolts, amplifier noise and spurious pickup had to be kept to a very low level. In these particular efforts, the noise problem was aggravated by the fact that we were measuring the charge on slowly moving, lowly charged particles, in a system that requires that the detector "see" the unobscured ion beam so as to receive the particles. This problem would not exist in the detection of particles emerging from an actual high-voltage accelerator system, because the pulse characteristics of the very fast particles would be of much higher frequency than that of the beam noise, the particle charge (and therefore the pulse height) would be 100 times as high, and the beam itself would be out of the field of view of the detector.

Detection pulse rise times and pulse durations determine the band pass requirements of a detector and its associated electronics; for our case, this band pass had to be from about 50 cps up to about 20 kc. In this region of the frequency spectrum, electromagnetic pickup from electronic equipment and microphonic pickup from sources of vibration are particularly severe for low level measurements. Initial attempts at charge detection, using conventional low noise audio amplifiers, yielded noise several orders of magnitude above the anticipated detection pulse. By very thorough electrostatic shielding, the use of low microphonic tubes, and batteries for B^+ and 6.3 volts, as well as the use of a very low noise commercial amplifier (millivac VS 68B) for the main amplifier, we finally achieved a noise level one order of magnitude above the expected particle pulse amplitude. The noise consisted of a low level random noise component and a much larger 120 cycle ripple component. The latter was directly attributable to the ion beam itself, from which it was

virtually impossible to geometrically shield the detector, since the detector had to see the beam in order to accept particles. Consequently, this particular experimental situation, that is, low level measurements of low frequency signals in the vicinity of an intense ion beam, required more sophisticated electronics to eliminate spurious noise without simultaneously attenuating the detection signal.*

This problem was at least partly solvable in principle, by using two identical detection systems, only one of which receives the charged particles, and subtracting the two output signals, prior to observing the pulses on an oscilloscope. In this way, spurious noise common to both detectors could be balanced out to zero. The scheme is shown in Fig. 2.

In practice we found that in this way we could only obtain a good null on the 120 cycle noise component for intervals on the order of a minute, which indicated that the spatial distribution of the noise was time-dependent.

C. Multiple Pass Experimentation

Multiple pass experimentation was resumed in an attempt to ascertain the particle trajectories within the experimental charging chamber, in view of previous inability to extract electrically measurable quantities of particles at the exit port. This study was undertaken to reveal whether the previously assumed azimuthal symmetry was present at the"extraction port," located 4-1/2 inches below the point of injection and oriented 90° to the injection plane, or whether the particles were missing extraction because they lay in a preferred plane. At the same time, as part of the diagnostic procedure, particle yield information at various axial distances below the point of injection was sought.

---

*In later work (discussed in Sections IF and IVE of this report) the 120 cycle noise was found to be principally due to stray electron currents. These currents are common to beam systems and easily bent magnetically, but we had considered that our geometry precluded noise from this source (erroneously).

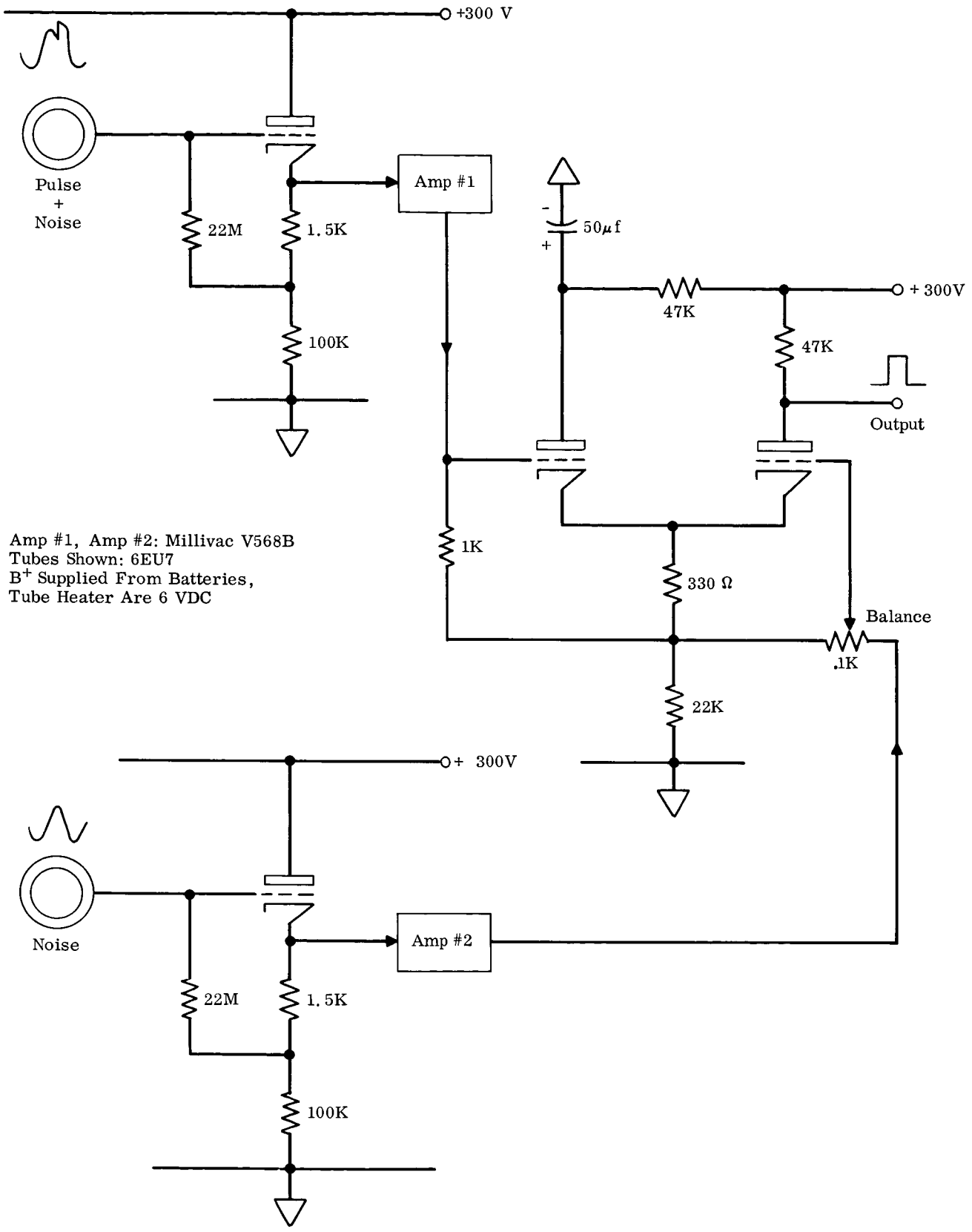

Fig. 2 Difference Amplifier

The experimental approach was to hang targets, consisting of paper coated with a thin layer of vacuum grease, from the interior surface of the grid structure at a given axial position, but at several angles (azimuths) at once. By perturbing only one axial position at a time, the possibility of "upstream" targets perturbing the particle trajectories sought at lower axial positions was avoided. For all of these experimental runs, an auxiliary target was placed directly across from the injector on the charging chamber housing, to verify that the particles were being properly repelled on the first pass. Experimental runs of, typically, one hour each were taken, while beam current, beam focus, dust chamber voltage, and other system parameters were maintained constant. Exposed targets were carefully scanned under a microscope by taking successive longitudinal sweeps across the target and moving the microscope stage transversely, by an amount equal to the field of view, between each sweep.

The experimental results showed that the planned azimuthal symmetry was present almost from the start of charging. Only a slight "polarization" of particle trajectories along the injection plane was noted. At the same time, particle yields diminshed rapidly with distance below injection. By 1/2 inch below the point of injection the yield was virtually zero. Particles observed on targets placed further down in the system showed typically 1/2 dozen particles on a one-inch by two-inch target, all randomly located. The very randomness of the particles in the lower locations indicated that they were scattered particles, and not due to orderly trajectories through the ion beam. Particles in comparably low concentrations had been previously observed when we first attempted to obtain large numbers of charged particles at the extraction port. Their low yield had precluded measurement of their charge electronically, since pickup and spurious noise invalidate such low "repetition rate" measurements. It is also probable that these scattered particles had very small charge.

We concluded from these results that the nonuniform electric field surrounding the grid wires was even more effective than our previous analytical studies had shown in strongly perturbing the particle trajectories. The "effective" grid wire diameter was thus much larger than tolerable, and could not be reduced by reducing the geometric size of the wire. These studies thus revealed that the confinement fields for multiple pass operation must be of a more tightly focusing nature, to avoid excessive stray scattering of the particles during the many passes required for full charge accumulation.

III. MODIFICATION OF RADIAL CONFINEMENT SYSTEM TO PLANE CONFINEMENT SYSTEM

The studies conducted with the helical grid system outlined in Section II of this report showed that a confinement system based on the action of a helically wound wire grid would lead to even greater scattering by the electric field in the neighborhood of the grid wire than had been anticipated, and that this scattering over a great number of passes accumulated to an overwhelming degree. It was apparent that a system should be sought that would:

1) require as little modification of the original ion beam apparatus and the associated charging chamber as possible, and,

2) provide tighter confinement than that obtainable with a grid confinement system.

It was deemed economical in time and money to engage in a brief effort in which a large amount of reliance was still placed on the high injection rate and the diversity in size and velocity of the injected particles, but using a confinement system that would provide somewhat tighter confinement of the particles.

A horizontal section of the revised system tried is shown in Fig. 3. The plane confinement system retained the original charging chamber, but interchanged the original grid confinement structure with a new electrode system that attempted to focus the particles within a plane, rather than allow azimuthal "drift". This new internal system was again mounted on the ceramic feed-thrus shown in Fig. 19 of Ref. 1. The inner electrode, of roughly rectangular cross section, was grounded, and shielded the beam centered within it from the influence of high voltage electric fields beyond it. The "slots" on each side of this electrode are aligned on the injection plane. Beyond the slot on each side is an electrode that consists of two

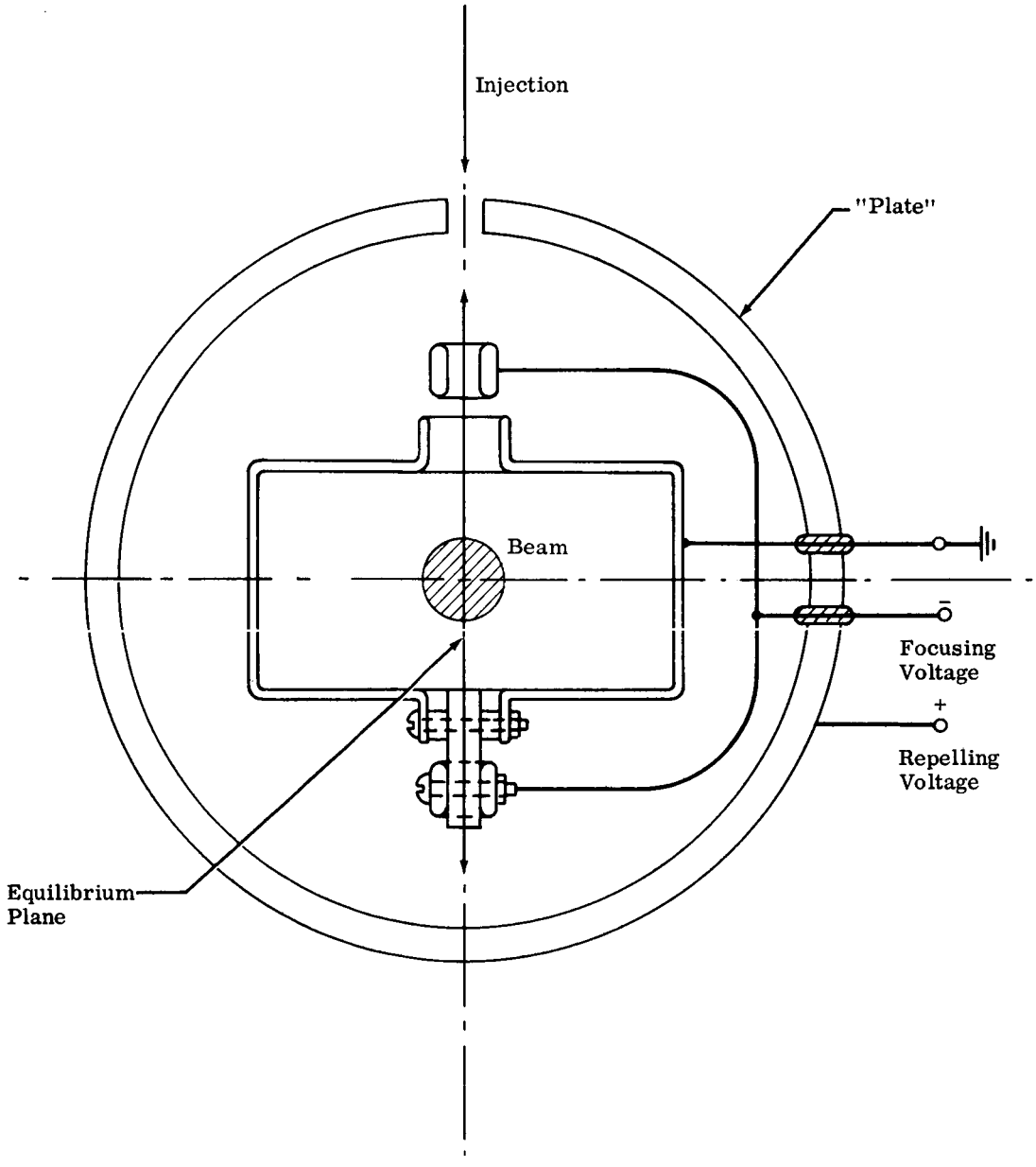

Fig. 3 In-Plane Charging System

vertical dural strips, 1/8 inch by 3/8 inch in cross section, with rounded edges to avoid high voltage sparking. Finally, we used the original brass outer cylinder of the charging chamber as the repelling electrode.

The role of the intermediate electrode is to provide focusing of the particles during their trajectories back and forth through the ion beam, to keep them oscillating in the injection plane as they fall under gravity. A negative potential was adopted for this electrode because this polarity would not repel the positively charged particles, but would provide focusing. Before this particular electrode geometry was chosen, various alternative electrode schemes were simulated on a 2 dimensional electrolytic plotting board, to investigate their respective field line configurations. This design showed good focusing qualities, as well as a "stopping vector", beyond the focusing electrode, that would direct the particle back toward the beam, independent of its depth of penetration into the "stopping" region.

Targets, consisting of vacuum grease-coated glossy paper bonded on glass microscope slides, were placed through the 1/8-inch opening between the focusing electrode and the grounded interior electrode. At particular values of focusing voltage and beam current, runs were taken at successively lower positions below the point of injection, and the targets were then examined under a microscope. Particle yields were found to be well collimated at positions corresponding to many passes through the beam, and then became more diffuse at lower positions, finally vanishing after a fall of about one inch*. During all these experimental runs, a target directly across from the injector verified that the particles were being repelled after their first ion beam traversal. There was some indication that, with lower focusing

---

*This "profile" is not seen on one target, but by observing the yield on targets placed at ever lower positions down the charging chamber.

voltages, collimation was improved further "downstream", but by this time the particles were highly reduced in number and statistics were poor.

This result was not surprising in view of the fact that electrostatic focusing depends on the charge to kinetic energy ratio of a particle. As particles fell to lower positions in the charging chamber, they acquired increasingly higher charge. Confinement with a fixed-potential lens system under these conditions eventually subjected the particles to over-focusing.

It thus was demonstrated that the design particle yields cannot be obtained by relying on high input rate and the diversity of particle input parameters, and that the particles must be tightly confined during the charging process in an electrode system in which the confining voltages are correlated to the time-dependent charge accumulation of the particles. For particles free to fall under gravity, this implies the need for spatial modulation of the confining voltages. For particles constrained to oscillate in a line, the need is for temporal modulation of the voltages.

IV. LINE CONFINEMENT PULSED SYSTEM

A. Concept of Line Confinement

1. General

The efforts previously described were based on the use of rather loose confinement systems. It had been judged that, in spite of the large losses inevitable in such systems, a considerable yield of suitably charged particles could be obtained through the very high injection rate of a population of particles rather diverse in mass and in injection vector velocity. Analysis of the charge and sizes of particles successfully extracted with various perturbations of the experimental system would then lead to an empirical optimization of the input parameters. This approach was dropped when it was found that the systems failed to extract sufficiently charged particles in detectable quantities. Our attention then was directed to the development of a tighter confinement system in which particles would be constrained to oscillate through the ion beam along a line. This system attempts to charge only one pulsed group of particles to the required field strength at one time; they are then extracted and a new group of particles is introduced into the system. The injector is alternately pulsed "on" and "off" in the course of a cycle, each new cycle beginning with the injection of a new group of particles into the system. Subsequent particle extraction is timed according to the amount of charge desired.

The confinement system, shown in Fig. 7 , consists of two identical electrostatic focusing systems "viewing" each other through the ion beam. These electrodes have cylindrical symmetry and are aligned on a common axis. Particles are reflected back toward the beam by the outer, cup-shaped, electrode and then focused by the adjacent cylindrical electrode. The repelling, or outer, electrode must have a

positive potential sufficient to reflect the particles; the focusing, or inner, electrode must have a potential adjusted to give a good focus through the beam. Because the focusing potential must not stop the particles, a negative potential whose magnitude is adjustable is applied to this electrode. Focal length of the lens system can be adjusted by varying the potential.

2. Electrode Design Parameters

The exact solution of charged particle trajectories within (arbitrary) electrostatic fields, subject to the proper boundary conditions, would have required a long-term computer program, possibly extending through the remaining contract time. Therefore, it was decided that the most expeditious design approach would be through approximate, but relatively quick, analytical methods, followed by a subsequent experimental validation of the electrode configuration finally adopted. The initial design procedure involved an investigation of the field equipotentials, arising from various tentative electrode configurations, by use of a two dimensional electrolytic tank. A typical lens design investigated in this way is shown in Fig. 4. This work revealed the focusing force lines pertaining to each geometry, and furnished a design incorporating minimum dispersion of the particles during their (basically defocusing) reflection by the repelling electrode. At the same time, the focusing field, between the focusing electrode and the interior, grounded, electrode, was optimized.

The axial potentials obtained from the electrolytic tank then served as input for a calculation of particle trajectories, which was based on an approximation technique employing finite difference equations (Reference 6, page 412). The results of this calculation showed that the present electrode configuration will produce focusing, with positive focusing voltages more efficient than negative voltages. Since these

- - - - - - -

*Ref. , page 412.

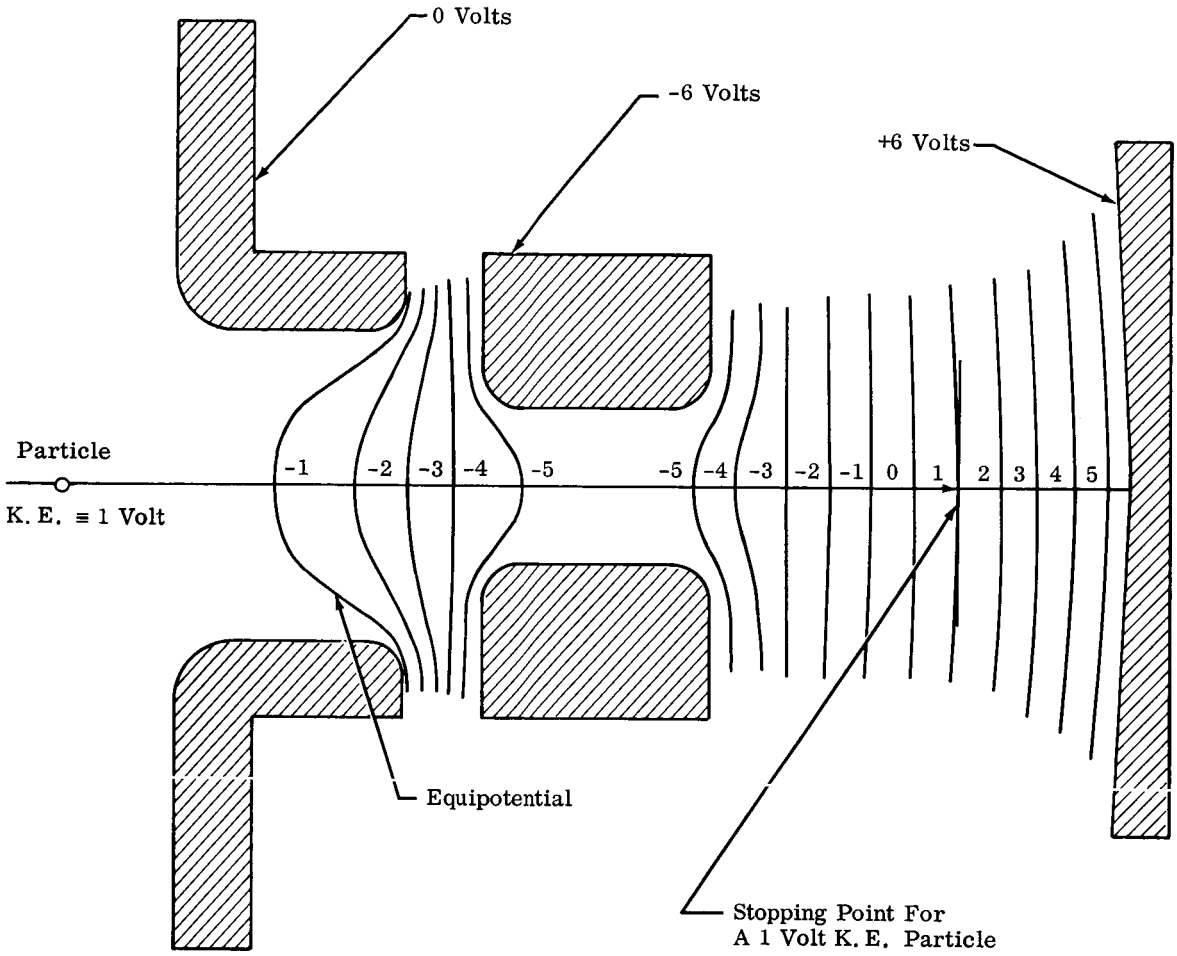

Fig. 4 Typical Electrolytic Lens Field Determination

theoretical results are only approximate, and are based on two dimensional potential determinations, the final experimental system was designed with sufficient versatility to modify both electrode configuration and focusing voltage requirements during later experimental runs.

3. Electrode Potential Modulation

Electrostatic lenses are characterized by focal lengths that depend on the voltages applied to the lens elements, as well as on the charge-to-kinetic energy ratio of the particles being focused. This dependence is given by the "small angle" ray equation for axially symmetric electrostatic fields:*

$$\frac{d^2r}{dz^2} = \frac{1}{\left[\frac{mv_0^2}{q} - 2\varphi\right]}\left\{\left(\frac{\partial r}{\partial z}\right)\left(\frac{\partial \varphi}{\partial z}\right) - \left(\frac{\partial \varphi}{\partial r}\right)\right\}$$

where

z = axial position in lens

r = radial distance from axis

φ = potential at (r, z)

q/m = charge-to-mass ratio of particle

v_0 = velocity of particle at entrance of lens region.

To maintain constant focusing properties during the charging process, this equation must remain unchanged during the charging history of the particle. By varying the potential as a function of time by a factor, $\alpha(t)$, with

$$\alpha(t) = (\text{const.})\,\frac{v_0^2(t)}{q(t)},$$

the focusing properties of the lens can be maintained invariant in time.

- - - - - - -

*See Appendix I for derivation.

In general, the particles' entrance velocity, $v_0(t)$, continues to increase during the charging period, because the augmented charge produces successively higher acceleration from the positive ion beam to the lens region. This velocity is given by:*

$$v_0^2(t) = V_0^2 + \frac{2\varphi_B}{m} q(t)$$

where we have defined

V_o = initial injection velocity

φ_B = potential from the edge of the beam to the entrance of the lens systems.

Consequently, the lens voltages must have a time-dependence given by:

$$\alpha(t) = (\text{const.}) \left\{ \frac{1 + \frac{2\varphi_B}{mV_0^2} q(t)}{q(t)} \right\} ,$$

with $q(t)$ defined as the charge acquired by the particle after being in the system for a time, t. The second term of the numerator in this expression is initially very small compared with unity, and the lens potentials vary inversely with the charge during this initial phase.

Equation (23) of Ref. 1 derives the equation relating particle charge as a function of time spent in the ion beam:

$$q(t) = 4\pi\varepsilon_0 R_p V_B (1 - e^{-\omega t}) ,$$

where

$4\pi\varepsilon_0$ = 1.11×10^{-10} f/m

R_p = radius of particle being charged

- - - - - - -

*See Appendix I.

V_B = ion beam acceleration voltage

ω = charging rate.

The present experimental system, however, requires that the particle spend a large amount of its time outside the beam during its reflection and focusing by the lens systems. Assuming that the charging is continuous (rather than in discrete "steps"), the above equation is valid if we modify ω to include the time spent outside the beam; this is done in Appendix I, where we define the new charging rate as ω'. At low values of accumulation, the charge is given by:

$$q(t) = 4\pi\epsilon_0 R_p V_B \left[1 - (1 - \omega' t + \frac{(\omega' t)^2}{2} + \ldots)\right]$$

$$\simeq 4\pi\epsilon_0 R_p V_B \omega' t = (\text{const.})\, t \ , \ \omega' t \ll 1 \ .$$

This means that the initial charge acquisition is linear, and that the lens voltages must initially be modulated in time by the function:

$$\alpha(t) = \frac{(\text{const.})}{t}$$

Since charge acquisition finally "saturates" at a value of

$$q(t \to \infty) = 4\pi\epsilon_0 R_p V_B \ ,$$

the lens potentials will finally reach a stationary value. The ratio of $\alpha(t)$ at infinity to $\alpha(t)$ at the start of charging is calculated in Appendix I, and has the value:

$$\frac{\alpha(t \to \infty)}{\alpha(t = 0)} = \left\{ \frac{1 + \left(\frac{\Phi_B}{\Phi_s}\right) \frac{4\pi\epsilon_0 R_p V_B}{q_0}}{\frac{4\pi\epsilon_0 R_p V_B}{q_0}} \right\}$$

where

φ_B = potential from beam to lens

φ_s = stopping potential after the first pass through the ion beam

q_0 = charge acquired after first traversal of ion beam.

For typical values used in the experimental system this ratio is about 1 percent.

Thus, the present experimental system, which is aimed at focused confinement of charged particles during charge accumulation, requires a decrease in lens voltages during charging in accordance with the theory of Appendix I. The lens voltage waveforms have been calculated as hyperbolas asymptotic to the final "saturation" voltage; typical decay times of about 1.0 second are calculated for the experimental system. Although this system has the disadvantage of requiring complicated electrode voltage modulation, it should provide much better confinement than could be obtained with the previous constant voltage systems. In principle, the amount of charge acquired can be raised to the theoretical limit, by increasing the charging time; alternatively, lower ion beam currents can be used with this system when this is desirable for some reason, again by increasing the charging time correspondingly. In practice, one would expect the charging time to have some optimum value, since increased charging time implies a greater number of traversals through the lens geometry and a lower survival probability for the particles.

B. The Mechanical System

1. General

The over-all ion beam apparatus, as described in Ref. 1 and also in Section II of this report, is retained in the pulsed charging system. On the other hand, the original charging chamber is replaced by the more compact pulsed charging apparatus shown in Fig. 5; the over-all experimental configuration is shown in Fig. 6. It should be noted that the actual charging region is now quite small, and a further reduction in size is practical for subsequent systems based on this technique.

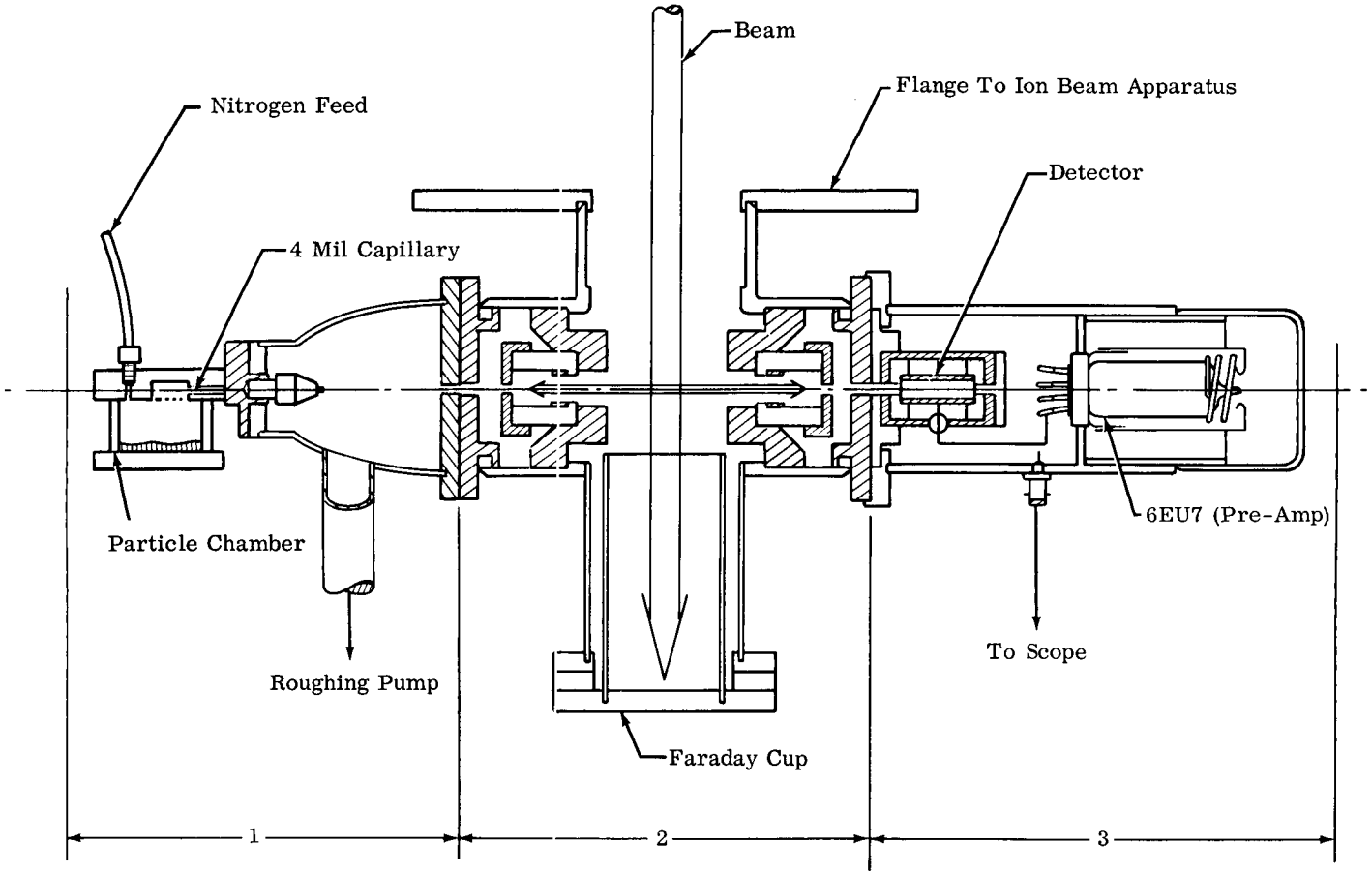

1 Injection Region
2 Charging Region
3 Detection Region

Fig. 5 Pulsed Charging Apparatus

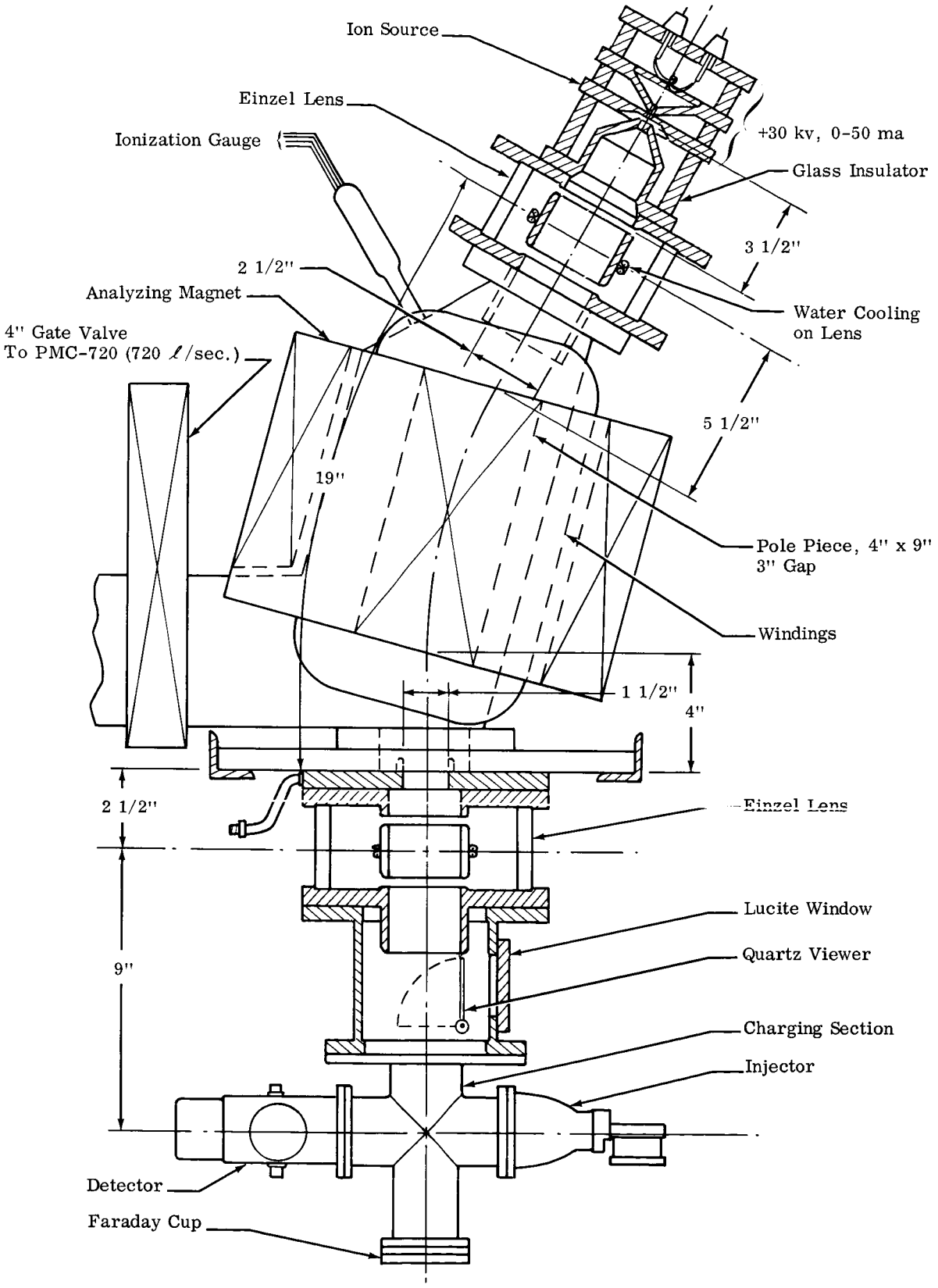

Fig. 6 Experimental System Configuration

The particle charging system consists of three major regions: the injection region, the charging region, and the detection region. The operation of the injector has been described in Section II. The second region, where particle confinement and charging takes place, consists of two identical electrostatic lens systems, one on each side of the beam, that reflect and focus the particles back and forth through the ion beam. Electrode voltages are brought in to the electrodes by way of insulating "feed-thrus" mounted on the vacuum wall of the charging chamber. Immediately below the lens systems is a faraday cup to monitor the ion beam current.

The detection region consists of an electrostatically shielded detection cylinder, aligned on the trajectory axis but outside the charging region, and a pre-amp which amplifies the detection pulses for their eventual observation on an oscilloscope. BNC connectors on the detector housing supply power to the pre-amp, and bring out the detection pulses. In the following treatment, the mechanical aspects of the charging system and of the detection system, will be discussed.

2. The Charging Chamber

The charging chamber used for the pulsed charging technique is a small, compact assembly that is accurately machined and aligned. The associated machine drawings are included in Appendix III and a full sized sketch of the system is shown in Fig. 7. The reflecting and focusing electrodes are machined in dural and all corners are well rounded to avoid high voltage sparking during operation. Both reflecting (or "repelling") electrodes have 1/16-inch holes at their centers; the hole in one electrode passes injected neutral particles into the charging region, while the hole in the opposite electrode passes extracted charged particles from the charging chamber. The repelling and focusing electrodes are aligned on machined nylon cylinders, whose impedance is sufficiently large to avoid electrical coupling of the high-voltage electrodes to each other, or to ground. These nylon

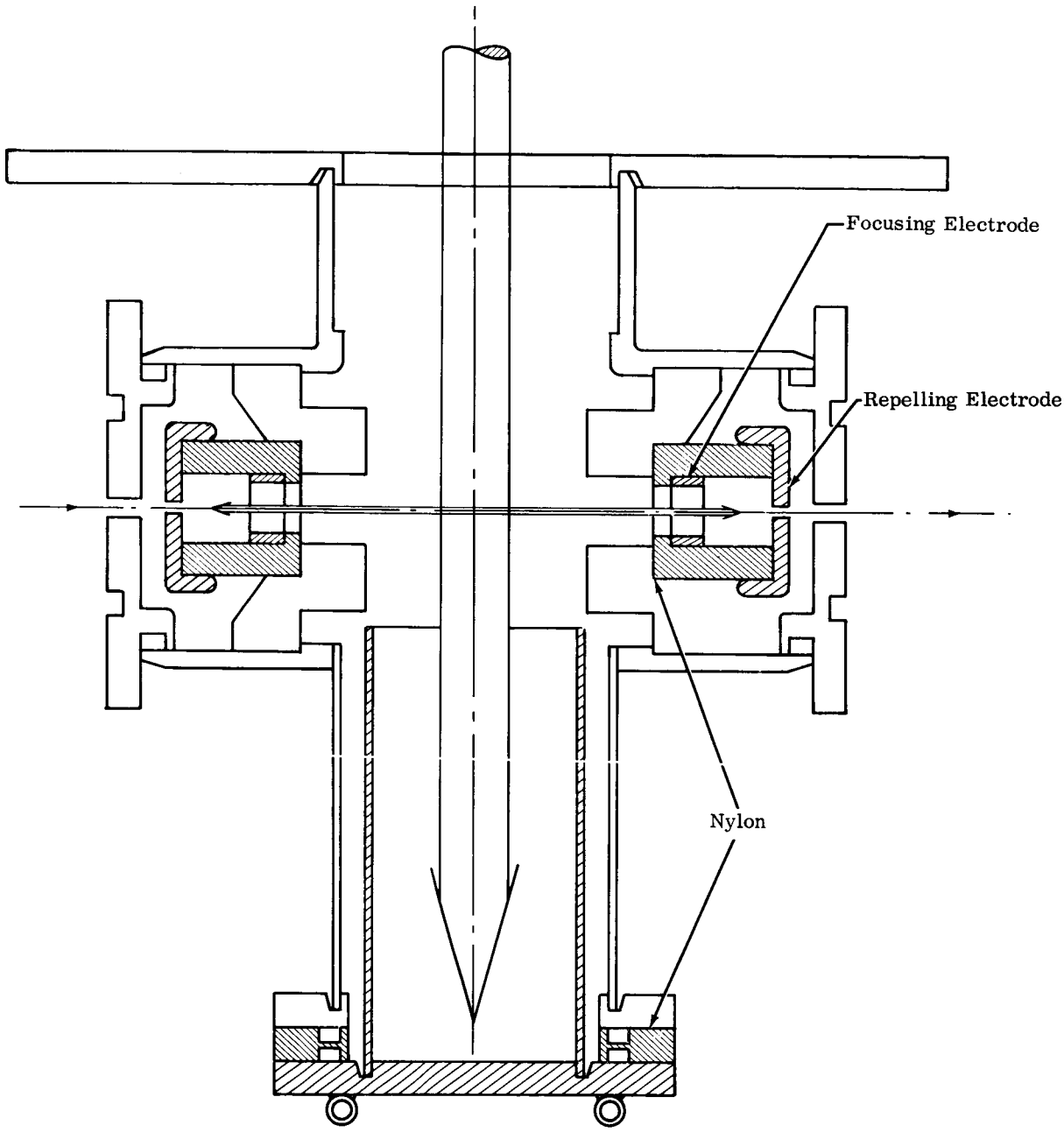

Fig. 7 Charging Assembly

insulators are, in turn, press-fitted into grounded coaxial cylinders of dural. The coaxial alignment of these electrostatic lenses focuses charged particles along the common axis of symmetry.

The housing for these two lenses is machined from a 2-inch brass "T". The "arms" of the T receive the lens elements described above, and the ion beam is focused down the vertical part of the T. The vertical part of the T also has a brass disk silver-soldered to it for installing the charging chamber on the ion beam apparatus. A faraday cup, consisting of 1-1/2-inch copper tubing silver-soldered to a brass disk, is located below the arms of the T. The faraday cup is water cooled through a single turn of 1/4-inch copper tubing soft-soldered to the bottom of the brass disk. Insulation from ground is assured by the use of a nylon spacer and nylon bolts to mount the faraday cup on the charging chamber. Finally, dural end caps, with O-rings, vacuum seal the charging chamber, and provide mounting surfaces for the injector and detector assemblies, respectively. These end caps, like the repelling electrodes, have holes at their centers to allow the passage of particles during the injection and extraction processes.

3. The Detector

Detection of charged particles by the induction of image charge on a cylindrical capacitor has been described in Ref. 1, and this discussion is limited to the experimental implementation of this detection technique. The experimental detection system is mounted at the extraction end of the charging system, and is coaxially aligned with the lens system in this chamber. Figure 8 shows the details of the present detection system, where the actual physical detector is a 1-inch-long, 1/4-inch-inside diameter, brass cylinder. The detection cylinder is placed inside a dural shield on nylon spacers, and this "cylindrical capacitor" is then bonded with epoxy to a nylon disk. Electrical connection with the detector is maintained

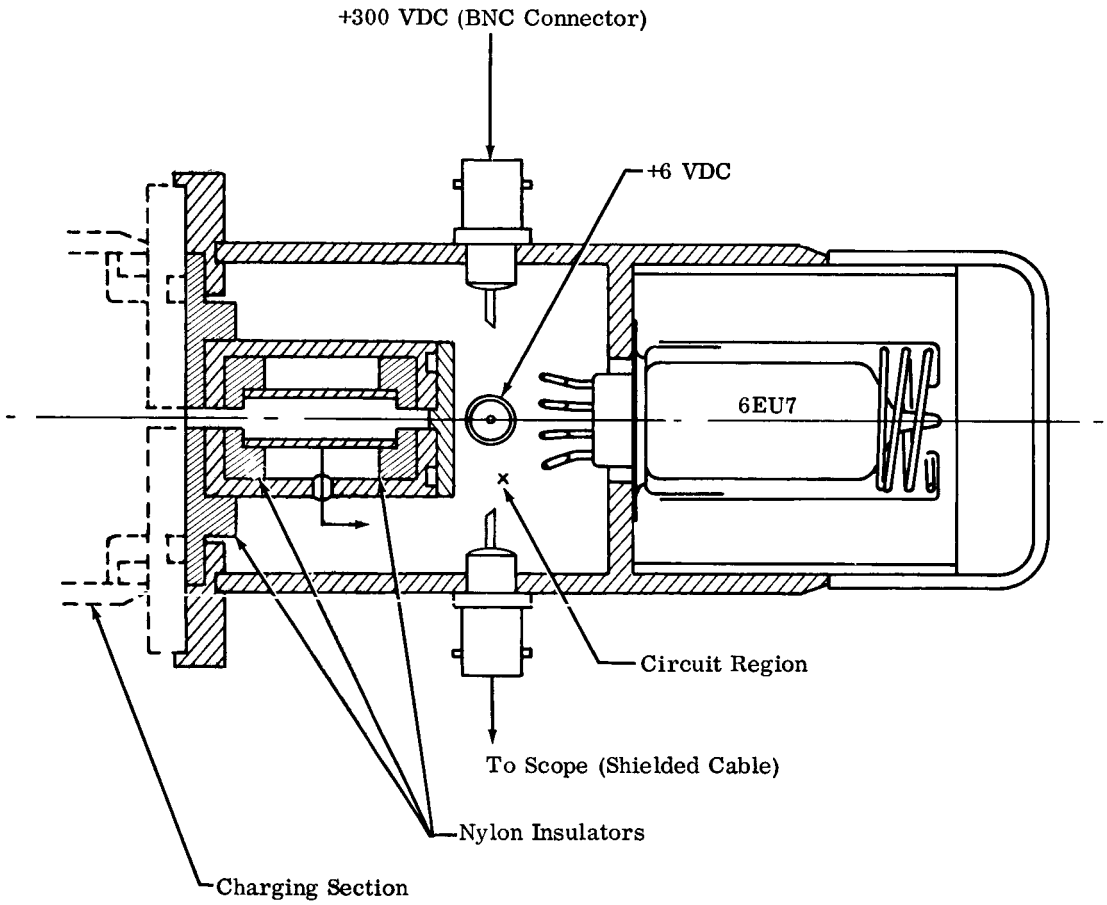

Fig. 8 Detection Assembly

through a solid copper wire passing through a hole in the shield, which is vacuum sealed with epoxy. Finally, a removable back cover on the shield serves as a target to collect particles that have passed through the detector; this provides a check on the alignment of the detection cylinder.

The detector unit is held against the end cap of the charging chamber by a brass "ring" that also centers the unit on the axis of the charging system. A 2-inch-inside diameter brass cylinder is silver-soldered to the ring and a disk, pressed into this cylinder, holds the 6EU7 tube socket. The schematic diagram of the pre-amp is shown later in Fig. 17, and is wired directly onto the pins of the tube socket, thus minimizing the capacity of the lead from the detector to the input grid of the 6EU7. Coaxial cables supply the 300 volt B^+ voltage and the 6.3 volt filament voltage to the pre-amp. Both voltages are derived from batteries to avoid the ripple normally associated with rectified power supplies. The output stage of the amplifier feeds a coaxial cable connected to a "545" oscilloscope with a type "D" plug-in unit. This oscilloscope combination provides a sensitivity of 1 mv/cm and can be synchronized only to sweep when particles are extracted from the system. In this way, noise pickup is greatly reduced and therefore higher particle charge detection sensitivity is feasible.

C. Electrical System

1. General

The basic electronics problem was to generate a repetitive set of the required waveforms, amplify them to kilovolt signals, and then to verify the final signals on an oscilloscope. The basic oscillator designed for this purpose is a free-running multivibrator with an adjustable period of 1 to 4 seconds; the "timing" signal thus generated fires a Schmitt trigger circuit to produce a 200-msec - duration, 25-volt, rectangular "gate" pulse. This gate pulse, of 1 to 4 second

"repetition period," provides the basic signal for subsequent pulse shaping, and also defines the steady state "on" period of the particle injector.

At the same time, the completion of the basic pulse fires several Schmitt trigger circuits in series to produce a final (particle extraction) pulse of 10 msec in duration. In this way, a rectangular extraction pulse is obtained that can be delayed from the initial injection pulse by a time period of from 1 msec to 1 second. At the termination of the 200 msec injection pulse the electrode voltages of the confinement system are caused to begin their hyperbolic decay. Timing relationships of the pulses are shown in Fig. 9. Finally, 6BK4 triodes amplify these signals to kilovolt magnitudes. A schematic diagram of the over-all electronic system is shown in Fig. 10.

2. Waveform Generation

As shown in the circuits in Figs. 11 and 12, waveform generation is initiated by a free-running multivibrator. The 250K potentiometer establishes repetition period from 1 second to 4 seconds, while the neon light flashes once each cycle for a visual check on repetition rate. Following this stage is a Schmitt trigger, or cathode coupled gate, circuit that is triggered by each negative pulse feeding through the 100 $\mu\mu$f coupling capacitor. Pulse width from this circuit is determined primarily by the 2.2 meg resistor in series with the .25 μf "feedback" capacitor; this time constant determines how soon, after being "turned off" by the incoming negative pulse, the first tube of the Schmitt trigger circuit draws current again, terminating the pulse. The rectangular gate pulse is coupled out through a 1N465 diode to a resistance divider, which prevents "undershoot" normally associated with this type of circuit.

The first half of the 12AT7, which receives the 200 msec gate pulse, is a cathode follower whose output is shaped by a diode pulse shaping network. It operates in

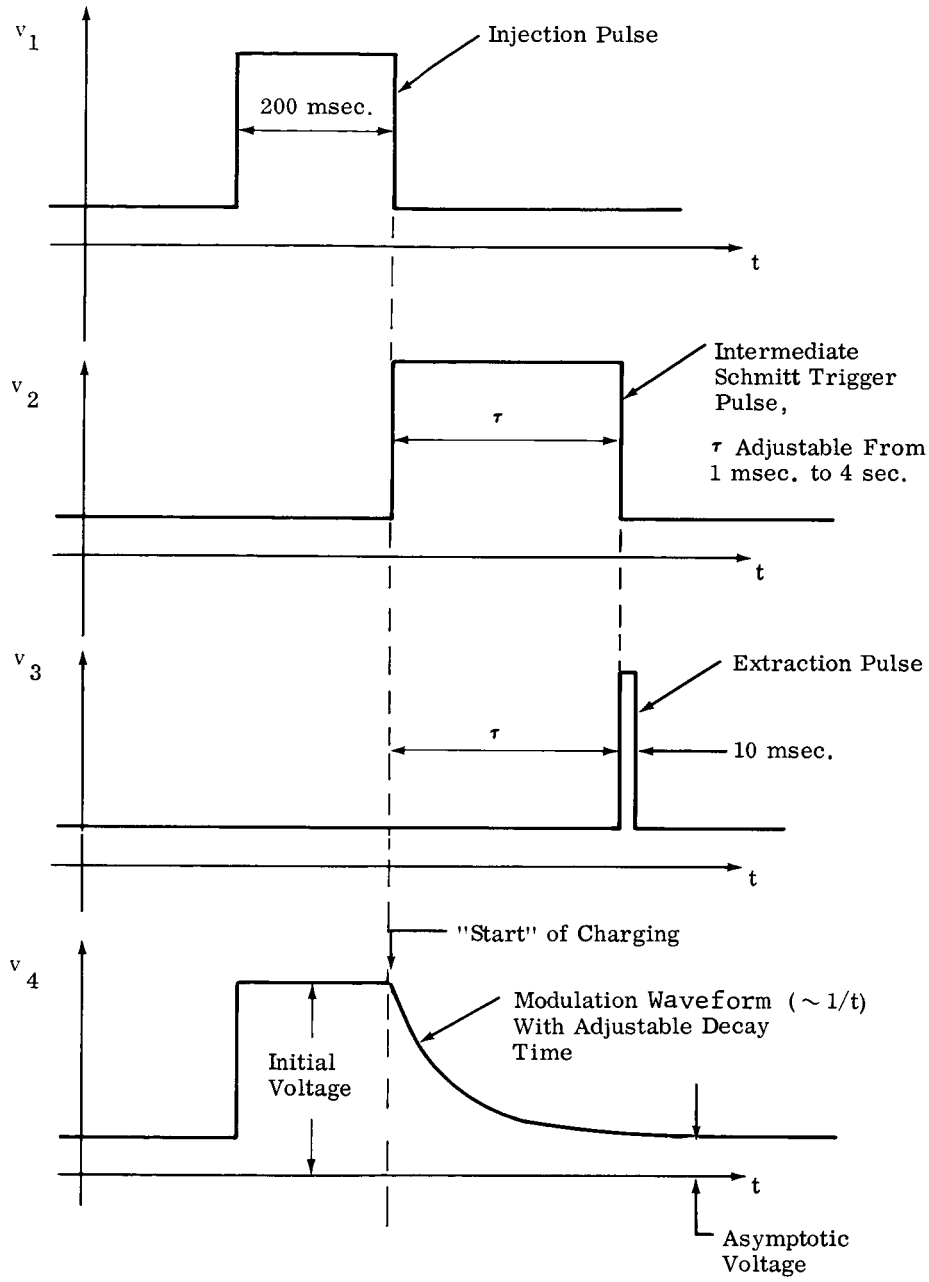

Fig. 9 Timing Relationship of Basic Waveforms

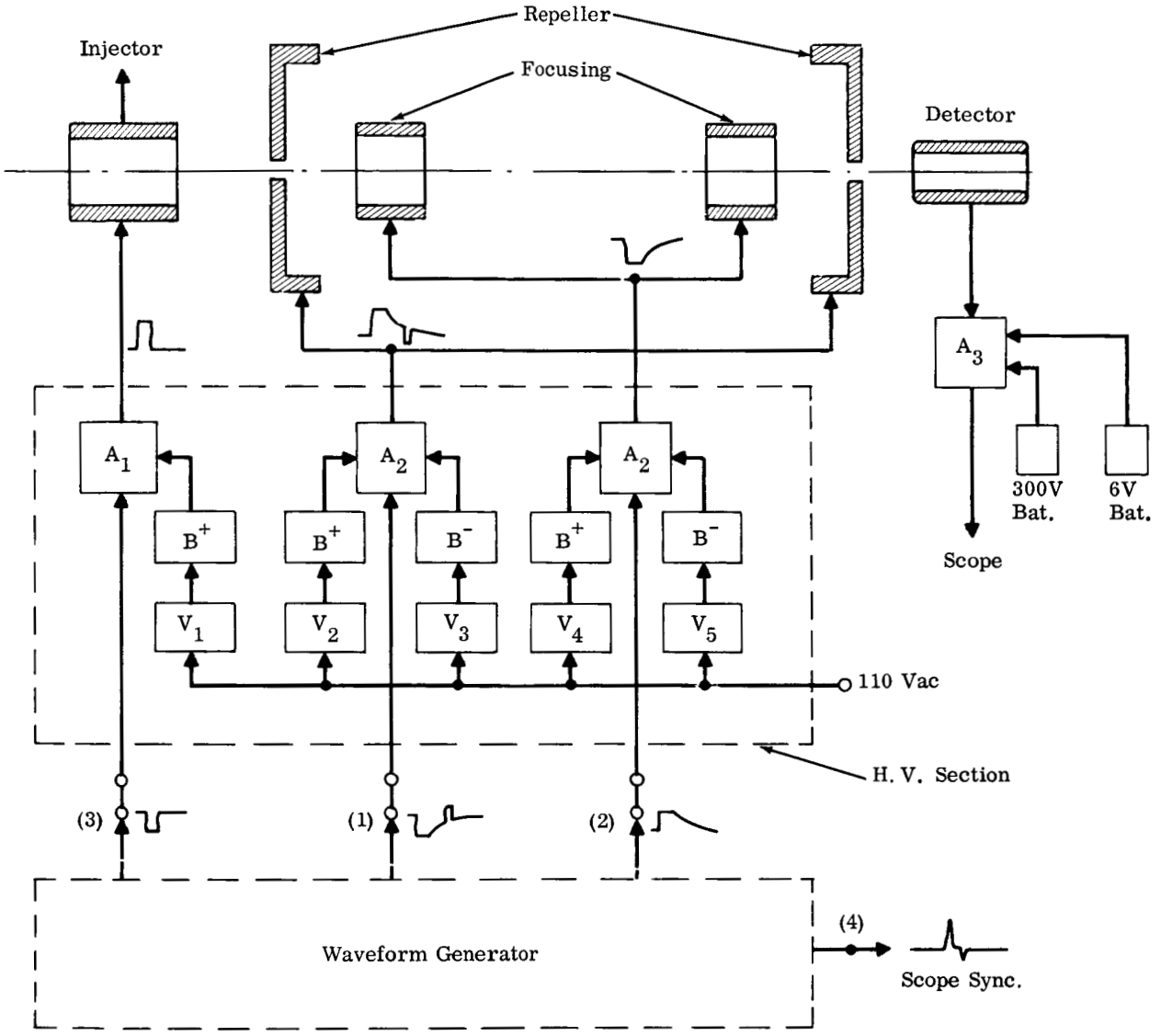

A_1 - Injector Amplifier
A_2 - Repeller Amplifier
A_3 - Detector Amplifier
B^+, B^- - 20kv, 5ma H. V. Power Supplies
V_1, ---, V_5 - 110 Volt, 60~, Variacs

Fig. 10 Block Diagram of Electronics

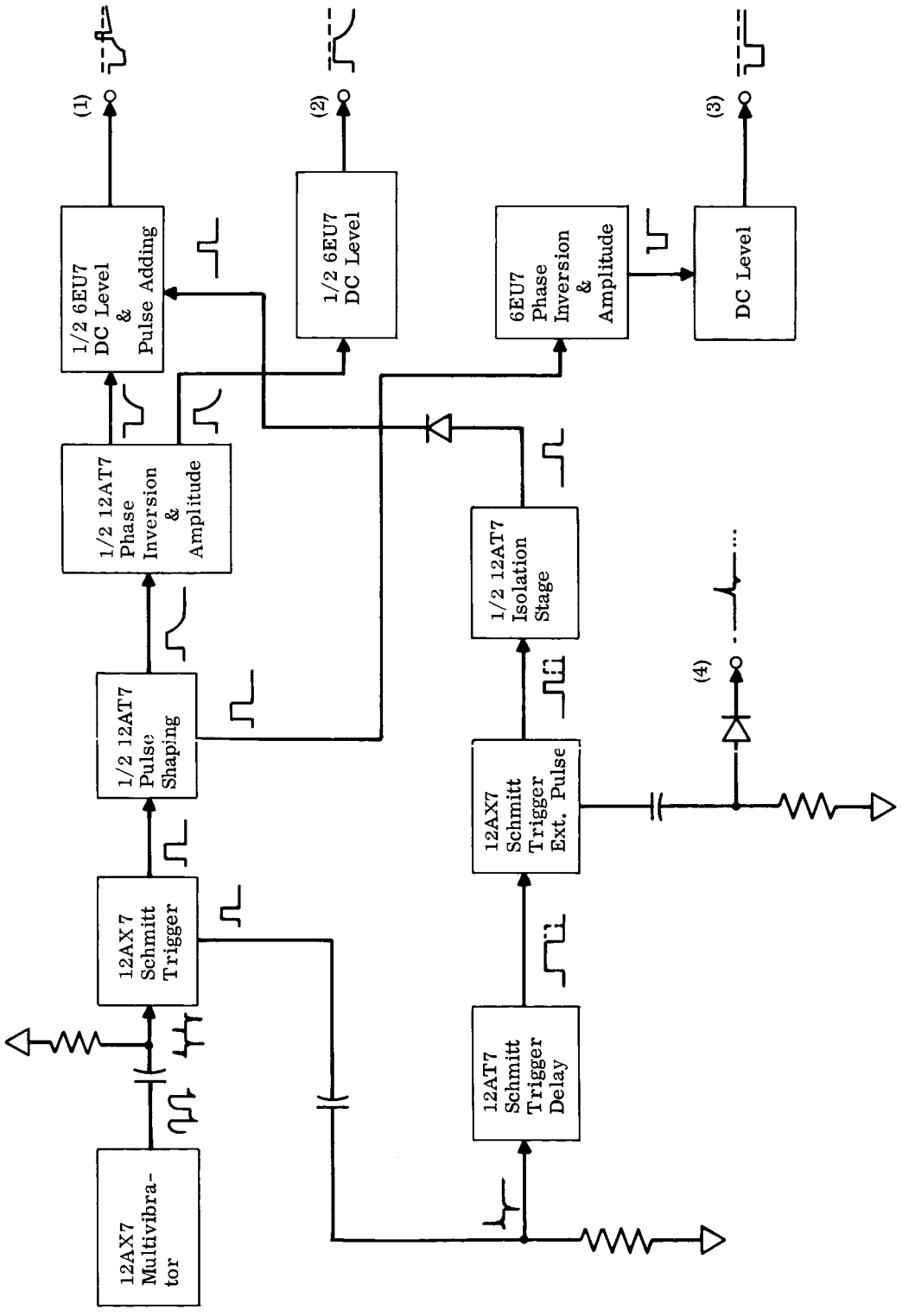

Fig. 11 Waveform Generator Logic

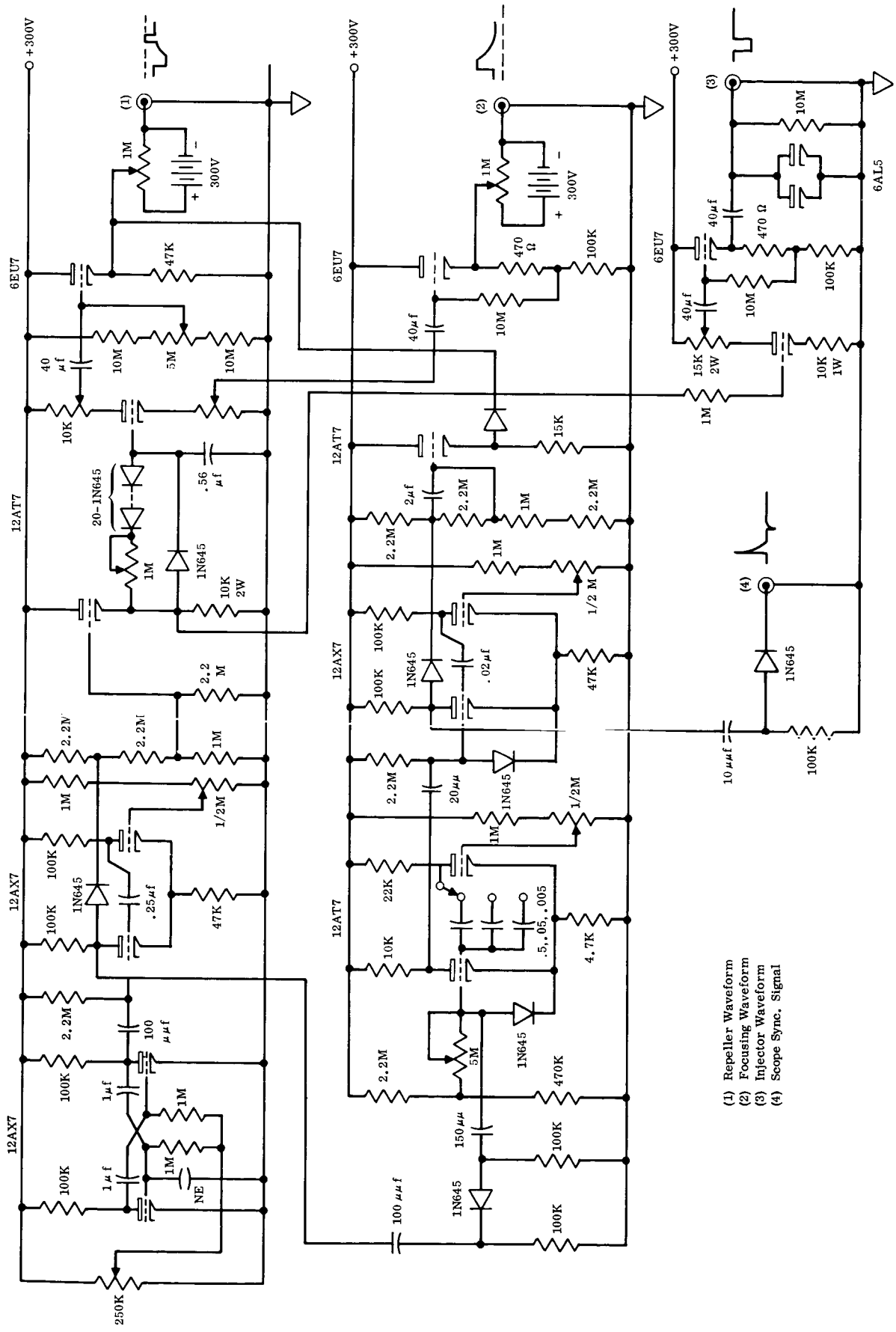

Fig. 12 Waveform Generator

the following manner. As the pulse rises and remains at its maximum, the lower 1N645 diode provides a low-resistance path for charging the .56 μf capacitor. When the cathode potential returns to its quiescent level, the capacitor is constrained to discharge through the 20 1N645 diodes and the 1 meg pot; but as the voltage is decreased, the nonlinear characteristics of the diodes increase the discharge resistance. The resultant wave shape followed, with 20 diodes in series, is very close to a hyperbola in time. Figure 13 shows the effect of varying the number of diodes.

The second half of the 12AT7 has a plate and a cathode resistor of 10K, which yields a plate and cathode gain of:

$$G_p = \frac{-\mu R_L}{\left[r_p + R_L + (1 + \mu) R_K\right]} \cong - \frac{\mu \quad R_L}{(1 + \mu) \quad R_K} \cong - 1 \cdot$$

$$G_K = \frac{+\mu R_K}{\left[r_p + R_L + (1 + \mu) R_K\right]} \cong + \frac{\mu \quad R_K}{(1 + \mu) \quad R_K} \cong + 1$$

Consequently, the plate and cathode signals are equal but out of phase; tube nonlinearities are also reduced because of the large amount of feedback. This stage feeds two cathode followers that have provision for adjusting the dc level of the output pulses.

Finally, to produce a delayed pulse, two Schmitt trigger circuits are placed in series with the initial trigger circuit. Each circuit is actuated by the negative pulse produced by the preceding (positive) gate signal going to zero. The intermediate trigger circuit has a variable pulse duration; fine adjustment is by means of the 5 megohm potentiometer and coarse adjustment is by means of switching in different capacitors. The final 10 msec pulse is fed out through a cathode follower that

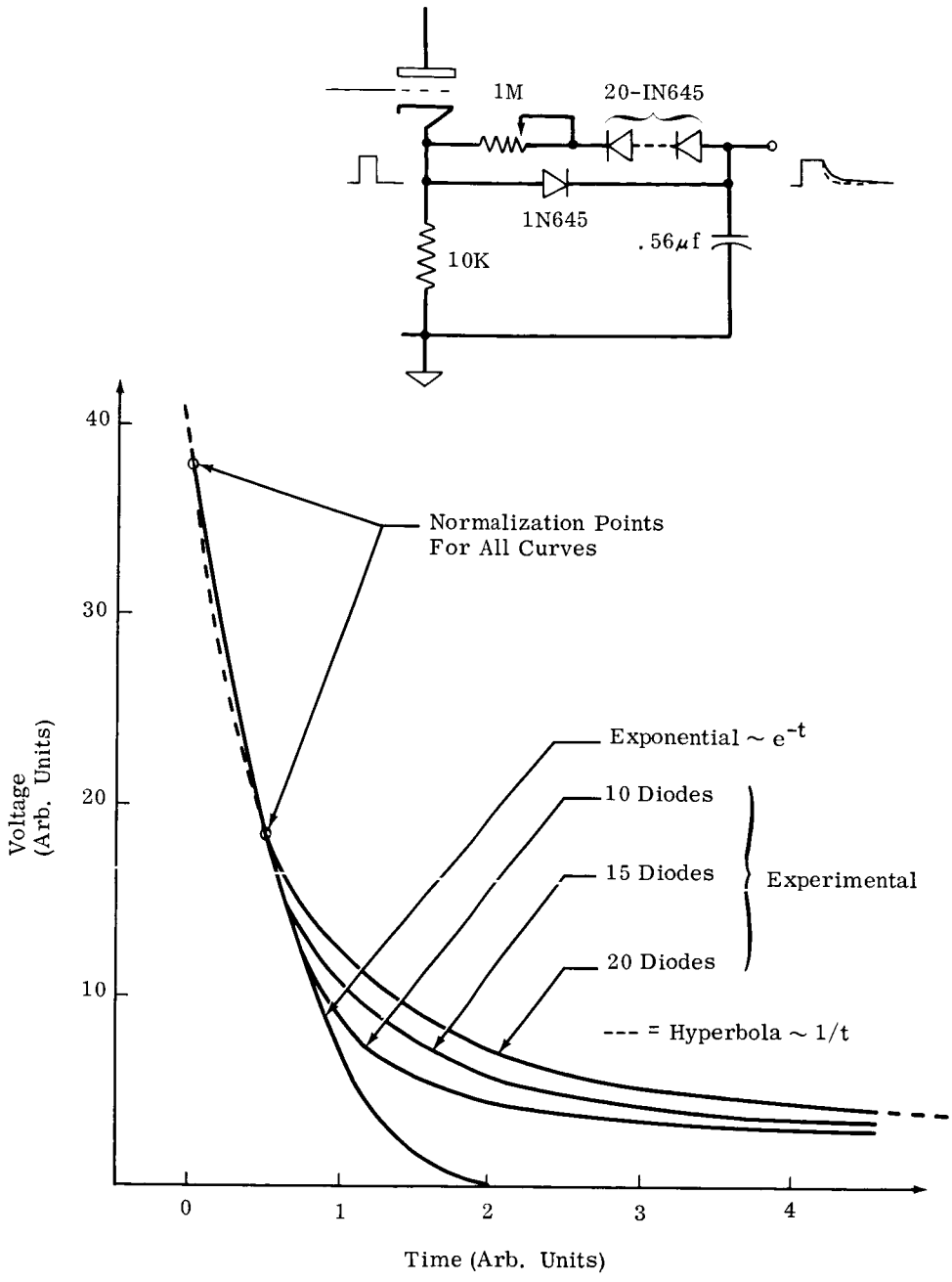

Fig. 13 Pulse Decay Dependence on Diode Number

has a diode to couple the signal into the repelling electrode waveform. This means that both repelling electrodes will receive the extraction signal. Consequently, only those particles that are heading toward the detector, during extraction will be detected and, on the average, one half of the charged particles will be lost.

3. High Voltage Amplification

The waveforms generated by the circuit described in Section IV.C2 are of low voltage, typically only 20 volts high. Unfortunately, the experimental system requires signal magnitudes in the kilovolt domain, and we have found that the high voltage triode, 6BK4, is convenient for such high voltage amplification. This tube has an amplification factor of 2,000, a voltage rating of 25kv, and a maximum plate dissipation of 25 watts. Transient response is determined by the output capacitance (tube and wiring) in parallel with the load resistance used; a load resistor of 20 meg is typical, while tube plus wiring capacitance is less than 10 $\mu\mu$f, thus:

$$t_R \approx RC \approx (2 \times 10^7)(10^{-11}) = .2 \times 10^{-3} = .2 \text{ msec} \quad .$$

This rise time is adequately fast for our purposes, but faster rise times are possible with smaller load resistors and using tubes in series for the proper over-all gain.

Caution must be exercised to keep the grid-to-cathode voltage negative for all input signal excursions, and this is why the waveforms described in Section IV.C2 are either adjusted negative with batteries, or "clamped" negative with diodes. Fig. 10 shows a block diagram of the experimental system, in which the A_1, A_2, A_3 are 6BK4 tube circuits, whose grids receive the low voltage waveforms. The B^+ supplies for these tubes are individual Plastic Capacitor Co. dc power supplies

(20 kv max @ 5 ma., 1 percent ripple) adjusted by 110 VAC variacs. B^- supplies are used to adjust the quiescent dc level of the final outputs, as shown in Figs. 14 and 15, which give the details of the H.V. circuit. The output cathode followers are used to achieve the proper dc level and to provide relatively very low (4.5k Ω) output impedance in the event that any current is drawn on the electrode. Individual B^+ supplies are needed because, with a power supply output impedance of ~1 meg, one tube drawing current would drop the B^+ on the other tubes using the same B^+ supply. Fig. 16 shows the plate curves for a 6KB4, along with a 10 meg "load line."

Because of the high voltage hazard in the vicinity of this circuit, the chassis (including B^+, B^-, and tube circuits) was enclosed in a lucite box with feed-thrus for the output voltages. X-rays must also be shielded, with proper placement of steel sheets (as indicated by a "survey"). The variacs were placed externally for ease of adjusting the dc voltages.

4. Detector Electronics

The charge detector is composed of a 1-inch-long, 1/4-inch-inside diameter, brass cylinder which is electrostatically shielded by an outer dural cylinder. The capacitance of this system, including the associated grid capacitance of the pre-amp input is about 10 μμf. A charged particle passing through this detection cylinder will induce an image charge on the cylinder, charging the cylinder-shield capacitance to a voltage given by charge divided by detector capacitance. The function of the pre-amp is to provide a very high input impedance to this capacitance and to isolate the detector from the remotely located post-amplifier.

The pre-amp employs a low noise, low microphonic, 6EU7 triode in a dc coupled cathode follower. The input impedance of such a stage is derived in Appendix II. This derivation yields an input impedance of 1,030 Meg for the system circuit

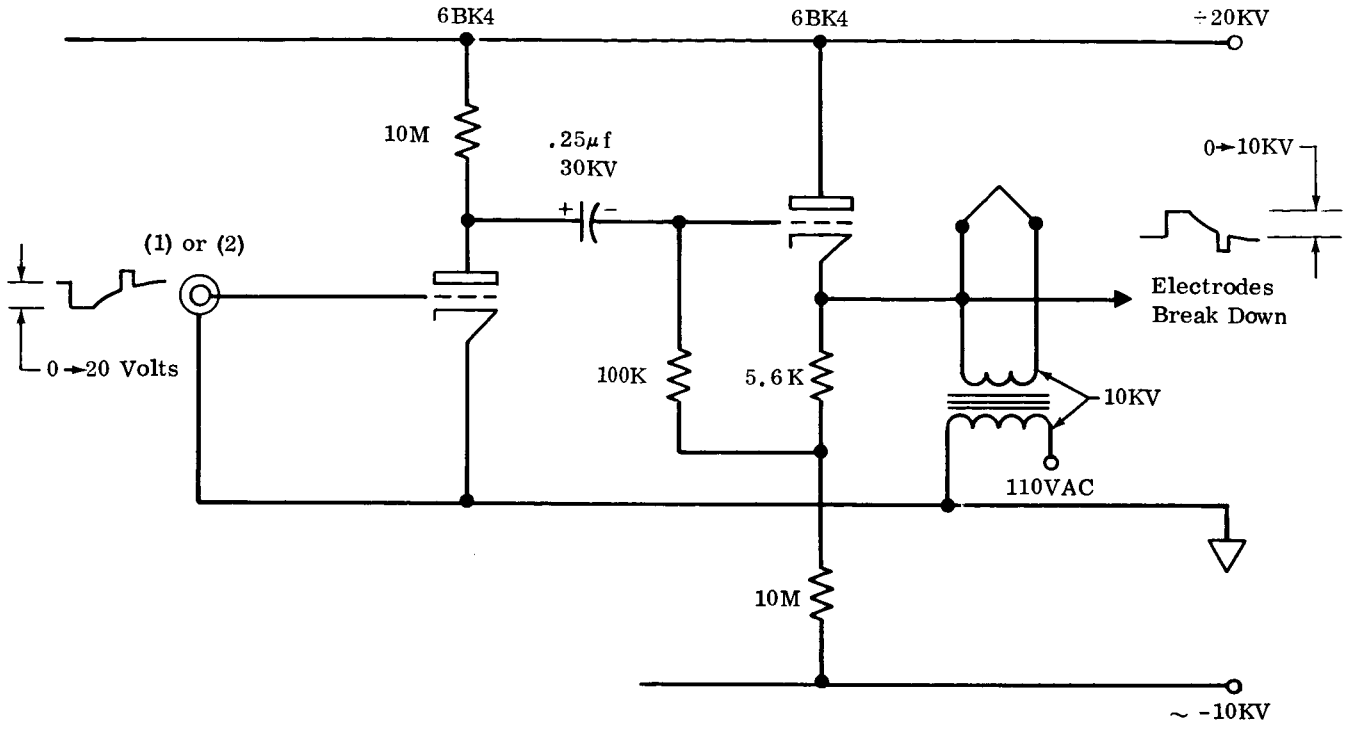

Fig. 14 Repeller H. V. Amplifier

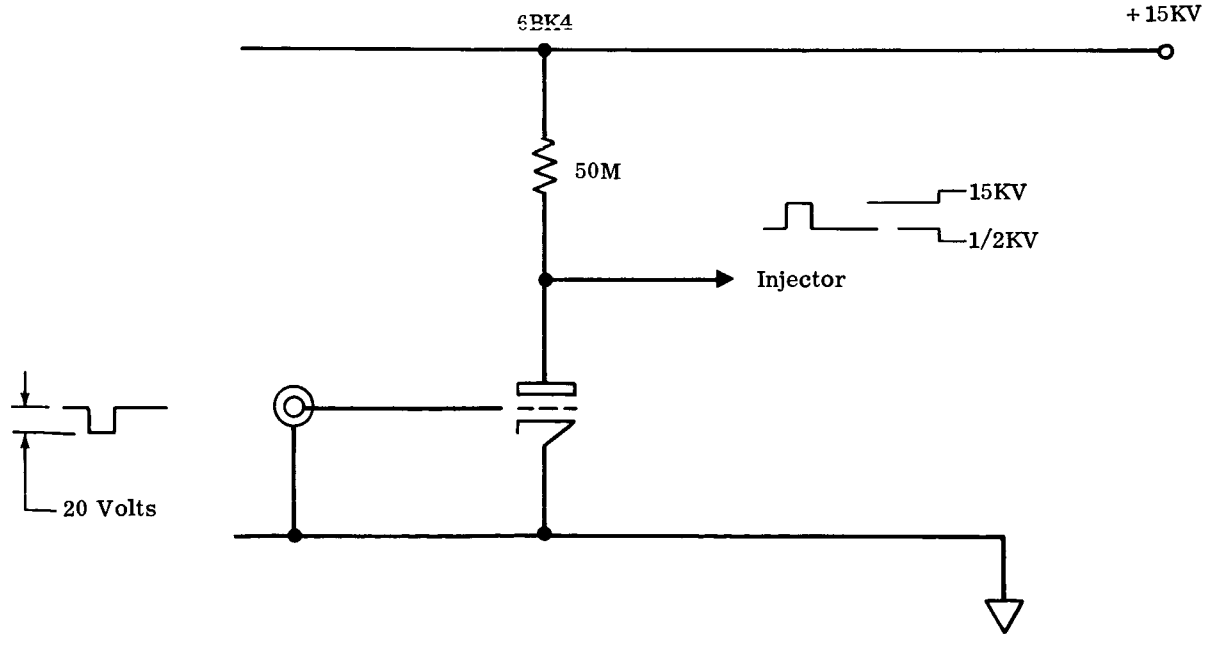

Fig. 15 Injector H. V. Amplifier

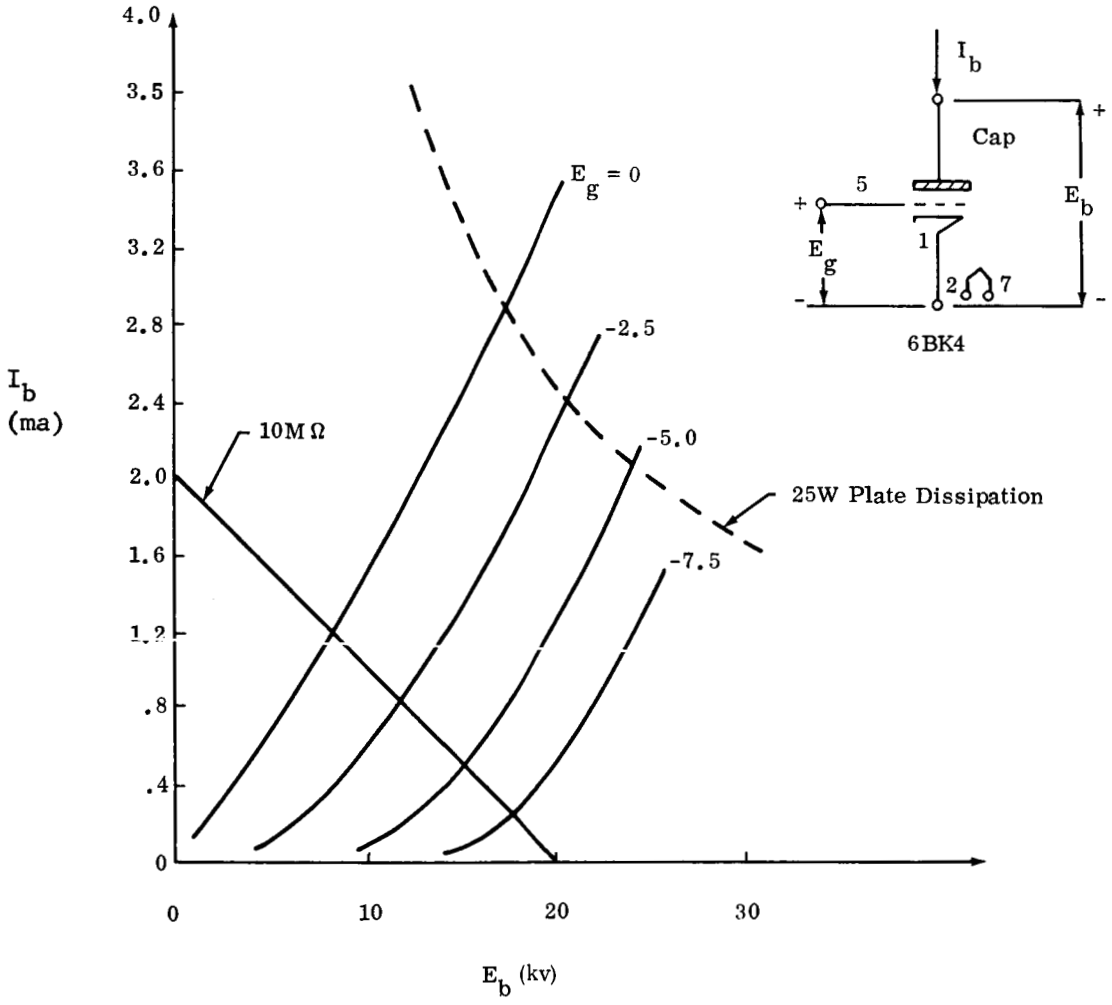

Fig. 16 Typical Plate Curves for 6BK4

parameters of Fig. 17. Consequently, the detector time constant is 10 μμf times 1,030 Meg, or 10 msec; since pulses of about 1 msec are anticipated, this low frequency response is adequate to measure detector pulse height.

It was found necessary to ground the triode plates and to supply a B^- voltage for the cathode circuits. This provides a negative dc level at the detection cylinder, which will avoid repelling the positively charged particles as they arrive at the detector cylinder.

D. The Modified Injector

Experimental work conducted with the injector outlined in Section IIA of this report proved that the basic concept of injection by entraining particles in an air stream flowing through a small tube is feasible. With the development of a pulsed system, however, it was felt that better collimation and higher feed rates would be highly desirable, and perhaps mandatory, especially during initial optimization studies. The reason for this is that the system requires relatively good alignment with respect to the focusing direction of the lenses, and that the injector must fire its particles in during the 200 msec time period when it is "on." With this in mind, we investigated the pattern of particle trajectories within the differentially pumped chamber (see Fig. 1) before the collimating aperture; we found that the particles are "sprayed" out into this region in a cone of about 40° (full angle) and that this angle is very sensitive to the gas pressure in the dust chamber. Low pressures tended to reduce the cone angle, while higher pressures caused the cone angle to "blow up." These effects can be attributed to the formation of a shock wave as the gas emerges from the tube into the low pressure (60μ) region. Since we can benefit only from those particles that enter the charging chamber within a cone of about 1°, a large cone angle in front of the collimating aperture implies a low yield in particles that can be suitably

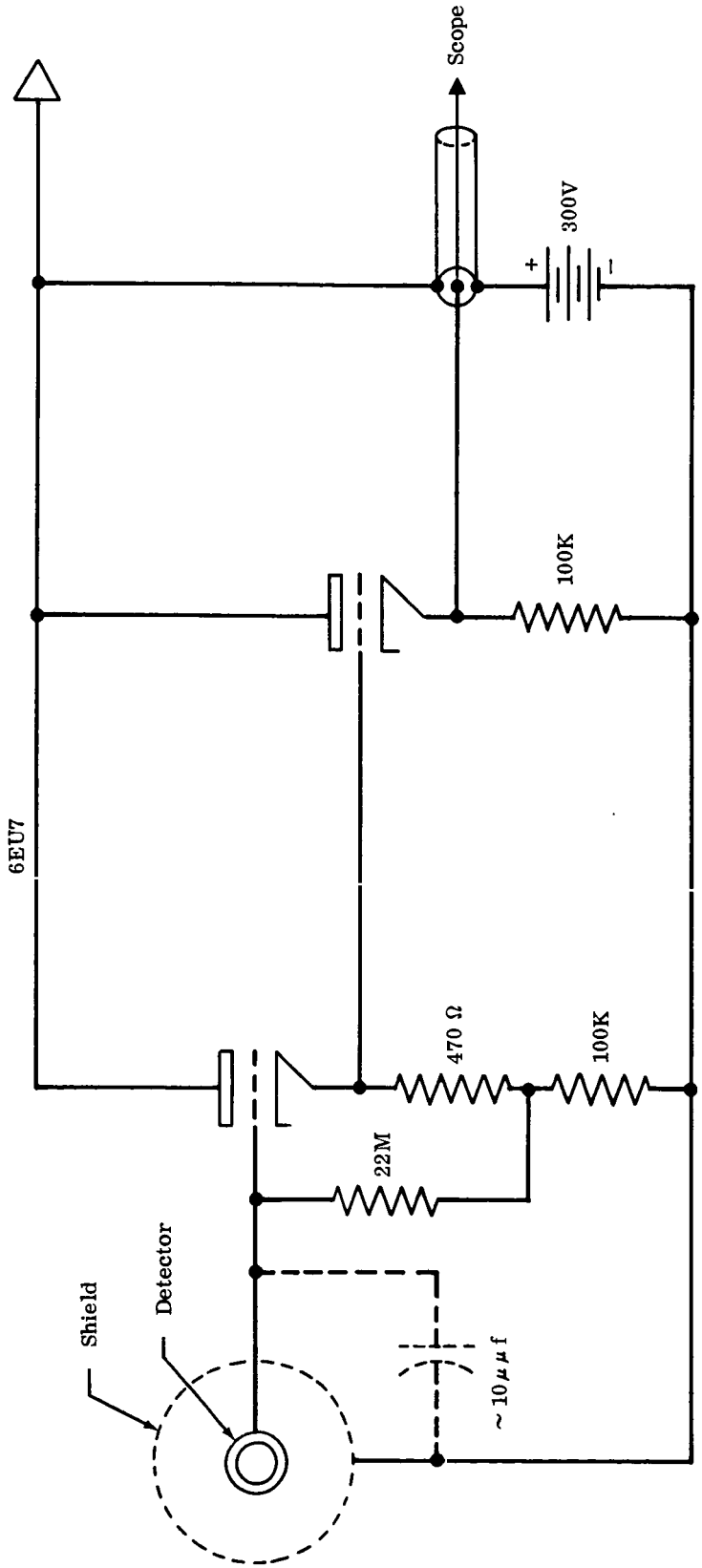

Fig. 17 Detector Amplifier

injected. Unfortunately, as we went to lower pressures to reduce the cone angle, the total number of particles flowing from the dust chamber through the tube diminished to such an extent that the effective injection rate decreased also. It was apparent that a new injector design was needed, if higher feed rates were to be made available for the pulsed charging line confinement technique.

Considerations motivating the design of the modified injector are as follows: To maintain a high particle input into the capillary from the dust chamber, the dust chamber gas density must be relatively high, the pressure required being of the order of one atmosphere. On the other hand, a lower pressure gradient across the capillary leads to a smaller cone angle and therefore, a higher density of particles in the 1° acceptance cone. A pressure gradient of about 1/2 an atmosphere was found to yield a cone angle of only several degrees; but if the differentially pumped chamber had a pressure of 1/2 an atmosphere, the air leakage into the experimental system's vacuum would be intolerable. This lead to the concept of using several differentially pumped chambers in series, each chamber having its own roughing pump.

The experimental injector designed to test this concept is shown in Fig. 18. The original dust chamber and 2-inch-long capillary is retained, but the capillary exits into a chamber whose pressure is adjusted by a needle valve. The needle valve is supplied with dried air at one atmosphere. As the particles leave the capillary, they travel about 1/32-inch through this chamber and then pass through a 0.010-inch hole into a second region that has a pressure of about 1,000 microns. At this pressure, the drag on the particles is small, and no appreciable decrease in velocity should take place in this chamber before they enter, again through a 0.010-inch hole, the third chamber, where pressure is about 60μ. A final aperture of 1/32-inch diameter collimates the particle stream to less than half a degree cone angle, and restricts the gas leakage into the main vacuum system.

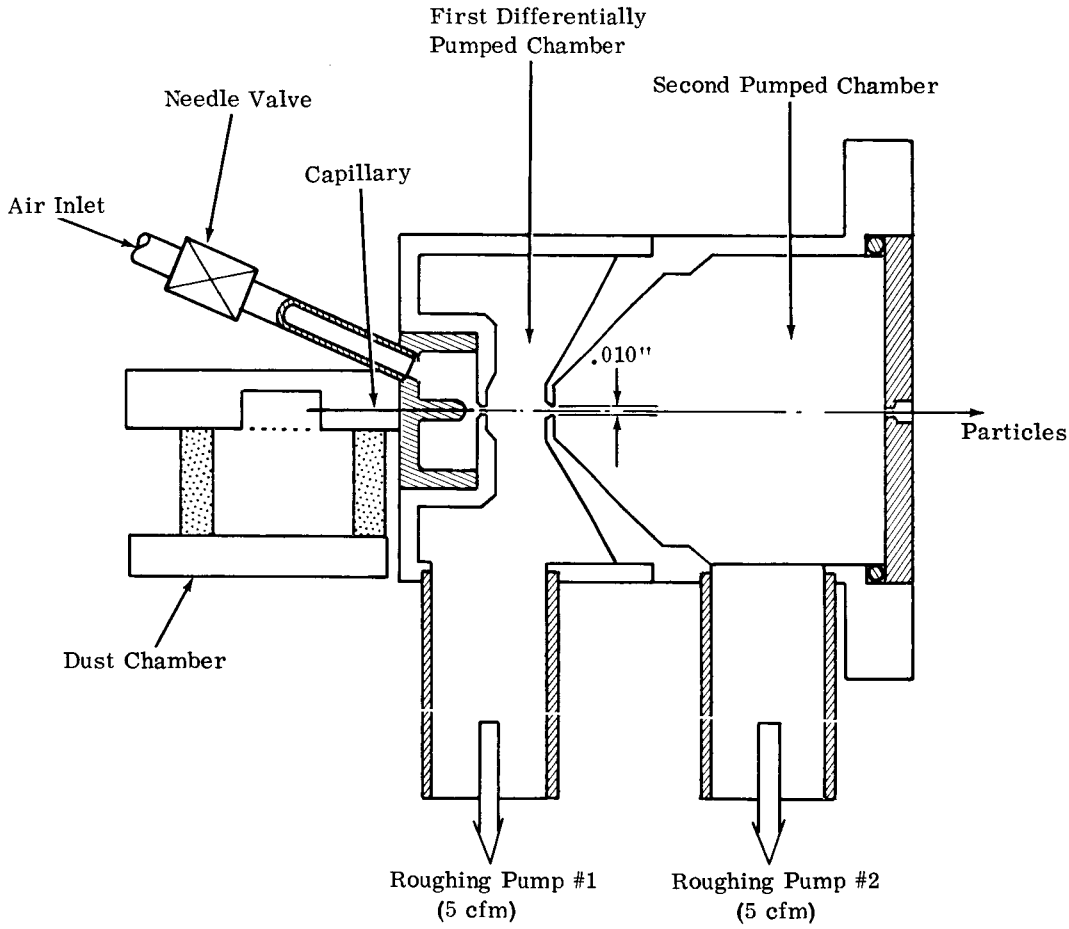

Fig. 18 Modified Injector Assembly

Our research showed that feed rates several orders of magnitude higher than those attainable with the original injector design are achieved with this design, provided care is taken to adjust the needle valve described above. From a theoretical point of view, the functioning of this adjustment may lie in its effect on the details of shock wave formation in the vicinity of the first .010-inch aperture. Since it should be expected that the particles' acceleration takes place mainly in the capillary, we felt that particle velocities obtained with this injector would be close to those obtained with the original injector. Actually it was later found that the velocities obtained were at least twice as high as those obtained previously. With the old injector we had found that a bucking potential of 2 kv was adequate for stopping particles after a single pass through a 1 ma proton beam. With the new injector, voltages of at least 6 kv were required with a 3 ma proton beam. The stopping potential for first pass operation is proportional to the third power of the injection velocity (second power due to kinetic energy and first power due to traversal time) and inversely proportional to the beam current.

Within the capabilities of our existing pumping system we were unable to maintain this bucking operation reliably because of concomitant intermittent electrical discharge of the electrodes through the ambient partially ionized gaseous environment. At the same time we are not able to operate reliably for long periods of time at proton beam currents in excess of 3 ma. Since our containment system requires that the particle be stopped and turned back at the end of each pass, the use of this injector was deferred, and the old injector was fitted to the pulsed line confinement charging system.

E. Experimental Procedure

The present line confinement system requires exact phasing between the operations of injection, charging, extraction, and final charge detection. This necessarily involves a great amount of experimental "tuning" of the system. Precautions common to this and previous confinement and charging systems that we have investigated include particle treatment and ion beam control. Particle treatment, prior to "charging" the dust chamber, is discussed in Section II of this report, and the operation of the basic ion beam apparatus is discussed in Ref. 1. Ion beam diameter, along with the alignment of the ion beam with the axis of the charging chamber, is adjusted and monitored with the help of an insertable quartz beam viewer located directly above the charging chamber, as seen in Fig. 6. At the same time, the faraday cup current reading is used to set the current of the ion beam. The latter two operations ensure that the proper ion beam conditions, as prescribed by theory for the particular experiment, are maintained in the charging region. After these preliminary adjustments are made, certain experimental procedures specific to the method of charging by line confinement must be followed.

This procedure is initiated by using an oscilloscope to observe the waveforms being produced by the "waveform generator" of Fig. 12. Failure to observe an output for the injector, output No. 3, means that the initial Schmitt trigger circuit must be adjusted to trigger on the multivibrator output; this adjustment is made by tuning the 1/2-megohm potentiometer for a dependable gate pulse output (caution must be exercised to keep the triggering threshold above the point where self-sustained oscillations occur). The injector pulse is used at a full amplitude of 20 volts, and is automatically "clamped" negative by the diode in the output circuit. Thus, this waveform may be connected directly to the injector high voltage amplifier (Fig. 15). With a lead from the output of the high voltage amplifier to the lower plate of

the dust chamber, the B^+ on the amplifier is adjusted, by varying the power supply variac, to a value of about 15 kv. At this point, a succession of particle "bursts" will be observed in the dust chamber at a repetition rate given by the period of the multivibrator setting, which is adjustable from 1 sec to 4 sec. Voltages are not critical, since the injector is either "on" or "off".

The waveform of the repelling voltage, at output No. 1, is observed on the oscilloscope next. Its decay rate is adjusted by the 1-Meg potentiometer in the pulse shaping diode network, described in Section IV.C, to conform to the theoretically predicted decay rate (see Appendix I). Output amplitude is tentatively set at about 1 volt and the waveform is carefully adjusted to remain below a level of -1 volt; this allows operation in the negative grid-voltage region of the input tube in the repeller high voltage amplifier. The waveform of the focusing voltage output No. 2, is now observed on the oscilloscope and will automatically have the same decay rate as the repelling waveform, since they are generated by the same pulse shaping network. The pulse amplitude is again tentatively set at about 1 volt and adjusted to remain below a level of -1 volt. Connecting these two outputs to their respective high voltage amplifiers, completes the adjustment of the (low voltage) repelling and focusing waveforms.

As seen in Fig. 11, the extraction pulse appears on the repelling waveform, and is generated by two Schmitt trigger circuits in series. Both of these trigger circuits are now adjusted to a proper "firing level" by their respective 1/2 Meg potentiometers, and the first trigger circuit has its pulse duration set at the desired "extraction time." Changing the dc level on the cathode follower that couples the 10 msec extraction pulse into the repelling voltage waveform, will adjust the amplitude of the extraction pulse as it appears on the repeller waveform; this pulse is adjusted to produce a zero level during extraction, to ensure a sufficient

drop in potential on the repelling electrode. Finally, the differentiated form of the extraction pulse at output No. 4, is fed into the "sync." input on the oscilloscope used for detection; in this way, a scope sweep is initiated as soon as charged particles are allowed to leave the charging region and travel toward the detection cylinder. The detection scope is operated with a sweep rate of about 1 msec/cm. With these adjustments of the injector, confinement, and extraction waveforms, the phasing and exact waveforms for the pulsed system are determined; the high voltage amplifiers must be considered next.

The injector high voltage amplifier mentioned above is activated by simply turning up its B^+ to about 15 kv. The repelling and focusing high voltage amplifiers, on the other hand, require more careful consideration. This is because, although the shape of the waveforms is determined by the (low voltage) waveform generator, the initial and final dc levels supplied to the electrodes are not arbitrary, but determine the initial and final focusing properties of the confinement lenses. Consequently, the variacs feeding the power supplies for the (focusing and repelling) B^+ and B^- voltages are adjusted, in conjunction with the amplitude of the input waveforms, for the proper initial and final dc levels. The initial repelling voltage is determined from the first pass stopping potential, and is typically around 2kv. The final repelling voltage is obtained theoretically from the ratio of final to initial electrode voltage, which has been derived on the basis of maintaining good focusing during charge accumulation (see Appendix I). This ratio is also valid for the focusing electrodes. The initial value of the focusing voltage, however, cannot be reliably calculated without an extensive program of analysis, and is most easily determined by experiment. The final high voltage waveforms are observed on an oscilloscope, operated in a dc mode, through a 1,000:1 attenuator probe. Since no probe with an input impedance as high as the 1,000 Meg Ω

required is commercially available, we designed and constructed the high voltage probe described in Section IIC of the Appendix.

The final phase of the experimental procedure is to verify that the detector pre-amp is in an operating state. This is most easily done by temporarily injecting a square wave on the detection cylinder and observing the resultant pre-amp output on an oscilloscope. A continuous check on the pre-amp is possible if the oscilloscope is dc coupled to the pre-amp and is operated in a dc mode; the dc level of the output cathode follower then serves as a check on the "operating point" of the two detector triodes. Pre-amp power is supplied by batteries for minimum noise operation, and we found that shielding of these batteries was essential in order to avoid 60~ pickup from adjacent electrical equipment. Noise pickup on the detector, directly attributable to the presence of the ion beam passing through the charging chamber, was greatly reduced by: (1) installing a small magnet under the lens region neighboring the detector; or (2) running the detection cylinder at a negative dc level. This information indicates that electron currents initiated by the ion beam are the primary source of "beam noise" at the detector.

In conclusion, the line confinement system requires a most detailed experimental procedure to adjust the experimental parameters properly. Most of these parameters may be calculated from the theory outlined in Appendix I. Experimental values must be found for the initial repelling and focusing voltages; the repelling voltage has been found to be about 2 kv., while the focusing voltage is still in question and requires additional study. Noise associated with the detector has been reduced to the point where it is no longer a problem for detection after multiple ion beam traversals, but requires further reduction for detection of particles which have executed only a small number of ion beam traversals.

V. CONCLUSIONS AND PLANS FOR FUTURE WORK

A significant achievement during the period of work covered by this report has been the experimental verification that charge is retained on the particles at least at temperatures up to 1400°K. Based on our experimental data, calculations were made to establish a lower limit for the amount of charge actually retained after the first pass of particles through proton beams of known intensities. The results of these calculations agreed with the results of previous theoretical charge accumulation calculations performed on the basis of zero net charge leakage. Since protons may be expected to leak almost instantaneously from micron size particles at the temperatures attained during first-pass operations, these results provided confirmation of our previous contention that leaking protons would carry electrons off with them in virtually a one-to-one correspondence, even in the presence of considerable field strengths (10^7 volt/cm) and high temperature (1400°K).

Several modifications were made to the charging system during the period of the contract. These redesigns were on the charging chamber, the injector, and the detector system.

In present work, we plan to perform detailed studies with the redesigned apparatus. These studies will be both experimental and analytical. The initial plan is to measure particle injection velocities obtained with the new injector as a function of input pressure and particle size. In support of and in extension of these studies, theoretical fluid mechanics studies of the effect of these parameters in the new injector will be pursued concurrently, applied to a simplified assumed model.

At the same time, the vacuum system will be improved to allow use of the higher bucking potentials required by the new injector system.

After the new injector has been studied (and modified, if necessary) and the parametric dependence of injection velocities determined, the device will be placed in operation on the new charging system. A series of single-pass runs will then be made with the new injector. The desired results here are q/m measurements as a function of beam intensity, input pressure, and particle size (and therefore implicitly as a function of injection velocity). Concurrently with this and the above-mentioned work, a detailed mathematical analysis will be conducted on the new confinement system, the object here being to see how the focusing can be optimized. In this analysis the electrostatic equations will be programmed for the IBM 7094 computer and parameter studies made. After making such refinements on the system as may be deemed advisable on the basis of this very detailed analysis, we will work toward resumption of the multiple pass studies.

APPENDIX I

MATHEMATICAL ANALYSIS OF PULSED CHARGING SYSTEM

A. Velocity and Charge Dependence of Electrostatic Focusing

If we consider a system of electrodes possessing axial symmetry, the potential distribution within this system has no azimuthal dependence, but depends on radial and axial position only:

$$\varphi = \varphi (r, z)$$

where

r = radius from axis of symmetry

z = distance along axis

This potential distribution gives rise to radial and axial forces on a charged particle given by:

$$F_r = - q\left(\frac{\partial \varphi}{\partial r}\right) = m\left(\frac{d^2 r}{dt^2}\right)$$

$$F_z = - q\left(\frac{\partial \varphi}{\partial z}\right) = m\left(\frac{d^2 z}{dt^2}\right)$$

These are the Newtonian equations of motion of the charged particle in the field region.

It is more convenient to reformulate the problem in terms of r and z, eliminating the time parameter. This is accomplished by rewriting the differential time operator as:

$$\frac{d}{dt} = \frac{dz}{dt} \cdot \frac{d}{dz}$$

$$\frac{d^2}{dt^2} = \frac{dz}{dt} \cdot \frac{d}{dz}\left(\frac{dz}{dt} \cdot \frac{d}{dz}\right) = \frac{d}{dt}\left(\frac{dz}{dt}\right)\frac{d}{dz} + \left(\frac{dz}{dt}\right)^2 \frac{d^2}{dz^2}$$

$$= \frac{d^2z}{dt^2} \cdot \frac{d}{dz} + \left(\frac{dz}{dt}\right)^2 \cdot \frac{d^2}{dz^2}$$

The radial force equation now becomes:

$$-\frac{q}{m}\left(\frac{\partial \varphi}{\partial \varphi}\right)\frac{dr}{dz} + \left(\frac{dz}{dt}\right)^2 \frac{d^2r}{dz^2} = -\frac{q}{m}\left(\frac{\partial \varphi}{\partial r}\right)$$

where the axial force equation has been used to evaluate (d^2z/dt^2), the axial acceleration. Solving for d^2r/dz^2 yields:

$$\frac{d^2r}{dz^2} = -\frac{q/m}{\left(\frac{dz}{dt}\right)^2}\left\{\left(\frac{\partial \varphi}{\partial r}\right) - \left(\frac{\partial r}{\partial z}\right)\left(\frac{\partial \varphi}{\partial z}\right)\right\}.$$

Thus far, the analysis has been rigorous; we now make the "small angle" approximation, where the axial velocity, dz/dt, will be taken to be the magnitude of the velocity vector. Thus, we have:

$$\left(\frac{dz}{dt}\right)^2 \cong v^2 = \left(v_0^2 - \frac{2q\varphi}{m}\right) \cdot \left(\frac{dr}{dt}\right) \ll \left(\frac{dz}{dt}\right),$$

defining v_0 as the particle speed at the entrance to the field region, where the potential is zero. This approximation reduces the differential equation governing the particle trajectory to the following form:

$$\frac{d^2r}{dz^2} = -\frac{1}{(m/q\, v_0^2 - 2\varphi)}\left\{\left(\frac{\partial \varphi}{\partial r}\right) - \left(\frac{\partial r}{\partial z}\right)\left(\frac{\partial \varphi}{\partial z}\right)\right\}.$$

In the general case, both the charge, q, and the entrance velocity, v_0, are functions of time:*

$$q = q(t)$$

$$v_0 = v_0(t)$$

We seek to modulate φ in such a way that the focusing characteristics of the system will not change with time. Assume that the electrode potentials are "modulated" in time by a function $\alpha(t)$, in the manner $\varphi(r, z, t) = \alpha(t)\,\varphi_0(r, z)$. This means that the functional form of φ is maintained, but its amplitude (at all field regions) undergoes an expansion or contraction given by the modulating function, $\alpha(t)$. $\varphi_0(r, z)$ is the spatial dependence of the field, which, if $\alpha(t)$ is normalized to $\alpha(t = 0) = 1$, is the electrostatic field at t = 0. If this potential is substituted into the trajectory equation above, we have:

$$\frac{d^2r}{dz^2} = -\frac{\alpha(t)}{\left(\frac{m \cdot v_0^2(t)}{q(t)} - 2\alpha(t)\varphi_0\right)}\left\{\left(\frac{\partial\varphi_0}{\partial r}\right) - \left(\frac{\partial r}{\partial z}\right)\left(\frac{\partial\varphi_0}{\partial z}\right)\right\}$$

$$= -\frac{1}{\left(\frac{m \cdot v_0^2(t)}{q(t)\alpha(t)} - 2\varphi_0\right)}\left\{\left(\frac{\partial\varphi_0}{\partial r}\right) - \left(\frac{\partial r}{\partial z}\right)\left(\frac{\partial\varphi_0}{\partial z}\right)\right\}.$$

Notice that the first term of the denominator is the only part of the differential equation that has a time dependence. Clearly, if this term is a "constant of the motion," the trajectory will be described by the same differential equation for all q(t) and $v_0(t)$, and the focal lengths will remain the same for all time. This means that the field must be modulated by a function:

- - - - - - -

*These times are very long compared to the propagation time of light in the system - therefore, the above electrostatic equation is valid for this "quasi-static" system.

$$\alpha(t) = (\text{const.}) \frac{mv_0^2(t)}{q(t)}$$

B. Velocity Build-up During Charging

When a charged particle approaches the positive ion beam from a lens, it slows down, passes through the ion beam, and then accelerates over to the other lens. On each side of the beam it travels through a potential, Φ_B, which is due to the presence of the positive charge in the ion beam. When the particle accelerates away from the beam through Φ_B, however, it has more charge on it than when it decelerates coming toward the beam. Consequently, the velocity of the particle as it enters the second lens, v_2, is greater than the velocity, v_1, which it had when leaving the first lens, by an amount obtainable from the relationship

$$\frac{1}{2} m(v_2^2 - v_1^2) = \Delta Q \Phi_B \quad ,$$

where ΔQ is the increment of charge acquired in the beam. Since v_1 and v_2 are nearly equal, we may use the approximation:

$$\frac{1}{2} m(v_2 - v_1)(v_2 + v_1) \cong \frac{1}{2} m(dv)(2v) = \Phi_B dQ \quad ,$$

or

$$d(\frac{1}{2} mv^2) = \Phi_B dQ \quad .$$

Integration yields

$$\int_{v=V_0}^{v=v_0(t)} d(\frac{1}{2} mv^2) = \Phi_B \int_{Q=0}^{Q=q(t)} dQ$$

$$\frac{1}{2} m v_0^2(t) = \frac{1}{2} m V_0^2 + \varphi_B q(t)$$

$$v_0^2(t) = V_0^2 + \frac{2\varphi_B}{m} q(t)$$

In this expression, V_0 is the injection velocity at t = 0, when q(t) = 0.

C. Electrode Voltage Modulation Requirements

In Part A we have derived the electrode potential time dependence required to maintain good focusing, when both the charge and the entrance velocity are time-dependent. In Part B we showed that the entrance velocity is directly related to the charge acquired by the particle. Consequently, the modulation function, $\alpha(t)$, may be written as a function of charge alone:

$$\alpha(t) = (\text{const.}) \left\{ \frac{1 + \frac{2\varphi_B}{mV_0^2} q(t)}{q(t)} \right\} .$$

Notice that the second term in the numerator is the ratio of the kinetic energy acquired by the particle, due to the beam potential, to the initial kinetic energy of the particle at injection.

1. Analysis for Charge Accumulation Small Compared to Full Charge

At the start of charging, q(t) is a small number, and the second term of the numerator is very small compared to unity. This leads to a voltage modulation that is initially inversely proportional to the charge:

$$\alpha(t) \cong (\text{const.}) \frac{1}{q(t)} \quad ; \quad \varphi_B q(t) \ll \frac{1}{2} m V_0^2$$

At the same time, initial charge acquisition is linear, since (see Ref. 1, p. 11):

$$q(t) = 4\pi\epsilon_0 R_p V_B \left(1 - e^{-\omega' t}\right)$$

$$= 4\pi\epsilon_0 R_p V_B \left[1 - \left(1 - \omega' t + \frac{(\omega' t)^2}{2} + \ldots\right)\right]$$

$$\cong 4\pi\epsilon_0 R_p V_B \omega' t = (\text{const.})t \quad .$$

In this equation we have:

1) assumed that charge acquisition is continuous, rather than in discrete "steps" as it crosses the beam, and

2) corrected the exponential coefficient, ω, to a new value, ω', that accounts for the time spent by the particle outside the beam.

Under these assumptions, the required initial voltage modulation is given by:

$$\alpha(t) = \frac{(\text{const.})}{t} \quad .$$

The constant in this equation is most accurately, determined experimentally; but an estimate of its value can be obtained by the following line of reasoning. "Time" may be conceived to start just as the particle receives its first reflection and focusing. At this moment, the charge of the particle, q_0, is due to the initial pass through the beam. Thus, we have

$$\alpha(t = 0) = (\text{const.})\frac{1}{q_0} \equiv \frac{\beta}{q_0}$$

The initial charge, q_0, is due to a sphere of πR_p^2 cross section in a "charge flux" of $i/\pi R_B^2$ for $\frac{2R_B}{V_0}$ seconds. This gives:

$$q_0 = i\left(\frac{R_p}{R_B}\right)^2 \frac{2R_B}{V_0} \text{ coulombs} ,$$

where

R_p = particle radius, m

R_B = beam radius, m

i = beam current, amps.

V_0 = injection velocity, m/sec

If $\alpha(t = 0)$ is now normalized to one, $\beta = q_0$, and we have:

$$\alpha(t) = \frac{\beta}{q(t)} = \frac{q_0}{4\pi\varepsilon_0 R_p V_B \omega'} \frac{1}{t}$$

$$\alpha(t) = \left(\frac{i(R_p/R_B)}{2\pi\varepsilon_0 V_0 V_B \omega'}\right) \cdot \frac{1}{t} .$$

This is the required constant, subject to the functional dependence of ω' on system parameters (derived in Appendix I E).

2. Analysis for Full Charging

At later times, both the charge acquired and the second term in the numerator of the modulation function lead to relatively large departures from a hyperbolic waveform. These effects become noticeable in the neighborhood of 25 percent to 30 percent of the maximum theoretical saturation charge. The situation is greatly improved by using a waveform of the form:

$$\alpha(t) = A + \frac{B}{t} ,$$

where B is the constant evaluated above, and A is a new "saturation" constant that is equal to the modulation function evaluated with the saturation charge. At the start of charging, the second term predominates; as saturation is approached, the leading term is most important.

Consider the modulation function:

$$\alpha(t) = (\text{const.}) \left\{ \frac{1 + \frac{2\varphi_B}{mV_0^2} q(t)}{q(t)} \right\}$$

$$= q_0 \left\{ \frac{1 + \frac{2\varphi_B}{mV_0^2} q(t)}{q(t)} \right\},$$

which has been normalized to unity at $t = 0$, where $\varphi_B q_0 \ll \frac{1}{2} mV_0^2$. At infinite time, this becomes:

$$\alpha(t = \infty) = q_0 \left\{ \frac{1 + \frac{2\varphi_B}{mV_0^2} 4\pi\varepsilon_0 R_p V_B}{\frac{mV_0^2}{4\pi\varepsilon_0 R_p V_B}} \right\}.$$

A simplification of this expression results if we know the stopping potential at $t = 0$, defined as φ_s, since:

$$q_0 \varphi_s = \frac{1}{2} mV_0^2$$

and

$$\alpha(t = \infty) = \left\{ \frac{1 + \left(\frac{\varphi_B}{\varphi_s}\right) \frac{4\pi\varepsilon_0 R_p V_B}{q_0}}{\frac{4\pi\varepsilon_0 R_p V_B}{q_0}} \right\}$$

where we are working with the dimensionless ratio of the saturation charge to the first pass charge. The first pass charge was evaluated on page 69, and the ratio becomes:

$$\frac{q_{max}}{q_0} = \frac{4\pi\epsilon_0 R_p V_B}{i\left(\frac{R_p}{R_B}\right)^2 \frac{2R_B}{V_0}} = \frac{2\pi\epsilon_0 V_0 V_B}{i(R_p/R_B)}$$

With reasonable system parameters, this ratio is about 300, and typical values of φ_B and φ_s are

$$\varphi_B \approx 10 \text{ volts}$$

$$\varphi_s \approx 1500 \text{ volts}$$

Thus, the asymptotic modulation voltage is:

$$\alpha(t = \infty) \cong \left\{\frac{1 + \frac{10}{1500}\ (300)}{300}\right\} = .01$$

Consequently, the proper modulation waveform should be a hyperbola of definite "decay time" with an asymptote at about 1 percent of its starting value.

D. Accelerating Potential Due to Beam Charge

Since the geometry of the beam passing down through the (grounded) vacuum system is very close to simple cylindrical symmetry, we will adopt this geometry for our calculations. Gauss' equation yields a radial electric field, ϵ_r, given by:

$$\vec{\nabla} \cdot \vec{\epsilon} = p/\epsilon_0$$

$$\iint_S \vec{\epsilon} \cdot \vec{ds} = \frac{1}{\epsilon_0} \iiint_V p dV = Q/\epsilon_0$$

$$\epsilon_r (2\pi r \ell) = \frac{Q}{\epsilon_0}$$

$$\epsilon r = - \left[\frac{d\varphi}{dr}\right] = \frac{Q}{2\pi\epsilon_0 \ell r}$$

$$\therefore d\varphi = - \frac{Q}{2\pi\epsilon_0 \ell} \frac{dr}{r}$$

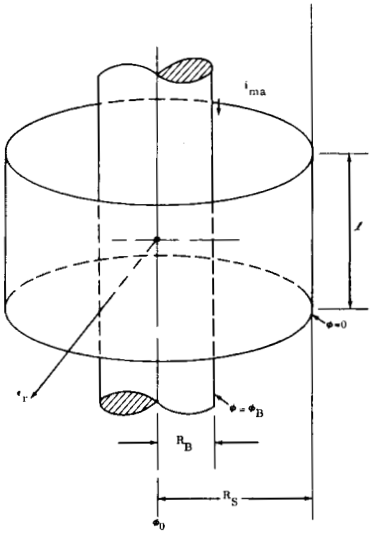

Fig. A1 Geometry for Beam Potential Analysis

Outside the beam, the internal charge, Q, is given by

$$Q = \frac{i}{v} \ell = \frac{\text{coul/sec}}{\text{cm/sec}} \text{ cm} = \text{coul.}$$

$$= \frac{i\ell}{(2eV_B/m)^{1/2}} \begin{cases} e/m = \text{proton charge-to-mass} \\ V_B = \text{beam voltage} \end{cases}$$

$$\int_0^{\varphi_B} d\varphi = \frac{i}{2\pi\epsilon_0 (2eV_B/m)^{1/2}} \int_{r = R_B}^{r = R_s} \frac{dr}{r}$$

$$\varphi_B = 7.51 \; i_{ma} \ln \left[\frac{R_s}{R_B}\right] \text{ volts; when } V_B = 30 \text{ kv}$$

Inside the beam, the charge contained within the surface s is given by:

$$Q(r) = \frac{i\ell}{(2eV_B/m)^{1/2}} \left[\frac{r}{R_B}\right]^2$$

$$\int_{\varphi_0}^{\varphi_B} d\varphi = \frac{-i}{2\pi\epsilon_0 (2eV_B/m)^{1/2}} \int_0^1 \left[\frac{r}{R_B}\right] d\left[\frac{r}{R_B}\right]$$

$$\varphi_0 - \varphi_B = \tfrac{1}{2}\left\{\frac{i}{2\pi\epsilon_0 (2eV_B/m)^{1/2}}\right\} = 3.75\ i_{ma}\ \underline{\text{volts}}$$

Consider a beam radius of R_B = 1/4 in., and a system radius of 3/4 in. and a current of 1 ma:

$$\ell n \left[\frac{R_S}{R_B}\right] = \ell n\ 3 = 1.1 \begin{cases} \varphi_0 - \varphi_B = 3.75\ \underline{\text{volts}} \\ \varphi_B = \dfrac{8.25}{12.00}\ \underline{\text{volts}} \end{cases}$$

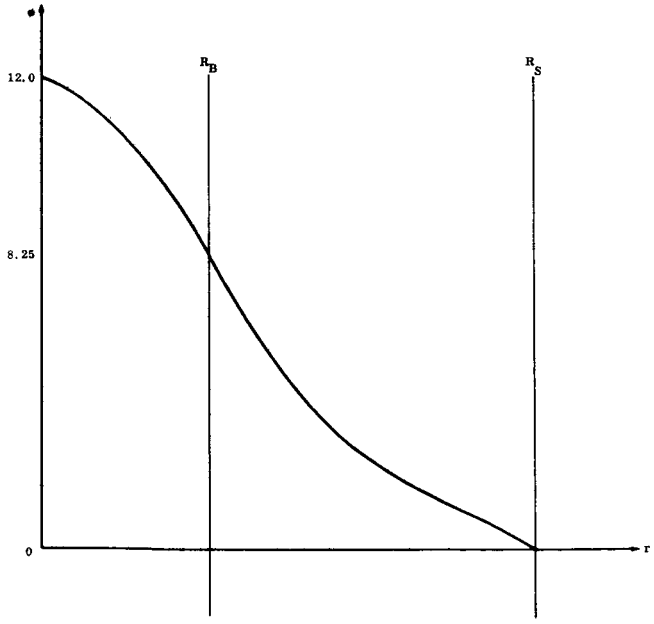

Fig, A2 Beam Voltage Profile

E. Modified Charging Rate

Reference 1 derives an equation for the amount of charge on a particle that has been continuously in the ion beam for a time, t. Page 11 of that reference gives:

$$q(t) = 4\pi\epsilon_0 R_p V_B \left[1 - \exp\left(-\frac{JR_p}{4\epsilon_0 V_B} t\right)\right]$$

$$\equiv A(1 - e^{-\omega t})$$

The actual system under consideration involves particle trajectories that pass through the beam, but have significant portions of their paths outside the beam. Physically, this means that the charging will proceed at a slower rate, given by the ratio of the time in the beam to the total time in the trajectory. Consider the three following time periods:

T_B = time to cross the ion beam,

T_0 = time to travel from the ion beam to the lens region, and

T_L = time spent being reflected and focused by the lens region.

The fraction of time that a particle is in the beam is given by the ratio:

$$f = \frac{T_B}{T_B + T_0 + T_L}$$

We will now define a new "charging constant":

$$\omega' = f\omega = \frac{\omega}{1 + \frac{T_0 + T_L}{T_B}}$$

which, when substituted into the Ref. 1 result, takes into account the time a particle spends outside the beam:

$$q(t) = A(1 - e^{-\omega' t})$$

Although the actual charge accumulation is acquired in steps, this continuous equation roughly represents a "time-average" of the particle's charge, which should be sufficiently accurate for predicting focusing time dependence. The three system time periods defined above are now evaluated.

1. Lens Time

Data taken with a two dimensional electrolytic plotting board, as well as from standard treatments of systems with axial symmetry, (e.g., Reference 6), indicate that the field between two electrodes is quite uniform along the axis of the system. This means that, as a first approximation, the potential between the two electrodes is linear along the symmetry axis, and that the axial force equations have solutions that represent motion under uniform acceleration.

The analysis is simplified if we divide the lens region into two zones:

a. Zone #1 represents uniform acceleration from the entrance of the lens to the center of the focusing electrode, and

b. Zone #2 represents uniform deceleration to zero velocity as the particle goes from the focusing electrode toward the repeller electrode.

We define the following system parameters:

R_B = radius of ion beam

ℓ_B = distance from beam to lens

ℓ_1 = length of Zone #1

ℓ_2 = length of Zone #2

v_0 = velocity at entrance of lens

v_1 = velocity at entering Zone #2

φ_1 = voltage on focusing electrode

φ_2 = voltage on repelling electrode

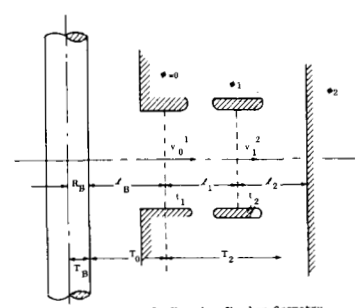

Fig. A3 Charging Chamber Geometry

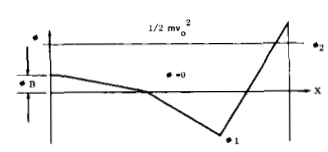

Fig. A4 Potential Profile in Charging Chamber

t_1 = time spent in Zone #1

t_2 = time spent in Zone #2

Figure A3 is a schematic representation of the electrode geometry employed for our lens system, showing the distances, velocities, potentials, and time durations required for the present calculational approach. At the same time, Fig. A4 illustrates the axial potential variation from the center of the beam to the repeller electrode, with ϕ_1 taken to be negative; $1/2\ mv_0^2$ represents the particle's initial kinetic energy, while $\left[1/2\ mv_0^2 - \phi\right]$ is the particle's instantaneous kinetic energy within the field region, which vanishes just short of the repeller electrode (the particle's "stopping point").

Under the assumption of uniform acceleration in the lens region, Zone #1 must have:

$$\ell_1 = v_0 t_1 + \tfrac{1}{2} a_1 t_1^2$$

where the acceleration in Zone #1, a_1, is evaluated by:

$$ma_1 = q\left[\frac{\varphi_1}{\ell_1}\right]$$

$$\therefore a_1 = \frac{q}{m}\left[\frac{\varphi_1}{\ell_1}\right]$$

Thus:

$$\frac{q}{2m}\left[\frac{\varphi_1}{\ell_1}\right]t_1^2 + v_0 t_1 - \ell_1 = 0$$

and use of the "quadratic formula" yields the solution:

$$t_1 = \frac{-v_0 + \sqrt{v_0^2 + 2\frac{q}{m}\varphi_1}}{\frac{q}{m}\left[\frac{\varphi_1}{\ell_1}\right]}$$

In Zone #2, the particle finally comes to rest and we have:

$$v_1 + a_2 t_2 = (v_0 + a_1 t_1) + a_2 t_2 = 0$$

or

$$t_2 = -\left[\frac{v_0}{a_2} + \frac{a_1}{a_2} t_1\right]$$

The entire lens time, T_L, is the sum of t_1 and t_2:

$$T_L = (t_1 + t_2) = -\left[\frac{v_0}{a_2} + \left(\frac{a_1}{a_2} - 1\right)t_1\right]$$

where

$$a_2 = -\frac{q}{m}\left[\frac{\varphi_1 + \varphi_2}{\ell_2}\right]$$

Substituting in the value of t_1 from above and the value of a_2 into the equation for T_L gives:

$$T_L = \left\{\frac{v_0}{\frac{q}{m}\left[\frac{\varphi_1 + \varphi_2}{\ell_2}\right]} + \left[1 + \frac{\ell_2}{\ell_1} \cdot \frac{\varphi_1}{\varphi_1 + \varphi_2}\right] \frac{\sqrt{1 + \frac{2q\varphi_1}{mv_0^2}} - 1}{\frac{q\varphi_1}{mv_0\ell_1}}\right\}$$

$$\text{or, } T_L = \frac{\ell_1/v_0}{\left[\frac{q\varphi_1}{mv_0^2}\right]}\left\{\frac{\ell_2}{\ell_1}\cdot\frac{\varphi_1}{\varphi_1+\varphi_2}+\left[1+\frac{\ell_2}{\ell_1}\frac{\varphi_1}{\varphi_1+\varphi_2}\right]\sqrt{1+\frac{2q\varphi_1}{mv_0^2}}-1-\frac{\ell_2}{\ell_1}\frac{\varphi_1}{\varphi_1+\varphi_2}\right\}$$

$$\therefore T_L = \frac{\ell_1/v_0}{\left[\frac{q\varphi_1}{mv_0^2}\right]}\left\{\left[1+\frac{\ell_2}{\ell_1}\cdot\frac{\varphi_1}{\varphi_1+\varphi_2}\right]\sqrt{1+\frac{2q\varphi_1}{mv_0^2}}-1\right\}$$

Notice that the term $(q\varphi_1/mv_0^2)$ is a time-independent factor, because of the electrode voltage modulation. This means that the time spent in the lens changes only by virtue of the entrance velocity increase, which is only of importance toward the region of saturation charge.

2. Intermediate Time

During the particle trajectory going from the edge of the beam to the lens region, the charged particle experiences an acceleration through the beam potential, φ_B. The shape of this potential, for cylindrical beam-to-vacuum wall geometry, is logarithmic. The resultant equation of motion leads to a definite integral that requires numerical integration for its evaluation. On the other hand, if the beam diameter is about as large as the distance to the lens entrance, then the beam potential along the trajectory is almost linear, and uniform acceleration may be adopted. This condition is fulfilled in our case. Consequently, we have:

$$a_0 = \frac{q}{m}\left[\frac{\varphi_B}{\ell_B}\right]$$

and

$$\frac{1}{2} a_0 T_0^2 + V_0 T_0 - \ell_B = 0$$

$$T_0 = \frac{-V_0 + \sqrt{V_0^2 + 2a_0 \ell_B}}{a_0}$$

$$T_0 = V_0 \left\{ \frac{\sqrt{1 + \frac{2\varphi_B}{mV_0^2} q} - 1}{\frac{\varphi_B}{m\ell_B} q} \right\}$$

Since the term $\left(\frac{2\varphi_B}{mV_0^2} q\right)$ is a small number for most of the charging period, and becomes comparable to unity only in the neighborhood of saturation charge, we may expand the square root in a Taylor series about $\left(\frac{2\varphi_B}{mV_0^2} q\right) = 0$. This procedure results in:

$$T_0 = \frac{\ell_B}{V_0} \left\{ 1 - \frac{1}{4} \left[\frac{2\varphi_B}{mV_0^2} q(t) \right] + \frac{1}{8} \left[\frac{2\varphi_B}{mV_0^2} q(t) \right]^2 + \ldots \right\}$$

Notice that we have used the injection velocity, V_0, as the velocity the particle has when it leaves the beam; this procedure is justified in the next section.

3. Beam Time

Except for the slight potential gradient within the beam itself, most of the increase in particle velocity is due to the potential, φ_B, from the ion beam to the lens region. However, when the particle returns to the ion beam, after being reflected and focused by the conservative fields outside the beam, it slows down through φ_B, and enters the beam with the same velocity that it had when it left the

beam. Consequently, the particle, except for second order effects within the beam, always crosses the beam with the same velocity, namely, the injection velocity, V_0. This effect gives rise to a beam time of:

$$T_B = \frac{R_B}{V_0}$$

4. Charging Rate

By combining the results of the three preceding sections, we can make an estimate of the modified charging rate. These results are:

$$T_L = \frac{\ell_1/v_0}{\left[\frac{q\varphi_1}{mv_0^2}\right]}\left\{\left[1 + \frac{\ell_2}{\ell_1}\cdot\frac{\varphi_1}{\varphi_1+\varphi_2}\right]\sqrt{1+\frac{2q\varphi_1}{mv_0^2}} - 1\right\}$$

$$T_0 = \frac{\ell_B}{V_0}\left\{1 - \frac{1}{4}\left[\frac{2q\varphi_B}{mV_0^2}\right] + \frac{1}{8}\left[\frac{2q\varphi_B}{mV_0^2}\right]^2 + \cdots\right\}$$

$$T_B = \frac{R_B}{V_0}$$

Since these parameters retain their initial values for a large part of the charging process, we may use the starting conditions:

$$v_0(t) \to V_0$$

$$\frac{2q\varphi_1}{mv_0^2} \to \frac{\varphi_1}{\varphi_s}, \quad q_0\varphi_s = \frac{1}{2}mV_0^2$$

$$q\varphi_B \ll \frac{1}{2} m V_0^2$$

where the initial stopping potential has been used.

The times spent in the three regions now assume the form:

$$T_L = \frac{2\ell_1}{V_0 \left[\frac{\varphi_1}{\varphi_s}\right]} \left\{ \left[1 + \frac{\ell_2}{\ell_1} \cdot \frac{\varphi_1}{\varphi_1 + \varphi_2} \right] \sqrt{1 + \left[\frac{\varphi_1}{\varphi_s}\right]} - 1 \right\}$$

$$T_0 = \frac{\ell_B}{V_0}$$

$$T_B = \frac{R_B}{V_0}$$

and the modified charging rate is determined by the time ratio:

$$\left[\frac{T_0 + T_L}{T_B}\right] = \frac{\ell_B}{R_B} + \frac{\ell_1}{R_B} \left\{ \frac{\left[1 + \frac{\ell_2}{\ell_1} \frac{\varphi_1}{\varphi_1 + \varphi_2} \right] \sqrt{1 + \varphi_1/\varphi_s} - 1}{\varphi_1 / 2\varphi_s} \right\}$$

We have previously shown that:

$$\omega' = \frac{\omega}{1 + \left[\frac{T_0 + T_L}{T_B}\right]} \quad (\text{sec})^{-1}$$

where ω is the charging constant as defined in Ref. 1, and ω' is the charging constant that has been modified for particle trajectory time outside the ion beam.

The above time ratio was evaluated for the initial phase of charging, when the velocity build-up due to the beam potential was quite small. As saturation charge

is approached, however, we must return to the more exact time-dependent solutions. These will only involve $T_L(t)$ and $T_0(t)$, since T_B remains invariant during the charging process. If we rewrite the time-dependent solution for $T_L(t)$ as:

$$T_L(t) \cdot v_0(t) = \frac{\ell_1}{\left[\frac{q\varphi_1}{mv_0^2}\right]} \left\{ \left[1 + \frac{\ell_2}{\ell_1} \cdot \frac{\varphi_1}{\varphi_1 + \varphi_2} \right] \sqrt{1 + \frac{2q\varphi_1}{mv_0^2}} - 1 \right\}$$

it will be noticed that the right-hand side of the equation is time-independent since

$$\varphi_1 = \alpha(t) \cdot \varphi_1(t = 0) = (\text{const.}) \frac{mv_0^2(t)}{q(t)} \cdot \varphi_1(t = 0)$$

and

$$\frac{q\varphi_1}{mv_0^2} = (\text{const.})\ \varphi_1(t = 0) \neq f(t)$$

At the same time

$$\frac{\varphi_1}{\varphi_1 + \varphi_2} = \frac{\alpha(t)\varphi_1(0)}{\alpha(t)\varphi_1(0) + \alpha(t)\varphi_2(0)} = \frac{\varphi_1(0)}{\varphi_1(0) + \varphi_2(0)} \neq f(t)$$

This means that $T_L(t) \cdot v_0(t)$ will be equal to its value at $t = 0$:

$$T_L(t)v_0(t) = T_L(0) \cdot V_0 ,$$

but

$$\frac{v_0(t)}{V_0} = \sqrt{1 + \left[\frac{\varphi_B}{\varphi_s}\right] \frac{q(t)}{q_0}}$$

which yields the final result:

$$T_L(t) = \frac{T_L(0)}{\sqrt{1 + \left[\frac{\varphi_B}{\varphi_s}\right] \frac{q(t)}{q_0}}}$$

The exact time-dependent solution for $T_0(t)$ has already been calculated to be

$$T_0(t) = \frac{\ell_B}{V_0} \left\{ \frac{\sqrt{1 + \left[\frac{\varphi_B}{\varphi_s}\right] \frac{q(t)}{q_0}} - 1}{\frac{1}{2}\left[\frac{\varphi_B}{\varphi_s}\right] \frac{q(t)}{q_0}} \right\}$$

where we have used the relation $1/2\ mV_0^2 = q_0\ \varphi_s$. Consequently, both time durations, T_L and T_0, will be influenced by the term, $\left(\frac{\varphi_B}{\varphi_s}\right) \frac{q(t)_{max}}{q_0}$, as saturation is reached. This term is evaluated in the next section, and amounts to about 2. If this is substituted into the above equations, we have:

$$T_L(\infty) \cong .6\ T_L(0)$$

$$T_0(\infty) \cong .7\ T_0(0)$$

Therefore, the variation in the modified charging rate is relatively small, and should not affect the voltage modulation requirement during most of the charging period.

F. Theoretical Typical System Parameters

1. Modified Charging Rate

The charging constant associated with continuous ion beam bombardment, ω, is given by (see Ref. 1, p. 11):

$$\omega = \frac{JR_p}{4\varepsilon_0 V_B} = \frac{iR_p}{4\pi\varepsilon_0 R_B^2 V_B}$$

Typical values for these parameters are

i = beam current $\cong 1 \times 10^{-3}$ amps.

R_p = particle radius $\cong 1 \times 10^{-6}$ m

$4\pi\varepsilon_0$ = fundamental constant = 1.11×10^{-10} f/m

R_B = beam radius $\cong 1/2 \times 10^{-2}$ m

V_B = beam energy $\cong 3 \times 10^{4}$ volts

With these parameters, the unmodified charging constant is:

$$\omega = \frac{(10^{-3})\ (10^{-6})}{(1.11 \times 10^{-10})\ (\tfrac{1}{4} \times 10^{-4})\ (3 \times 10^{4})} = 12.0 \text{ sec}^{-1}$$

or

$$(1/\omega) = .083 \text{ sec.}$$

The initial time ratio, from p. 81, is determined by the equation:

$$\left[\frac{T_0 + T_L}{T_B}\right] = \frac{\ell_B}{R_B} + \frac{\ell_1}{R_B}\left\{\frac{\left[1 + \frac{\ell_2}{\ell_1}\frac{\varphi_1}{\varphi_1 + \varphi_2}\right]\sqrt{1 + \varphi_1/\varphi_s} - 1}{\varphi_1/2\varphi_s}\right\}$$

From the machine drawings of the physical system, and from preliminary indications of voltage requirements, reasonable values for this equation are:

ℓ_B = distance from beam to lens = 2 cm

ℓ_1 = distance of lens focusing = 1.5 cm

ℓ_2 = distance of lens repelling = 1.6 cm

R_B = beam radius = .5 cm

φ_1 = focusing potential (initial) = 1 kv

φ_2 = repelling potential (initial) = 2 kv

φ_5 = stopping potential (initial) = 1.5 kv

Thus:

$$\left[1 + \frac{\ell_2}{\ell_1} \frac{\varphi_1}{\varphi_1 + \varphi_2}\right] = \left[1 + \frac{1.6}{1.5} \cdot \frac{1}{3}\right] = 1.36$$

$$\sqrt{1 + \varphi_1/\varphi_s} \qquad = \sqrt{1 + 2/3} \qquad = 1.29$$

$$\varphi_1/2\varphi_s \qquad = 1/3 \qquad = .333$$

or

$$\left[\frac{T_0 + T_L}{T_B}\right] = \frac{2}{1/2} + \frac{3/2}{1/2}\left\{\frac{.740}{.333}\right\} = 4 + 6.70$$

$$= 10.7$$

This gives a modified charging constant given by:

$$\omega' = \frac{\omega}{1 + \dfrac{T_0 + T_L}{T_B}} = \frac{12.0}{11.7} \simeq 1 \text{ sec}^{-1}$$

or

$$(1/\omega') \cong 1 \text{ sec.}$$

Consequently, with a 1μ radius particle, a 1 ma ion beam with a beam diameter of about 1/2 inch, we would expect a system time constant of about 1 sec. The electric field at the surface of the particle would then have an ideal value given by:

$$\varepsilon = \frac{q(t)}{4\pi\varepsilon_0 R_p^2} = \frac{4\pi\varepsilon_0 R_p V_B (1 - e^{-1})}{4\pi\varepsilon_0 R_p^2}$$

$$= \frac{V_B}{R_p}\left(1 - \frac{1}{2.72}\right) = \frac{3 \times 10^4}{1 \times 10^{-4}}\ (1 - .367)$$

$$\cong 200 \times 10^6 \text{ v/cm}$$

$$\cong 200 \text{ Mv/cm}$$

Effects of changing beam currents, beam radius, and particle size are readily calculated by taking ratios of these results.

2. Asymptotic Voltage Ratio

As saturation charge is reached, the modulation function, $\alpha(t)$, will reach a limiting value. This function has the form:

$$\alpha(t) = \frac{\left[\alpha_0\right]\left[1 + \frac{2\varphi_B}{mV_0^2} q(t)\right]}{q(t)}$$

and its limiting value is given by:

$$\alpha(\infty) = \frac{1 + \left[\frac{\varphi_B}{\varphi_s}\right] \frac{q_{max}}{q_0}}{\frac{q_{max}}{q_0}}$$

where

$$\left[\frac{q_{max}}{q_0}\right] = \frac{2\pi\epsilon_0}{i}\left[\frac{R_B}{R_p}\right] V_0 V_B$$

Typical values for the system are:

$2\pi\epsilon_0$ = fundamental constant = $.555 \times 10^{-10}$ f/m

i = beam current = 10^{-3} amps.

R_B = beam radius = $1/2 \times 10^{-2}$ m

R_p = particle radius = 1×10^{-6} m

V_B = beam energy = 3×10^{4} v

V_0 = injection velocity = 2×10^{1} m/sec

φ_B = beam potential = 12 v

φ_s = initial stopping potential = 1.5×10^{3} v

yielding:

$$\left[\frac{q_{max}}{q_0}\right] = \frac{(.555 \times 10^{-10})}{(10^{-3})}\left[\frac{1/2 \times 10^{-2}}{1 \times 10^{-6}}\right](2 \times 10^{1})(3 \times 10^{4})$$

$$= 170$$

and

$$\left[\frac{\varphi_B}{\varphi_s}\right]\left[\frac{q_{max}}{q_0}\right] = \left[\frac{12}{1500}\right](170) = 1.36$$

This leads to an asymptotic modulation function value of:

$$\alpha(\infty) = \frac{2.36}{170} \cong .014$$

whence

$$\frac{\alpha(t = \infty)}{\alpha(t = 0)} = .014$$

APPENDIX II

ELECTRONIC CIRCUIT THEORY

The electronic circuits required for many aspects of our pulsed system are mainly well-known circuits, such as, multivibrators, Schmitt trigger circuits, etc; although these circuits had to be designed for our specific needs, the basics of their operation is well treated in standard texts.* Work on these circuits primarily required patient application to find the exact parameters for dependable system operation. The circuit components finally adopted for our system are shown in Section IV C of this report. Several electronics problems, however, were specific to the microparticle charging work and required detailed calculations. These are:

1) the input impedance to the detection pre-amp;
2) the output impedance of the h.v. amplifiers feeding the electrodes; and
3) the frequency compensation required in order to observe the h.v. waveforms on an oscilloscope. These topics are discussed in the following treatment.

A. Detector Input Impedance

The detector input stage is a high input impedance cathode follower using a low noise, low microphonic, 6EU7 triode. The input impedance of this stage determines how rapidly the induced charge will drain off the detection capacitor. This current drain must be slow compared to the particle transit time through the detector. With an expected exit velocity in excess of 30 m/sec, and a detection cylinder 1 inch long, the detection pulse length requirement is of the order of:

$$t_{pulse} = \frac{2.54}{3 \times 10^3} \cong 1 \text{ msec}$$

- - - - - - -

*For example, see Ref. 7.

Consequently, the input time constant, τ_D, must be at least 10 msec, to faithfully reproduce the top of the detector pulse. It is from this pulse height that the particle's charge is measured, so that we must have the condition:

$$\tau_D = C_D Z_{in} > 10 \text{ msec}$$

where

C_D = capacity of the detector $\cong$ 10 $\mu\mu$f

Z_{in} = cathode follower input impedance,

which leads to a minimum input impedance of

$$(Z_{in})_{min} = \frac{10 \times 10^{-3} \text{ sec}}{10 \times 10^{-12} \text{ f}} = 10^9 \Omega$$

$$= 1{,}000 \text{ M}\Omega$$

The input circuit, with its "equivalent circuit," is

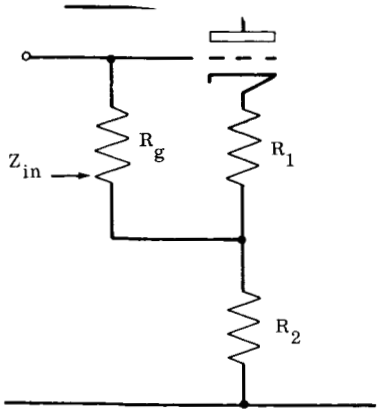

Fig. A5 Input Circuit

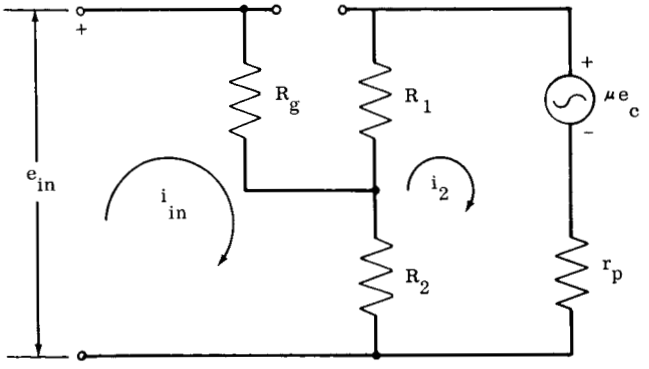

Fig. A6 Equivalent Input Circuit

The equivalent circuit yields the following loop equations:

$$i_{in}(R_2 + R_g) - i_2 R_2 = e_{in}$$

$$-i_{in} R_2 + i_2(R_1 + R_2 + r_p) = -\mu e_c$$

But the voltage from grid to cathode, e_c, is given by:

$$e_c = e_{in} - i_{in}R_2 + i_2(R_1 + R_2)$$

and the loop equations become:

$$i_{in}(R_2 + R_g) - i_2R_2 = e_{in}$$

$$- i_{in}(1 + \mu)R_2 \quad + i_2\left[(1 + \mu)(R_1 + R_2) + r_p\right] = - \mu e_{in}$$

Therefore, using Cramer's rule:

$$i_{in} = \frac{\begin{vmatrix} e_{in} & -R_2 \\ -\mu e_{in} & \left[(1 + \mu)(R_1 + R_2) + r_p\right] \end{vmatrix}}{\begin{vmatrix} (R_2 + R_g) & -R_2 \\ -(1 + \mu)R_2 & \left[(1 + \mu)(R_1 + R_2) + r_p\right] \end{vmatrix}}$$

$$= e_{in} \frac{(1 + \mu)(R_1 + R_2) + r_p - \mu R_2}{(R_2 + R_g)\left[(1 + \mu)(R_1 + R_2) + r_p\right] - (1 + \mu)R_2^2}$$

$$\therefore \left[\frac{e_{in}}{i_{in}}\right] = \frac{R_g\left[(1 + \mu)(R_1 + R_2) + r_p\right] + R_2\left[(1 + \mu)R_1 + r_p\right]}{r_p + R_2 + (1 + \mu)R_1}$$

If we assume that $R_g \gg R_2$,* the second term in the numerator may be neglected, and we are left with:

$$\left[\frac{e_{in}}{i_{in}}\right] \equiv Z_{in} = \frac{R_g}{\dfrac{r_p + R_2 + (1 + \mu)R_1}{r_p + (1 + \mu)R_2}}$$

- - - - - - -

*22MΩ $\gg$ 100kΩ

The circuit components used are:

$R_1 = 470\,\Omega$

$R_2 = 100\,k\Omega$

$R_g = 22M\Omega$

$\mu = 100$

$r_p \cong 70k\Omega$

These values lead to an input impedance given by

$$Z_{in} = \frac{22M\Omega}{\frac{218k\Omega}{10,170k\Omega}} = 22M\Omega(46.6)$$

$$= 1,030\ M\Omega$$

This result means that the detector electronics has a low frequency response down to about 100 cps (10 msec), and should allow a virtually undistorted detection pulse to appear on the oscilloscope for a definitive charge measurement.

B. Output Impedance of High Voltage Amplifiers

The high voltage amplifiers that "drive" the system's electrodes must maintain their voltages in the presence of small stray currents being picked up by the electrodes, from secondary emission electrons created by ion beam impacts on metallic surfaces and/or from ionization of residual gas molecules in the vacuum system. This means, from an electronics point of view, that the output impedance of the amplifier must be low. The output impedance is defined as the ratio of a change in output voltage to a change in output current

$$R_0 \equiv \left[\frac{e_0}{i_0}\right]$$

where we may define:

e_o ≡ output voltage when no current is drawn from the output terminals

i_o ≡ output current when the output terminals are shorted (by, say, a large capacitor, to block dc).

The equivalent circuit for the output stage is that for a cathode follower:

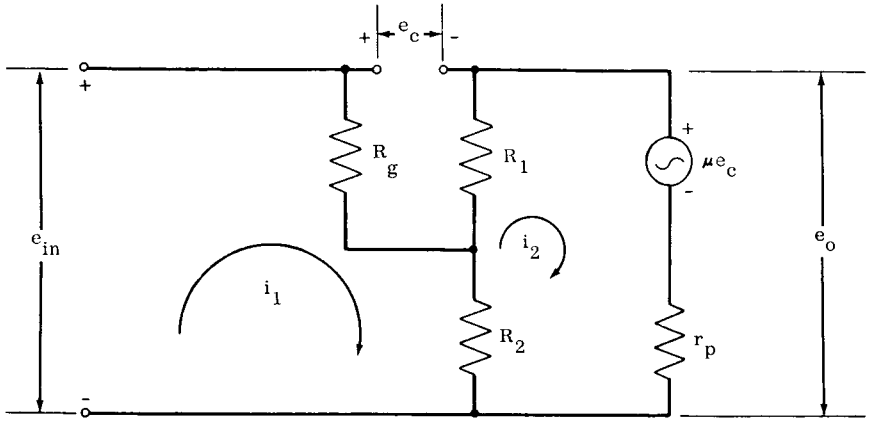

Fig. A7 Equivalent Output Circuit

with the loop equation given by

$$i_1(R_g + R_2) - i_2R_2 = e_{in}$$

$$- i_1R_2 + i_2(R_1 + R_2 + r_p) = - \mu e_c$$

The grid-to-cathode voltage, e_c, is obtained from

$$e_c = e_{in} - \mu e_c - i_2 r_p$$

$$e_c = \frac{e_{in}}{1 + \mu} - i_2 \frac{r_p}{1 + \mu}$$

and the loop equations become

$$i_1(R_2 + R_g) - i_2R_2 = e_{in}$$

$$-i_1R_2 + i_2\left(R_1 + R_2 + \frac{r_p}{1 + \mu}\right) = - e_{in} \frac{\mu}{1 + \mu}$$

Solving for the current i_2 yields:

$$i_2 = e_{in} \frac{\begin{bmatrix} R_2 + R_g & 1 \\ -R_2 & -\frac{\mu}{1+\mu} \end{bmatrix}}{\begin{bmatrix} R_2 + R_g & 1 \\ -R_2 & R_1 + R_2 + \frac{r_p}{1+\mu} \end{bmatrix}} =$$

$$- e_{in} \left\{ \frac{\mu R_g - R_2}{R_g\left[(1+\mu)(R_1 + R_2) + r_p\right] + R_2\left[R_1(1+\mu) + r_p\right]} \right\}$$

The output voltage, e_0, is given by

$$e_0 = \mu e_c + i_2 r_p = \frac{\mu}{1+\mu} e_{in} + i_2 r_p \left[1 - \frac{\mu}{1+\mu}\right]$$

$$= \frac{\mu}{1+\mu}\left[e_{in} + i_2 \frac{r_p}{\mu}\right]$$

Substituting in the value of i_2 yields:

$$\frac{e_0}{e_{in}} = \frac{\mu}{1+\mu} \left\{ \frac{R_g(1+\mu)(R_1 + R_2) + R_g r_p + R_2\left[(1+\mu)R_1 + r_p\right] - R_g r_p + R_2 \frac{r_p}{\mu}}{R_g\left[(1+\mu)(R_1 + R_2) + r_p\right] + R_2\left[R_1(1+\mu) + r_p\right]} \right\}$$

$$\therefore \frac{e_0}{\mu e_{in}} = \frac{R_g(R_1 + R_2) + R_2(R_1 + r_p/\mu)}{R_g\left[(1+\mu)(R_1 + R_2) + r_p\right] + R_2\left[(1+\mu)R_1 + r_p\right]}$$

If the output is shorted, the output current that results is given by

$$i_0 = \frac{\mu e_c}{r_p}$$

but in this situation, the grid voltage, e_c, is just the input voltage and

$$i_0 = \frac{\mu e_{in}}{r_p}$$

Thus, the output impedance is given by:

$$R_0 = r_p \cdot \frac{R_g(R_1 + R_2) + R_2(R_1 + r_p/\mu)}{R_g\left[(1 + \mu)(R_1 + R_2) + r_p\right] + R_2\left[(1 + \mu)R_1 + r_p\right]}$$

The circuit values of these components are:

$R_1 = 5.6\text{k}\Omega$

$R_2 = 10\text{M}\Omega$

$R_g = 100\text{k}\Omega$

$\left.\begin{array}{l}\mu \cong 2{,}000 \\ r_p \cong 10\text{M}\Omega\end{array}\right\}$ 6BK4, see Fig. 16 for typical plate curves.

These values give an output impedance of $4.5\text{k}\Omega$. Thus, if we draw steady state currents as large as $50\ \mu\text{a}$ on these electrodes, the voltages on the electrodes will drop by an amount given by:

$$\Delta e_0 = (4.5 \times 10^3)(50 \times 10^{-6})$$

$$= .225 \text{ volts}$$

which is quite acceptable. Since electrode voltages will range from kilovolt levels down to tens of volts, and since the stray electron currents will diminish as the electrode voltage is modulated downward, this small voltage drop will be negligible.

C. Frequency Compensation in High Voltage Probe

When kilovolt signals are to be displayed on an oscilloscope, three requirements must be fulfilled:

1) the signals must be attenuated down to the volt domain;

2) the measurement must not draw appreciable current from the circuit; and

3) transient response should not be impaired by the attenuator.

The first two requirements are generally fulfilled by simply using a large resistor in series with the 1MΩ scope impedance; a 1,000 MΩ resistor would reduce a 10 kv signal to about 10 volts at the scope. The third requirement is more subtle; this is because there is always some capacity across the 1MΩ scope resistor, which will charge up slowly if it is in series with a large resistor.

Consider the following circuit, where e_{in} is the kilovolt signal and e_0 is the observed scope signal:

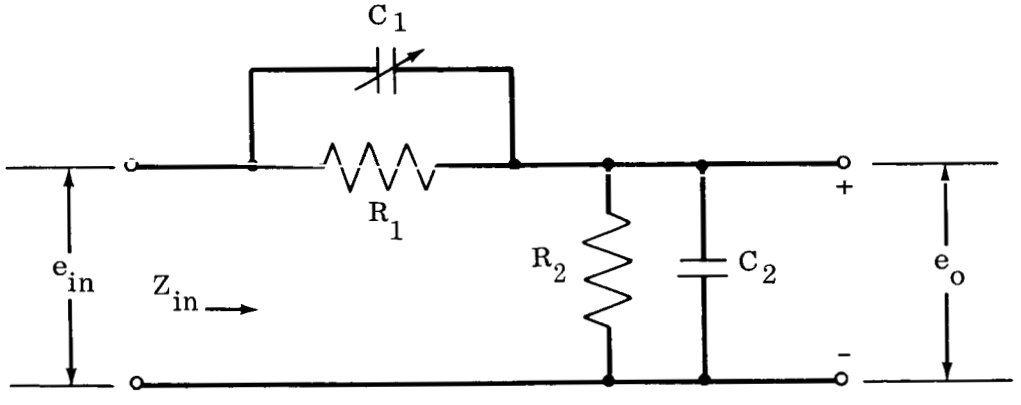

Fig. A8 High Voltage Probe

$$e_0 = \left[\frac{e_{in}}{Z_{in}}\right] \frac{R_2 \frac{1}{C_2 s}}{\frac{1}{C_2 s} + R_2} = \left[\frac{e_{in}}{Z_{in}}\right] \frac{R_2}{1 + R_2 C_2 s}$$

$$Z_{in} = \left\{ \frac{R_1 1/C_1 s}{1/C_1 s + R_1} + \frac{R_2 1/C_2 s}{1/C_2 s + R_2} \right\} = \left\{ \frac{R_1}{1 + R_1 C_1 s} + \frac{R_2}{1 + R_2 C_2 s} \right\}$$

$$\text{or, } Z_{in} = \frac{R_1 (1 + R_2C_2s) + R_2(1 + R_1C_1s)}{(1 + R_1C_1s)(1 + R_2C_2s)}$$

$$\therefore \left[\frac{e_0}{e_{in}}\right] = \frac{(1 + R_1C_1s)(1 + R_2C_2s)}{R_2(1 + R_1C_1s) + R_1(1 + R_2C_2s)} \cdot \frac{R_2}{(1 + R_2C_2s)}$$

$$= \frac{R_2}{R_2 + R_1 \dfrac{1 + R_2C_2s}{1 + R_1C_1s}}$$

$$= \frac{R_2}{R_2 + R_1} \neq f(s) \quad \underline{\text{if}}: \quad R_1C_1 = R_2C_2 \; ; \; C_1 = \frac{R_2C_2}{R_1}$$

Consequently, a small (h.v.) trimmer capacitor across R_1 will result in good transient response of the attenuator. If the "intrinsic" capacity of R_1 is already too large, then C_2 can be increased.

The experimental h.v. probe designed for this work uses a 1,000 MΩ , high voltage, resistor with a lucite tube surrounding the 6-inch-long resistor. At the low voltage end, a BNC connector allows a scope (operated in a "dc" mode)* to be connected to the resistor by a coaxial cable. A small wire, connected by one end to the cable shield, is made to move along with the end of a plastic screw toward the h.v. end (outside the lucite shield). Thus, the trimmer capacitor, C_1, is varied until a good square wave is observed on the scope, with the "cal. output" of the scope feeding the h.v. end of the resistor; this calibrates the unit for observing our

- - - - - - -

*If the scope is operated on "ac" the internal coupling capacitor will attempt to rise up to the kv dc level.

h.v. waveforms. Notice that the cable capacitance is part of C_2, and that the cable and attenuator must be calibrated together as a unit.

APPENDIX III

MACHINE DRAWINGS OF PULSED SYSTEM FOCUSING ASSEMBLY

The focusing assembly designed for the pulsed charging system is based on machining a brass 2-inch "T". The vertical part of the T has a brass plate silver-soldered to it for mounting the assembly on the ion beam apparatus, and the electrodes are placed in the two arms of the T that face each other. At the same time a 2-inch copper tube is silver-soldered onto the T to provide a support for the faraday cup, while the actual electrodes are mounted on nylon cylinders within the arms of the T. End caps, vacuum sealed with O-rings, complete the assembly. Machine drawings of these parts are shown on the following pages, and a sketch of the assembled system is shown in Fig. 5.

NOTE:

Brass "T" is turned by upper I.D. for a press fit with a 2" copper tubing, which extends 2 1/2" beyond "T". Tubing is then silver soldered to "T" and trimmed up inside. After 3" Diam., 1/4" thick brass ring is silver soldered to tubing, surfaces marked "M" are lightly machined for flatness and concentricity. Finally, upper 6 3/4" Diam. brass disk is silver soldered to "T". Discrete use of dilute hydrochloric acid and sand-blasting clean assembly.

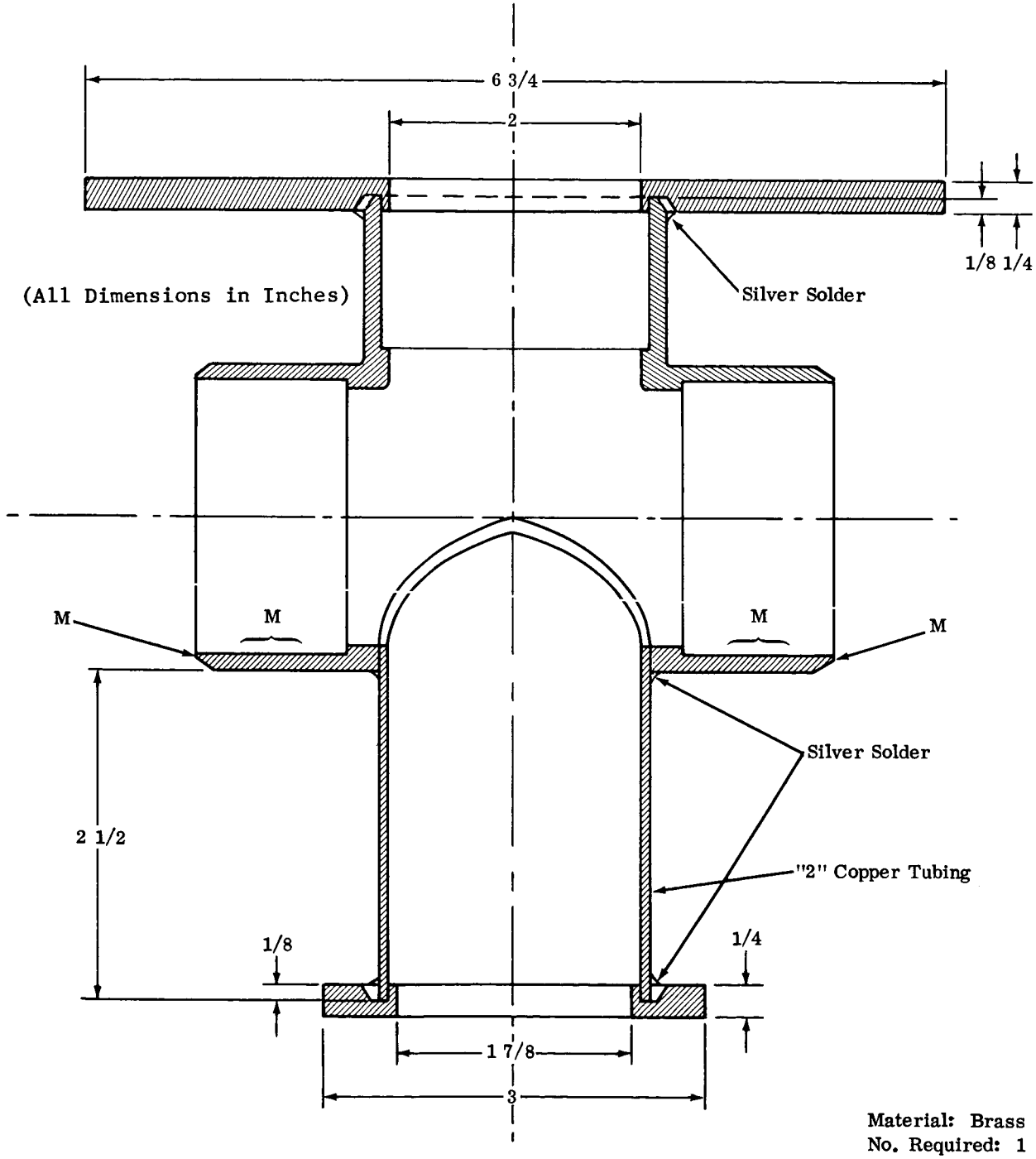

Material: Brass
No. Required: 1

Fig. A9 Housing Assembly

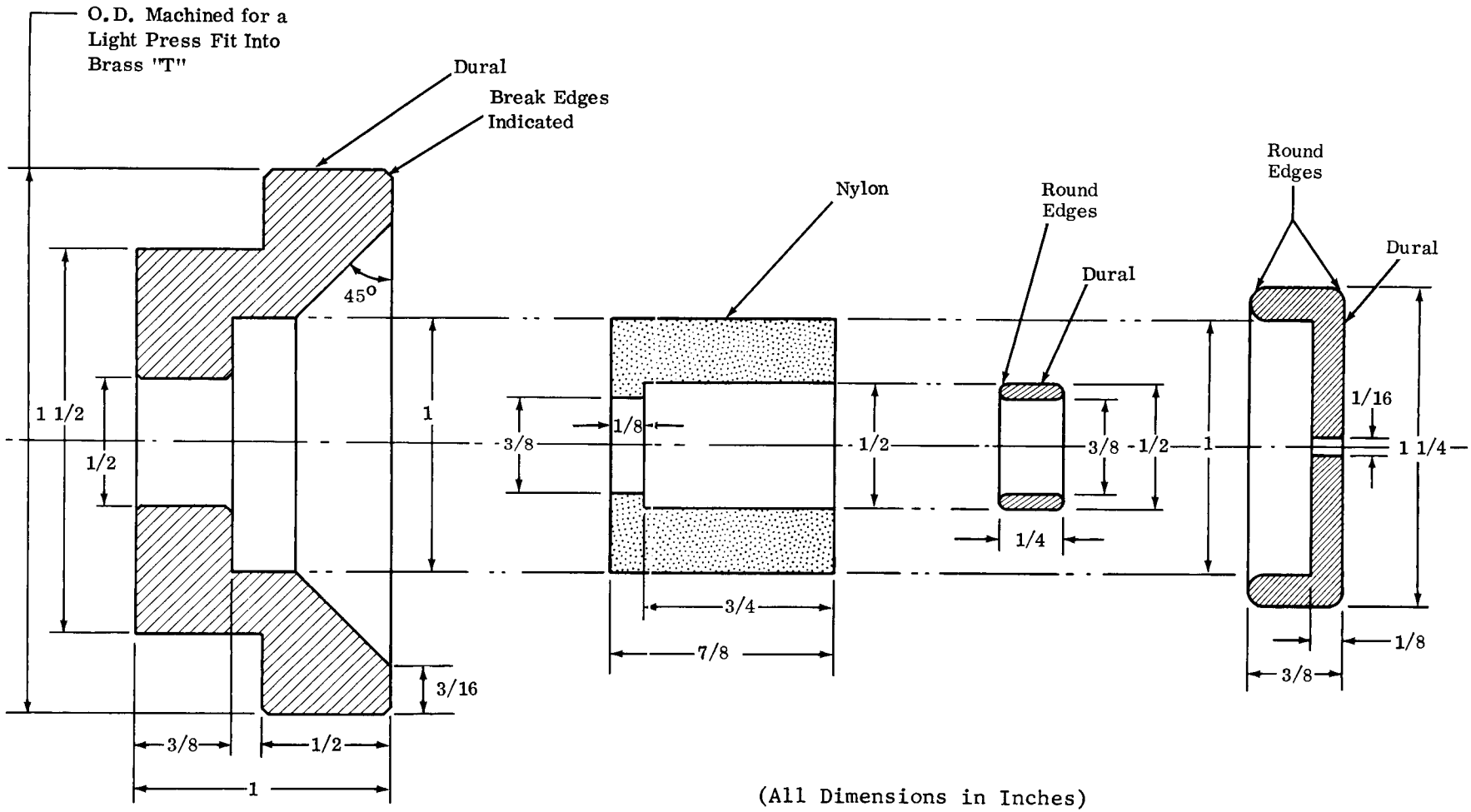

(All Dimensions in Inches)

Material: Nylon & Dural
No. Required: 2

Fig. A10 Focusing Assembly

(All Dimensions in Inches)

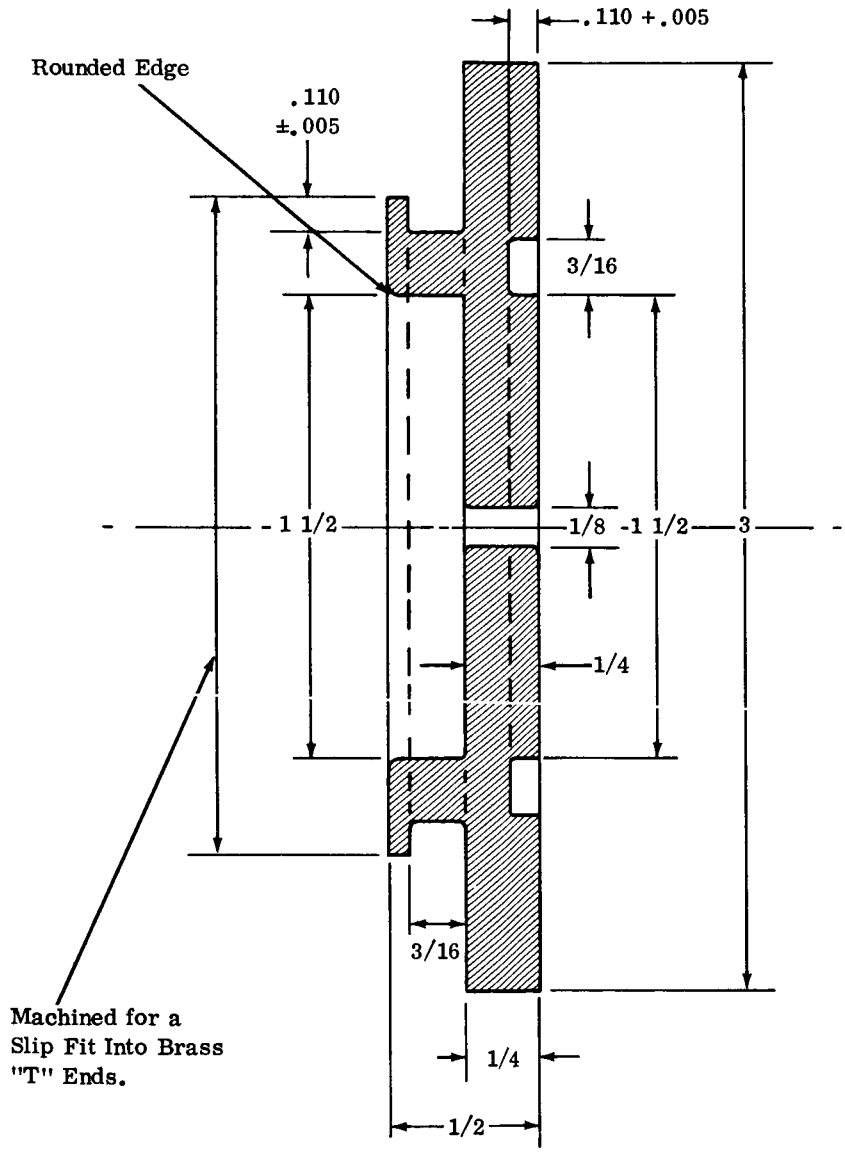

Material: Dural
No. Required: 2

Fig. All End Plate

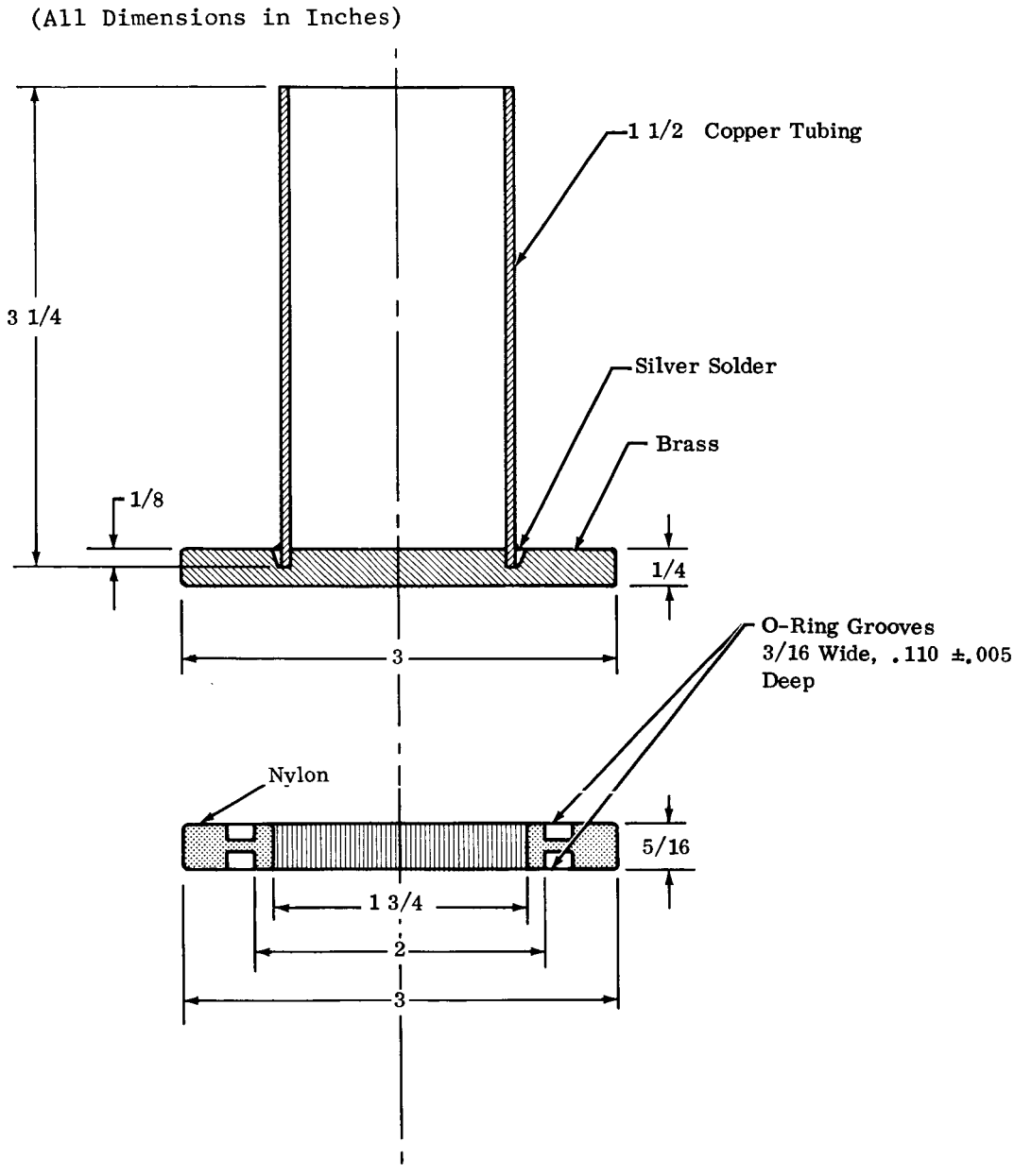

Material: Nylon, Brass, & Copper
No. Required: 1

Fig. A12 Faraday Cup Assembly

APPENDIX IV

CHARGE NEUTRALIZATION BY AMBIENT GAS

The charge on the micron-sized particles can be neutralized by field ionization of the neutral gas molecules surrounding the charged spheres. The subject of field ionization of neutral gases has been studied in detail by Müller et al. (Ref. 5). In Ref. 5, Müller gives the results of his analysis for the geometry of the field emission microscope. Applying his results to our problem leads to a conservative answer due to the fact that the electric field of a charged sphere falls off faster than $r^{4/3}$, the spatial dependence of the field used by Müller. The results of this analysis show that for the charging times involved in our system, this form of charge neutralization is not appreciable until one attains surface field strengths of about 120 Mv/cm in a hydrogen atmosphere. At this field strength the charge neutralization, as calculated for Müller's geometry, amounts to about 17 percent of the charge accrued. The actual percentage is lower because of the conservativeness of using results for Müller's geometry.

In the analysis that follows, the rate of charge neutralization for a charged sphere immersed in a neutral gas is derived under the assumption that every gas atom striking the sphere is ionized. This assumption is actually very good only at high field strengths. At low field strengths one must actually perform a barrier penetration analysis. However, the results attained herein and those of Müller can be compared so as to attain an estimate of how conservative we are in the previous result. From Fig. A13, we can see that at high field strengths Müller's results give neutralization rates at least 20 times higher than those for our geometry.

The gas molecules surrounding a charged sphere are attracted to the sphere by the dipole force on the gas molecule due to the nonuniform electric field. As per Müller, we define a radius of capture, r_c, ($r_c > r_0$, where r_0 is the radius of the

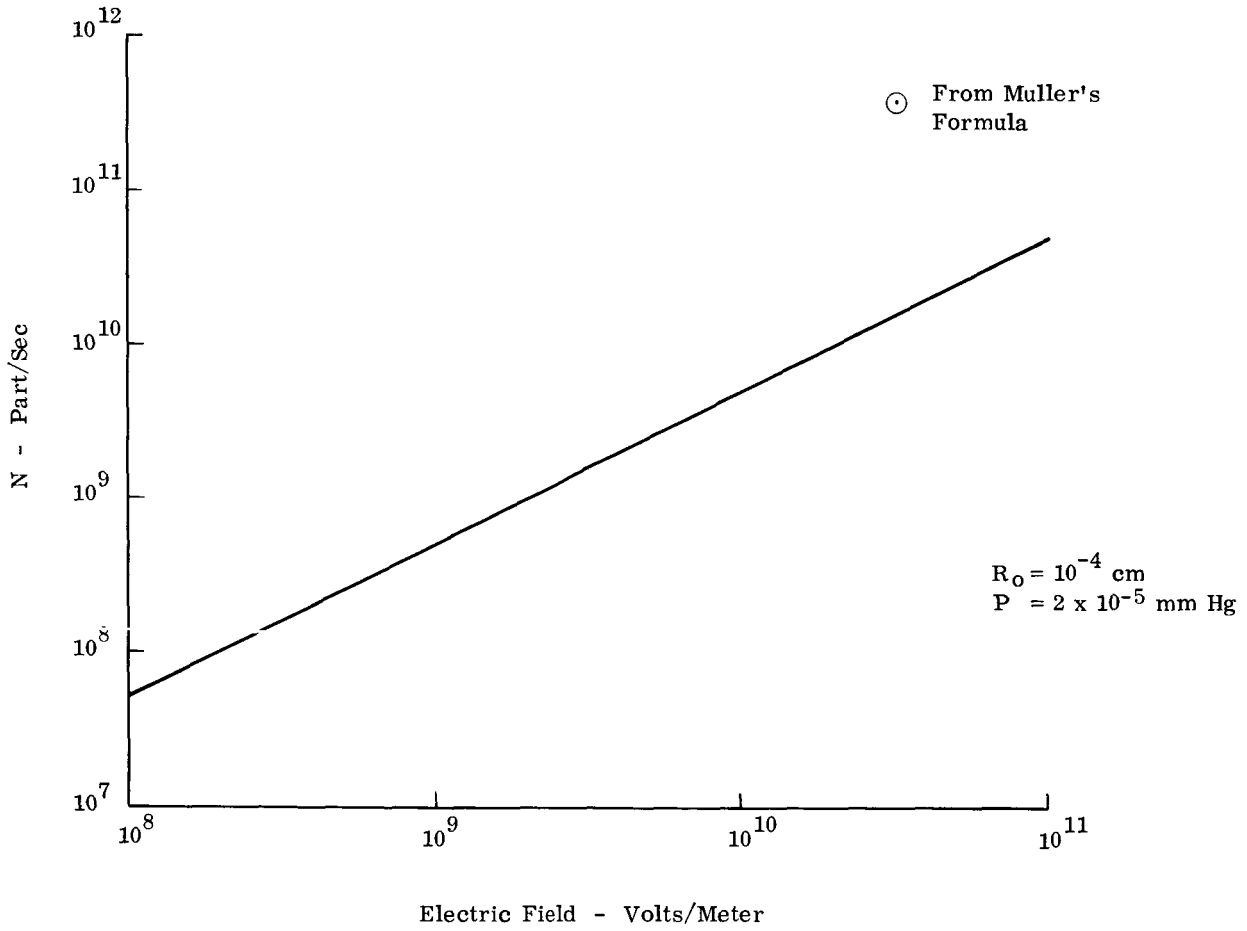

Fig. A13 Number of Charges Neutralized Per Sec Versus Electric Field Strength

sphere). The distance r_c is defined as that distance at which the dipole attraction is just equal to the centripetal force of a tangentially approaching molecule of polarizability α and mass m.

Mathematically, this is expressed

$$-\alpha E \frac{dE}{dr} = \frac{mv^2}{r_c} \tag{1}$$

where

E = electrostatic field due to charged sphere

v = mean gas velocity.

The electrostatic field of a charged sphere of radius, r_0, is given by:

$$E = \frac{q}{4\pi\epsilon_0 r^2} = \frac{E_0 r_0^2}{r^2}, \tag{2}$$

where

E_0 = the electric field strength at $r = r_0$.

Substituting into Eq. (1) we have

$$\alpha \left[\frac{E_0 r_0^2}{r_c^2}\right]\left[\frac{2E_0 r_0^2}{r_c^3}\right] = \frac{mv^2}{r_c} . \tag{3}$$

$$r_c^4 = \frac{\alpha E_0^2 r_0^4}{mv^2/2} = \frac{\alpha E_0^2 r_0^4}{\frac{3}{2}kt} , \tag{4}$$

utilizing the fact that

$$mv^2/2 = 3/2\ kT , \tag{5}$$

where

k = Boltzmann's const.

T = absolute temperature.

$$\therefore \quad r_c = \frac{\alpha^{1/4} E_0^{1/2} r_0 (2/3)^{1/4}}{(kT)^{1/4}} \tag{6}$$

The number of gas molecules, N, striking a sphere of radius, r_c, per unit time when immersed in an ordinary gas at pressure P is given from kinetics as:

$$N = \frac{P}{(2\pi mkT)^{1/2}} 4\pi r_c^2 \tag{7}$$

Substituting for r_c we get:

$$N = \frac{P}{(2\pi mkT)^{1/2}} 4\pi \frac{\alpha^{1/2} E_0 r_0^2 (2/3)^{1/2}}{(kT)^{1/2}} \tag{8}$$

$$N = \frac{4.09\, P \alpha^{1/2} E_0 r_0^2}{m^{1/2} kT} \tag{9}$$

Figure A13 is a plot of N vs. E_0 for a 1μ radius particle in a hydrogen atmosphere. Inclusion of the barrier penetrability would lower this curve by orders of magnitude in the low field area ($E \leq 100$ Mv/cm), the separation becoming more pronounced as the field is lowered. From this derived result one can see that the amount of time spent in charging the particle to a given field strength is going to put severe restrictions on the gas pressure that can be tolerated. If the times are large then the gas pressure must be correspondingly low. In our system the charging times ($\tau \simeq 1$ sec) are relatively short; hence ordinary ion beam systems vacuum can be tolerated ($P \simeq 10^{-6}$ mm Hg).

APPENDIX V

EFFECTS OF FIELD IONIZATION ON CHARGE RETENTION

It is pointed out in Ref. 1 that the high temperature to which the micron-size particles are heated as a result of the charging process may result in a charge leakage problem. It was indicated that the temperature peak could not be kept below 1000°K when charging with milliampere beam currents. The direct effect of this high temperature is to increase the diffusion of captured protons out of the tungsten spheres. This might or might not have constituted a problem, depending on whether the protons diffused out as ions or as neutrals.

The binding energy of the ground state electron in hydrogen is 13.6 ev, while the energy required to remove an electron from the tungsten lattice is 4.54 ev; therefore, one might expect that each proton escaping from a tungsten lattice would have a high probability of removing an electron with it and emerging from the tungsten as a neutral hydrogen atom. The probability for this mode of emission really depends upon the time that the ion spends in the vicinity of the surface. Our feelings on this question were that because of the somewhat nebulous understanding of the diffusion of atoms in metals and the number of factors still unknown, the solution to the problem lay in the performing of the experiments.

Even if we had found that the protons diffused out of tungsten as protons in appreciable quantities we were prepared to overcome this difficulty through the use of helium ions. These ions diffuse through metals only at very high temperatures often only near the melting point (see Ref. 1, page 21). An estimate of the maximum sputtering coefficient of tungsten by helium ions was made based on known data of helium ions on copper and the data of nitrogen ions on copper and tungsten (see Ref. 8 & 9). It was found that the maximum sputtering coefficient for helium on tungsten should be less than 0.05. Therefore, sputtering would not

be a problem. Since the binding energy for a singly charged helium ion is 24.6 ev and the time it would spend in the tungsten is orders of magnitude larger than that for protons, the relatively few helium ions that might leak would have a much greater affinity for picking up electrons on the way out. This makes use of helium look very attractive.

Another point of concern was that of field ionization. At first thought the very existence of the field ion microscope's high efficiency would lead one to believe that even if protons were to diffuse out as neutral hydrogen atoms, the high electric field at the tungsten surface would result in their becoming ionized again. If this indeed happened a charge loss would occur. However, careful study of E.W. Müller's paper (see Ref. 5) clearly shows that for the case where a neutral is moving out from the surface at diffusional velocity the probability for ionization is less than 10^{-6} for a field strength of 250 Mv/cm. Hence, reionization does not constitute a serious problem.

The high ionizing efficiency of the field ion microscope is obtained only as the result of an experimental arrangement that does not exist in our system. In the field ion microscope, as the atom approaches the tip, the ionization probability at first increases rapidly, unitl a critical distance outside the surface is reached. The ionization probability then abruptly goes to zero. At this point the energy of the outer electron of the atom becomes lower than that of the Fermi sea electrons in the metal. Hence there is no available level for the electron to go to in the metal. As can be seen from Fig. 2b of (Ref. 5) the region of maximum ionization is only a few angstroms in depth. We can see from these curves that the ionization probability for gas atoms on a single pass to the tip is extremely small. This is due to the high velocity resulting from dipole attraction. At the surface, those atoms which have not been ionized are reflected and again move out

into the region of high ionization probability. They are, however, drawn back by the dipole force. After accommodation to the low tip temperature, usually 20°K, the atoms perform a slow hopping motion as they are pulled back to the surface by dipole attraction. On the average, by this process, the reflected molecule will reside in the zone of high ionization probability for a relatively long period of time. The latter phenomenon gives rise to the high ionization efficiency of the microscope.

In the case of neutral hydrogen gas emerging from a tungsten surface at some 1000°K to 1500°K, as in our system, the total ionization probability should correspond to the value for a single pass, which is extremely low. This, ironically, is one case where the high temperature helps us.

APPENDIX VI

ANALYSIS OF INJECTION VELOCITY*

The tungsten particles are injected into the charging section by an aerodynamic accelerator.

Since the injection velocity is an important parameter in the experiment, the following analysis has been carried out in an attempt to verify experimental determinations. The model describes the "old" injector, used for the bulk of our work. The particles pass through a 0.004" diameter tube which connects two chambers; one at essentially atmospheric pressure and the other at a vacuum of about 5×10^{-2} torr. In their passage they are entrained and accelerated by the gas flow between the chambers, and are fired out into the vacuum chamber (see Fig. A14).

Derivation (Ref. Shapiro, The Dynamics and Thermodynamics of Compressible Fluid Flow, Vol. 1)

Friction coefficient of the tube (laminar flow, fully developed):

$$f = \frac{16\mu}{V\rho D} = \frac{16\mu}{V^{*}\rho_0 D}\left[\frac{V^{*}}{V_1}\right]\left[\frac{\rho_0}{\rho_1}\right]$$

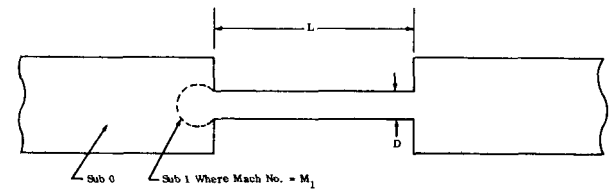

Fig. A14 Pressure Chamber Configuration

$$\left[\frac{V^{*}}{V_1}\right] = \frac{1}{M_1^{*}} = \left\{\frac{1 + \frac{\gamma - 1}{2} M_1^2}{\frac{\gamma + 1}{2} M_1^2}\right\}^{1/2}; \qquad \left[\frac{\rho_0}{\rho_1}\right] = \left[1 + \frac{\gamma - 1}{2} M_1^2\right]^{\frac{1}{\gamma - 1}}$$

Gas flow in a tube of high L/D across which a high pressure ratio exists will be dominated by the wall friction losses in the tube. If the back pressure is in the 10^{-3} torr range, the compressible nature of the flow requires that the exit flow be sonic. Solution of the adiabatic, one dimensional, steady flow equations shows

- - - - - - -

*Contribution of Dr. Richard Oman and Dr. Reuben Chow, Fluid Mechanics Section, Grumman Research Department.

that all fluid properties can be expressed in terms of the upstream (stagnation) conditions and the ratio of specific heats of the gas (γ), with the local Mach number as a parameter. Since the Mach number increases monotonically from a very low inlet value to unity at the exit, we can also use the sonic state (denoted by an asterisk) as a convenient reference.

We will employ Stokes Drag Law to calculate the forces on the particles, as the Reynolds number for these particles is extremely low. We ignore acceleration in the entrance region, where velocity is very low, and in the exit region where the mean free path of the gas molecules exceeds the diameter of the particles. Collisions of particles with the walls will undoubtedly be an important factor, reducing the actual bead velocity by a considerable factor. Since the momentum loss in a single wall collision is unknown, and we have no good method of estimating the mean number of collisions per bead in traversing the tube length, it seems reasonable to treat the "upper limit" case of no collisions. The fact that most of the aerodynamic acceleration takes place in the last part of the tube greatly increases the validity of ignoring the effects of wall collisions.

The following is a brief outline of the aerodynamic calculations conducted to determine the exit velocity of the beads.

With the known conditions we have the expression:

$$4f\left[\frac{L}{D}\right] = \frac{7.5}{P_0 M_1}\left\{1 + 0.2\, M_1^2\right\}^3 \qquad \left(\gamma = \frac{c_p}{c_v} = 1.4\right)$$

Also the choking condition at the exit requires that:

$$4f\left[\frac{L}{D}\right] = \frac{1 - M_1^2}{1.4\, M_1^2} + 0.86\ \ell n\left[\frac{1.2\, M_1^2}{1 + 0.2\, M_1^2}\right]$$

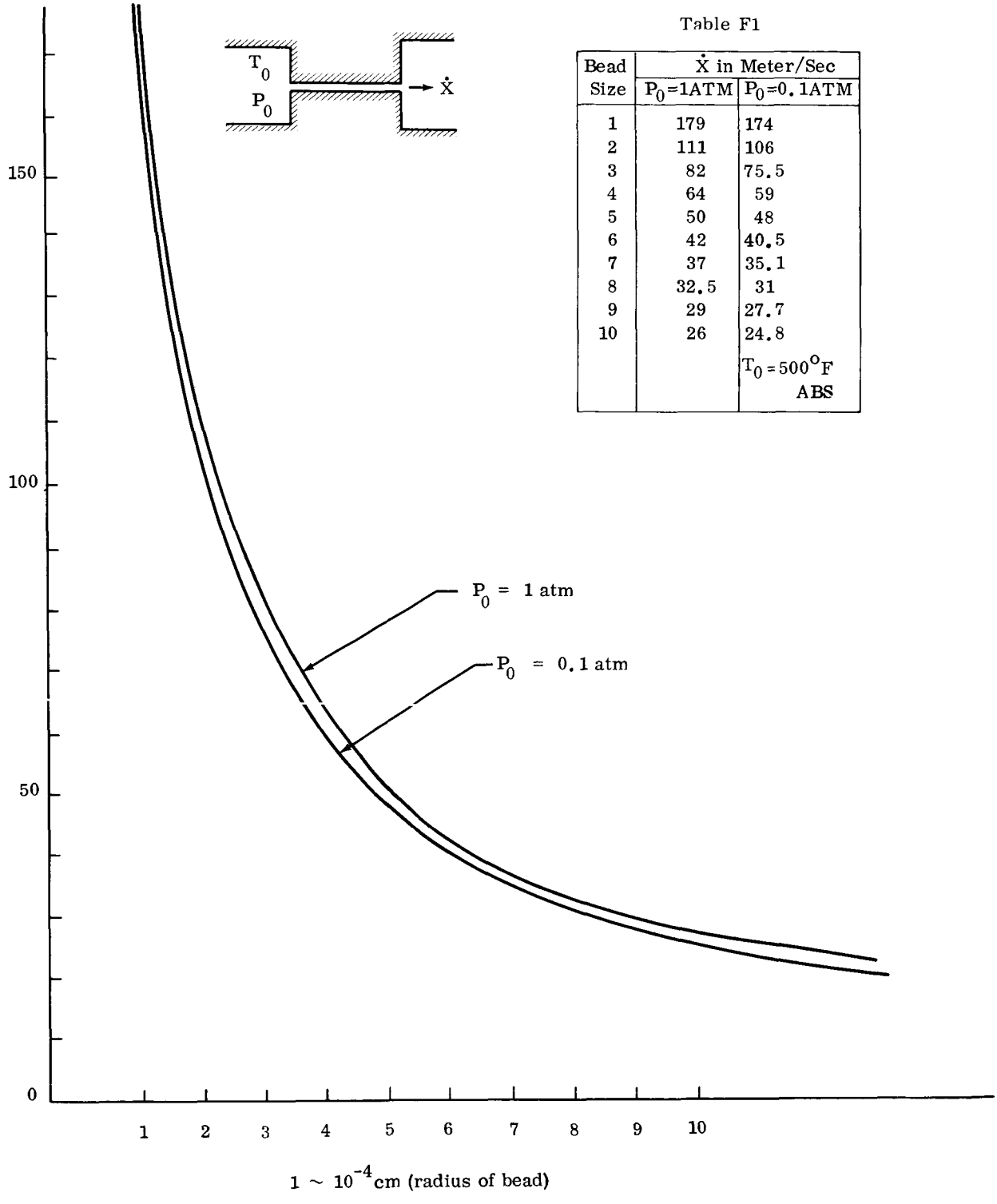

Table F1

Bead Size	$\dot{X}$ in Meter/Sec	
	P_0=1ATM	P_0=0.1ATM
1	179	174
2	111	106
3	82	75.5
4	64	59
5	50	48
6	42	40.5
7	37	35.1
8	32.5	31
9	29	27.7
10	26	24.8
		T_0 = 500°F ABS

Fig. A15 Particle Velocity Versus Pressure

An approximation for M_1 that satisfies both conditions:

$$M_1 = 0.0954\ P_0$$

and

$$M^* = \left[\frac{V_1}{V^*}\right] \sim \sqrt{\frac{\gamma + 1}{2}}\ M_1 = 0.104\ P_0$$

The velocity distribution along tube is very close to linear

$$\therefore \frac{V(x)}{V^*} = \tilde{x} + \left[\frac{V_1}{V^*}\right](1 - \tilde{x}) = \tilde{x} + 0.104\ P_0(1 - \tilde{x}) \quad \text{where } \tilde{x} = x/L$$

For a simple model:

$$m\ddot{x} = 6\pi\mu\frac{d}{2}\{V - \dot{x}\} \equiv \text{Stokes Drag Law.}$$

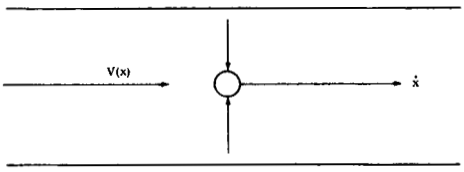

Fig. A16 Simplified Model for Velocity Calculations

we obtain:

$$\ddot{\tilde{x}} + \left[\frac{18\mu}{d^2\rho_s}\right]\dot{\tilde{x}} = \left[\frac{18\mu}{d^2\rho_s}\right]\left[\frac{V^*}{L}\right]\left[(1 - ap_0)\tilde{x} + ap_0\right] \quad \text{where } a = 0.104$$

with boundary conditions $\tilde{x} = \dot{\tilde{x}} = 0$ at $t = 0$:

Solution of the differential equation is as follows:

$$\tilde{x} = \left[\frac{ap_0}{1 - ap_0}\right]\left\{\left[\frac{m_2 e^{m_1 t} - m_1 e^{m_2 t}}{m_2 - m_1}\right] - 1\right\} \text{ (tube length/sec)}$$

where

$$m_{1,\,2} = -A \pm \left[A^2 + 2A\left(\frac{V^*}{L}\right)(1 - ap_0)\right]^{1/2}$$

$$A = \frac{9\mu}{d^2 \rho_s} \quad \text{sec}^{-1}$$

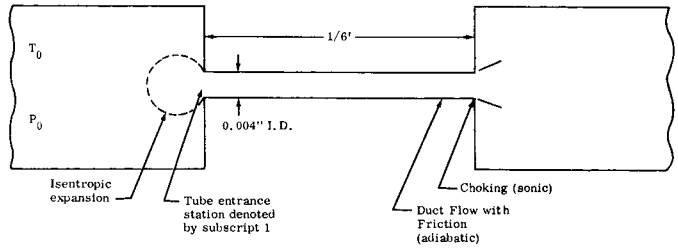

Fig. A17 Pressure Chamber Configuration Showing Operating Conditions

Operating Conditions

T_0 $\sim 500^{\circ}$F abs.

μ $\sim$ const = 118 x 10^{-7} # mass/sec ft

ρ_s = beads density = 18.9 gm/c.c.

= 1180 # mass/ft^3

γ = bead radius = 10^{-4} to 10^{-3} cm = $\frac{d}{2}$

P_0 = 0.1 to 1 atm.

V^* = sonic velocity based on T_0^* = $(\gamma RT^*)^{1/2}$ = 1042 fps

L = 1/6 ft

Results

I. Gas Flow:

$$\left[\frac{V_1}{V^*}\right] = M_1^* = a p_0 = 0.104\, p_0 \; ; \; a = 0.104, \; P_0 \text{ in atm}$$

Linear velocity distribution is a good approximation in the tube

$$\left[\frac{V}{V^*}\right] = \frac{X}{L} + \left[\frac{V_1}{V^*}\right]\left(1 - \frac{x}{L}\right) = \tilde{x} + a p_0 (1 - \tilde{x}), \quad 0 \leq \tilde{x} \leq 1$$

II. Bead Velocity at the Exit of the Tube

$$\dot{x} \text{ (in meters per sec)} = \frac{-A + \left[A^2 + 2A\left(\frac{V^*}{L}\right)(1 - ap_0)\right]^{1/2}}{19.7(1 - ap_0)}$$

$$A = \left[\frac{9\mu}{d^2 \rho_s}\right] \text{ in units of } \sec^{-1}$$

Figure A15 clearly shows that the particle velocity is extremely insensitive to input gas pressures (over our operating range), but very sensitive to particle radius.

APPENDIX VII

EXPERIMENTAL DETERMINATION OF CHARGE-TO-MASS RATIO FOR FIRST PASS PARTICLES

The principle involved in this experiment is simply that of equating the initial kinetic energy of the microparticle to its potential energy when stopped by a bucking voltage. Particles are injected through the beam, becoming positively charged in the process. In the absence of bucking voltage, these particles come to rest on a piece of mylar tape after leaving the beam. A bucking voltage is applied to oppose the motion of particles coming through the beam. This voltage tends to prevent the particles from reaching the tape. That bucking voltage which is just sufficient to prevent particles from reaching the tape is then recorded.

The kinetic energy of the microsphere is:

$$\frac{mv_o^2}{2} + V_B q$$

where

- m --- mass of particle
- q --- charge on particle
- v_o --- particle injection velocity
- V_B --- voltage due to beam

With a bucking voltage, V_o, we have:

$$\frac{mv_o^2}{2} + V_B q = V_o q$$

Solving for q/m we have

$$q/m = \frac{v_o^2}{2(V_o - V_B)}$$

In typical experiments we have found:

$v_o > 30$ m/sec

$V_o = 540$ volts

$V_B = 80$ volts

Hence:

$q/m \geq 1$ coul/kgm.

We know that in order for particles to be positively charged they must be no smaller than 1/2 micron in diameter (the range of 30 kv protons in tungsten), and from microscopy we put an upper limit at about 1 1/2 microns in diameter. This gives limits to an obtained first-pass charge of between 0.36 percent and 1.08 percent, of maximum obtainable charge.

REFERENCES

1. Favale, A. J., Swanson, F. R., Rossi, M. L., Wolkowitz, W., and Hall, K. , Improved Particle-Charging Technique, Grumman Research Department Report RE-152, February 1962

2. Shelton, H., et al , Final Technical Report on Artificial Meteorite Studies, GM-TR-0127-00384.

3. Friichtenicht, J. F., Micrometeoroid Simulation Using Nuclear Accelerator Techniques, Nuclear Instruments and Methods, Vol. 28 (1964) No. 1, North Holland Publishing Company, Amsterdam, Holland.

4. Vedder, J. F., Charging and Acceleration of Particles, Review of Scientific Instruments, Vol. 34, No. 11, American Institute of Physics.

5. Miller, E. W. and Bahaden, K., Field Ionization of Gases at a Metal Surface and the Resolution of the Field Ion Microscope, Physical Review, Vol. 102, No. 3, May 1, 1956.

6. Zworykin, V., al, Electron Optics and the Electron Microscope, John Wiley & Sons, N. Y. 1945.

7. Seely, Samuel, Electron-Tube Circuits, McGraw Hill 1950.

8. O. C. Yonts, et al, "High-Energy Sputtering," Journal of Applied Physics, Vol. 31, #3, March 1960, p. 447.

9. M. Bader, et al, Sputtering of Metals By Mass-Analyzed N_2^+ and N^+, NASA TR R-105.